# Coupled, Data-Driven, and Real-Time Modeling and Control of Sewer Systems and Water Resource Recovery Facilities

by

Sara C. Troutman

A dissertation submitted in partial fulfillment
of the requirements for the degree of
Doctor of Philosophy
(Environmental Engineering)
in The University of Michigan
2020

Doctoral Committee:

Associate Professor Branko Kerkez, Co-Chair
Professor Nancy G. Love, Co-Chair
Professor Glen Daigger
Professor Seth Guikema
Professor Peter A. Vanrolleghem, Université Laval

Sara C. Troutman

stroutm@umich.edu

ORCID iD: 0000-0002-6809-7959

# DEDICATION

To Millie, for boldly going your own way, knowing where home is, and recognizing the beauty in simple things.

# ACKNOWLEDGEMENTS

There are a number of people to whom I must express gratitude for helping me reach this point. "Nothing of me is original. I am the combined effort of everyone I've ever known." (Chuck Palahniuk)

I'd like to thank my committee members Glen Daigger, Seth Guikema, and Peter Vanrolleghem, who assisted me in improving my dissertation through feedback, course instruction, and conversation. Seth's risk analysis course grounded the concepts of probability and uncertainty for me to more broadly understand how people consider information and make decisions. Peter gave both time and effort to share his expertise and help me build upon my ideas. Finally, Glen has always been enthusiastic to join in conversation about all things wastewater and provided a practical view to my research efforts and applications.

To my advisors Branko and Nancy, thank you for the guidance you have provided me throughout the past five years. I consistently leave our meetings with more excitement about my research and the confidence to identify and tackle new challenges. My outlook on research and the work I have and will continue to do has benefited from the passion, enthusiasm, and vision you articulate and display in all of your efforts. I have grown as a both researcher and person because of the consideration and kindness you show to me and others. (Not to mention that my figure standards are much higher as a result of five years of design indoctrination.)

I also want to recognize the operators and managers at GLWA and DWSD who gave tours of facilities, provided access to data and information, and allowed researchers to ask a lot of questions. Much of my work would not have been possible without your assistance.

I have been privileged to work alongside amazing peers in both the Real-Time Water Systems Lab and the Environmental Biotechnology Group at the University of Michigan. I could not have been part of better groups. It was a wonderful experience to be mutually invested in the research of each one of you through thoughtful and patient feedback, rantings, questions, comments, doubts, and dissension. And then to the friends I've made, thank you for making my time in graduate school feel like home, never failing to make me laugh, and helping me to take better care of myself: Rachel Vitali, Evan McLean, Emily Crossette, Anne Menefee, Brandon Wong, Kevin Fries, Matt Bartos, Abhiram Mullapudi, Brooke Mason, Ernesto Martinez, Jack Schmidt, Meagan Tobias, Stef Escobar, Greg Ewing, Sara Rimer, Jackie Fortin, Nate Schambach, Jeseth Delgado Vela, Zerihun Bekele, Caroline Van Steendam, Leonard Cheung, Jimmy Yonts, Enrique Rodriguez, Brett Wagner, Hollie Adejumo, Cheng Yang, Heather Goetsch.

Finally, I can never sufficiently thank my wonderful family. To my grandparents, Nancy, Leroy, Albert, and Betty, your hard work and dedication to family has shaped my values and inspired me my entire life. It was also my grandfather, Albert, who took me on my first tour of a wastewater treatment plant when I was in high school; that marked the beginning of my love of wastewater treatment. And to my parents, Margaret and Joel, and brother, Jacob, you set me on my current path as well as walked with me every step of the way. Thank you for being present, supportive, invested, and loving in every sense. I wouldn't be where I am today without you and I love you immensely.

# TABLE OF CONTENTS

# LIST OF FIGURES

**Figure**

# LIST OF TABLES

**Table**

# LIST OF APPENDICES

**Appendix**

# ABSTRACT

Within the urban water cycle, the challenges posed in the operation of combined sewer systems include changing storms, evolving regulations, and impacts to environmental health. While building bigger infrastructure is one way to solve issues such as sewer overflows, budgetary constraints and increasing stresses to the system, such as climate change, limit the feasibility of this option for many communities and utilities. One alternative is posed by an increasing availability of sensors and data algorithms. Rather than building bigger, the use of real-time data and remote actuation provides a new avenue to autonomously adapt performance of the entire existing system.

While promising, there are outstanding knowledge gaps that must be closed to bring the idea of smart wastewater systems to fruition. 1.) Sewer systems are highly dynamic and spatially heterogeneous. Thus a static, one-size-fits-all modeling approach will not accurately reflect the real-world system. This dissertation addresses this by presenting a data-driven toolchain that learns from historical sensor measurements to estimate current and future combined sewer conditions. By evaluating this toolchain on sensor data collected across the Detroit combined sewer network, it is discovered that wastewater and stormwater flow components exhibit distinct spatial and temporal variation, underscoring the importance of flexible re-calibration using the most relevant window of data. 2.) The efficacy and feasibility of real-time control across the sewershed poses a number of challenges. In particular, objectives for control across the scale of a city often force trade-offs between flood reduction and water quality; without informing control decisions based on these trade-offs, unintended consequences will affect performance across the system. To address this challenge, this dissertation introduces a real-time control algorithm to balance loads across distributed sewer assets and equalize combined sewer flow. The algorithm is

evaluated in a simulated subsection of the Detroit combined sewer network. Trade-offs between flow and water quality objectives are evaluated to inform algorithm parameterization and considerations toward implementation. 3.) While the individual control of either sewer networks or water resource recovery facilities (WRRFs) has been explored separately, the opportunity to link these system components must consider the impact that sewer control has on WRRF operation and performance. By focusing on chemical phosphorus treatment, this dissertation quantifies the impact that WRRF influent dynamics and chemical addition has on treatment efficacy and efficiency. Namely, leveraging these two strategies together, phosphorus treatment is maintained or even improved, while chemical consumption is reduced. These findings exemplify benefits that can be accomplished by coupling the control and operation of system-wide assets.

# CHAPTER 1

# Introduction and Overview

The management of the urban water cycle is readily acknowledged as one of our most important environmental challenges. This is particularly true in the context of wastewater and stormwater, which continue to be the sources of some of our most pressing environmental woes. While the explicit separation of storm and sewer infrastructure has yielded a number of benefits over the past decades, many communities still operate combined sewer systems. The integration of stormwater and wastewater into the same pipe network poses a number of challenges, including urban flooding, sewer overflows, highly variable wastewater treatment performance, strict regulatory decrees, and even impacts to public health. While these issues have been noted for decades [1], aging infrastructure and increasing severity of storms are only further exasperating the situation [2, 3].

Decision makers and operators of urban wastewater systems continue to be tasked with meeting increasingly stringent regulations, while operating aging systems with shrinking budgets. For those communities that can afford it, construction of new and bigger assets (e.g., storage basins, pipes) poses one viable solution. For example, the city of Chicago has developed and constructed an $4 billion tunnel and reservoir plan (TARP) to capture storm and sewer water for the last several decades [4]. By most accounts, the new deep tunnel system has performed well, reducing harmful overflows and increasing the amount of water treated before being discharged to Lake Michigan [5]. Most communities across the US and world do not, however, have enough money

to respond in a similar fashion. More realistically, most municipalities work with limited annual budgets, which allow them to fix one small component of the system at a time — with the hope that the overall collection system and treatment plant will benefit over the long term. As has been noted, however, smaller individual fixes may not lead to overall improvements and may, in some cases, lead to worse performance [6, 7]. This begs the question: what alternatives exist to expensive and massively disruptive new construction, and how can we build water infrastructure that adapts to the rapidly changing urban water cycle?

The recent affordability and availability of sensors and wireless communication technologies has resulted in a growing abundance of new resources to support water management. This, in concert with remote actuation (e.g., gates, valves, pumps), enables a paradigm shift in the way that urban wastewater systems are viewed and managed. Rather than a static, passive system, the vision of *smart wastewater systems* is one in which sensors provide a comprehensive look into real-time sewer and wastewater treatment conditions. Similar to self-driving cars, the behavior of distributed infrastructure assets can be autonomously adapted to enhance the performance of existing systems. Toward this vision, the goal of this dissertation is to enable real-time and data-driven modeling and control of urban wastewater systems by evaluating the role of real-time data in decision-making.

Throughout this dissertation, the specific focus will be on the *urban wastewater system*, which includes both the sewer network (stormwater and wastewater drainage and conveyance) and the water resource recovery facility (WRRF, formerly known as the wastewater treatment plant, WWTP). The span this dissertation is illustrated in Figure 1.1.

Realization of this vision demands the closure of key knowledge gaps, which must be addressed to begin bringing autonomous wastewater systems to fruition:

- We do not yet understand how to develop flexible, real-time models of combined sewer systems. These systems are temporally dynamic and spatially heterogeneous. To leverage the real-time sensor data that capture these nuances, a data-driven modeling toolchain must learn from historical measurements and

incorporate flexible re-calibration using the most relevant window of data.

- We do not understand the scalability of algorithms for the real-time control of entire, city-scale combined sewer systems. Real-time control of sewer systems has been demonstrated with a number of control approaches and algorithms. There is a need to assess the scalability of these approaches to control vastly distributed sewer assets in a coordinated fashion. Furthermore, impacts of sewer control must be considered in light of trade-offs between water quantity and quality objectives, particularly when they are competing.

- We do not understand the impact of collection system control of treatment operations. On their own, sewer networks and WRRFs are complex systems. Considering and balancing decisions and objectives across both of these components is rarely done. However, leveraging control actions to impact and benefit the collection system *and* WRRF presents an exciting opportunity. Quantification of these potential benefits in terms of treatment performance and operational considerations is still needed.

To advance and build upon the idea of smart urban wastewater management, and bridge these knowledge gaps, this dissertation builds upon environmental engineering, data science, and systems analysis. The specific contributions of this dissertation include:

**Chapter 2.** A data-driven toolchain for the modeling of combined sewer flows using signal processing and machine learning (frequency filtering, Gaussian processes, system identification). The toolchain learns from historical sensor data to support real-time forecasting and flexible model re-calibration. The methodology is evaluated across a large, three-year dataset collected by sensors in the Detroit combined sewer network.

**Chapter 3.** A real-time control algorithm that balances loads across distributed sewer storage assets. The algorithm is applied for the equalization of combined sewer flow and is evaluated in a simulated subsection of the Detroit combined

sewer network. Most importantly, the approach is evaluated to analyze trade-offs between flow and water quality objectives, which is presently missing from current literature.

**Chapter 4.** A study that evaluates the impacts of collection system control on WRRF treatment performance. Motivated by regional environmental concerns, we quantify the impacts of WRRF influent dynamics and chemical addition on chemical phosphorus treatment. Specifically, this examines sewer control scenarios from Chapter 3 and ferric chloride dosing strategies, and assesses implications for treatment efficacy and efficiency.

## 1.1 Background

### 1.1.1 Combined Sewers, Wastewater Treatment, and Water Quality

Combined sewer systems integrate stormwater flows into the wastewater sewer network (Figure 1.1a), resulting in flows that exhibit distinct, and often undesirable, peaks during precipitation and snowmelt. These peak events are superpositioned over the more periodic diurnal wastewater dynamics, making comprehensive modeling and forecasting a challenge. The combined stressors on these systems often lead to adverse conditions at the WRRF, which can detrimentally impact surrounding water quality and sewer operation [1].

**Combined sewer overflows.** Storage basins in combined sewers divert, collect, and store excess combined flow during precipitation events, so as to not overwhelm the downstream WRRF. Once the system is less inundated, the aim is to slowly reintroduce the stored combined flow back into the system where it can be treated at the WRRF. However, when the capacity of these basins is exceeded, combined sewer overflow (CSO) events result, whereby stormwater and wastewater from these basins are discharged into a surrounding water body such as rivers. This is often done with little (e.g., primary and disinfection only) to no treatment (Figure 1.1b) [1].

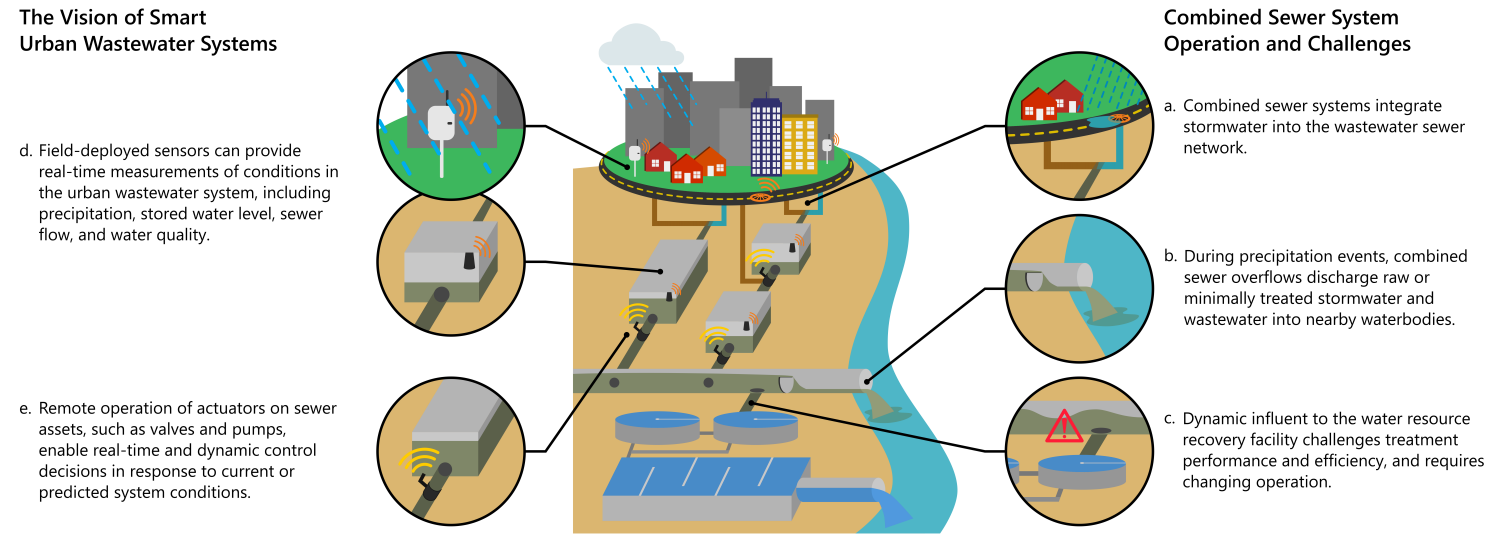


Figure 1.1: Overview of combined sewer and smart urban wastewater systems. Callouts a.–c. highlight operation and challenges of combined sewer systems, as well as their interaction with the downstream WRRF. Callouts d.–e. highlight opportunities for sensing and control to facilitate smart urban wastewater management.

**Dynamic treatment challenges.** Sewer storage basins and CSOs are intended to buffer the downstream WRRF from being overwhelmed by excess stormwater. However, the influent to the WRRF is still impacted by precipitation effects, with impulses of stormwater and variation in pollutant concentrations and mass loads. This is also the case for separated sewer systems, where stormwater infiltrates into aging sewer pipes [8]. The dynamic WRRF influent challenges treatment processes by reducing the efficiency and efficacy of treatment performance (e.g., washout of solids and microorganism populations from clarifiers and bioreactors) or requiring dynamic treatment operation (e.g., chemical dosing, aeration, pumping) (Figure 1.1c) [9, 10].

**Flooding and sewer backups.** Blockages in the sewer system during precipitation events can result in sewer overflows and backups of both stormwater and wastewater into residential areas and nearby water bodies [11, 12]. Further, overutilization of sewer storage can cause them to overflow and result in localized network flooding.

### 1.1.2 Sewer Sensor Data and Modeling

Urban wastewater systems are as dynamic and complex as the cities that they underpin. Wastewater generation patterns and stormwater runoff depend on dynamics that change under a variety of conditions [13–15]:

- Seasonal weather patterns (e.g., warm spring rain on existing snow increases stormwater volumes and changes rainfall-runoff dynamics via snowmelt)
- Variability in storm characteristics impacted by climate change (e.g., more frequent and severe storm events inundate sewer infrastructure assets beyond their design capacity) [15]
- City development and population change (e.g., landuse change alters rainfall-runoff dynamics; growth or contraction of urban populations impacts wastewater generation patterns)

- Infrastructure aging, and retrofit and new construction (e.g., aging sewer pipes experience increased infiltration; augmentation of sewer infrastructure impacts flow routing)

Due to these dynamics, estimating current or predicted sewer conditions with a static model of the underlying physical system will not be sufficient. Rather, the modeling approach must be flexible to continuously incorporate variable, dynamic, and uncertain features and inputs.

The traditional, physically-based modeling approach in water resources and civil engineering relies on a thorough physical characterization of the entire urban water system. This includes the generation of wastewater patterns and precipitation-driven stormwater runoff, as well as the routing of these flows (and pollutants and other water quality constituents) throughout the pipe network. Herein, this is referred to here as *physical modeling*. An example of this is the description of open channel flow and surface runoff through Saint-Venant equations, a system of partial differential equations formulated through a physics-based understanding of underlying hydrologic and hydraulic processes [16]. While the act of formulating this physical modeling approach has greatly grown our understanding of hydrologic and hydraulic processes, their use in real-time modeling at a urban system-scale is limited for several reasons: 1) large amounts of data are required to calibrate these highly detailed and parameterized models, 2) laborious effort is needed to update the model configuration as the city changes through time, and 3) model complexity makes continuous re-calibration in real-time computationally burdensome — if not infeasible — for a typically-resourced water utility [17–20]. This creates motivation to consider alternative uses of data science-based methods to enable a new generation of data-driven modeling approaches.

Advancements in sensing and wireless communication technologies have enabled the deployment of sensors throughout the urban wastewater system (Figure 1.1d) [21]. By deploying an array of sensors in these environments, utilities now have an unprecedented opportunity to leverage real-time monitoring of system conditions, including precipitation, water level, flow, and water quality parameters. However,

monitoring is only one application of these abundant data resources. Indeed, the development and calibration of system models from historical and real-time sensor data stands to enhance our understanding of these dynamic water systems, as well as provide current and future estimates of system conditions. In application, this will better inform control decisions and enable improved operational response to and anticipation of storm events [22, 23].

The growth of real-time data resources motivates research into and assessment of data-driven modeling approaches for describing stormwater and sewer hydrologic processes. As their name suggests, these approaches build mappings between system input and output data using statistical features and relationships that are observed in the data. As data-driven modeling is often used as a catch-all term, there are a number of approaches that are classified under this umbrella, including regression, decision trees, genetic algorithms, and neural networks, to name a few [24]. These techniques can be applied in the context of a black-box system, without knowledge of the internal structure, learning solely from characteristics of the data. One of the most common examples of this in the field of hydrology and sewer modeling has been neural networks [25–31]. There are pros and cons to this black-box approach; while it doesn't require underlying knowledge of the system, extracting a physical interpretation of the system from the learned model is unclear, if not impossible [32]. There are several techniques to embed some degree of physical knowledge of the underlying system into the data-driven model [33] or apply data-driven modeling in conjunction with physical models, largely in developing a data-driven/black-box model for physical model outputs or errors (between model and measured outputs) [34, 35]. More research is needed to combine the benefits of physical understanding and data-driven methods.

In any application of data-driven models, one of the most important questions pertains to the volume, age, and quality of data that will be used to calibrate a data-driven model in order to accurately represent the system and thus make model predictions [14, 23]. It is likely the answer to this question will vary based on model structure, ability for data pre-processing, and system characteristics (e.g., rate of city or urban wastewater system change). This thus highlights a need for a data-driven

modeling toolchain to take advantage of data resources and be flexible for continuous re-calibration using the most relevant historical measurements.

### 1.1.3 Coordinated Real-Time Control for Distributed Sewer Assets

Beyond providing real-time estimates or predictions of sewer conditions, the deployment of sensors and the addition of remotely-controllable actuators to urban wastewater systems enables significant potential to use real-time control [22]. While local control can improve the operation of a single asset, of more fundamental interest is the coordinated control across the system- and city-scales. By leveraging a real-time look at the entire urban wastewater system, the aim is to steer the entire system of distributed assets and actuators toward a system-wide goal via coordinated decisions (Figure 1.1e). In fact, there has been significant development in system-wide control to achieve this [22, 36]. There has been documented success of these efforts toward objectives of mitigating flooding and overflows, and maximizing flow to the downstream WRRF.

Research efforts into real-time control of urban wastewater systems have largely focused on water *quantity* objectives, such as minimizing flooding and CSOs [37–40], and maximizing flows to the WRRF [41]. However, the ability of system-wide real-time control to simultaneously trade-off water quantity and water *quality* objectives (e.g., minimizing pollutant release, performing treatment processes in distributed stormwater assets) remains an open area of research. To our knowledge, there are very limited studies in this area [37].

There are a number of research efforts towards realizing the goal of coordinated real-time control; most of this work has focused on the development of control algorithms [37, 41, 42]. Additional attention must be dedicated to moving the field of real-time control in urban wastewater systems from computational and lab-based studies to real-world implementation. This includes understanding how operators interact with automated and decision support systems [43, 44], maintaining sewer conveyance and WRRF performance requirements that may not be directly incorporated into control objective functions, and investigating and balancing system-wide

trade-offs.

### 1.1.4 Coupled Evaluation of Sewer and WRRF Controls and Operations

WRRF treatment performance is inevitably impacted by the dynamic conditions of the sewer system. Changes in inflows are driven by wastewater and stormwater dynamics. Inflow fluctuations will impact a number of treatment conditions, including chemical addition, energy requirements, and sludge production [9, 10]. In the particular case of chemical phosphorus removal during WRRF primary treatment, the efficacy and efficiency of metal salts to react with and precipitate soluble phosphorus species varies with influent conditions and other operational variables [45]. As a result, a number of dosing strategies for metal salts have been devised to account for changes in influent conditions, with varying degrees of success. These have included constant dose, doses proportional to influent flow or pollutant load, and feedback control to tune the dose in response to effluent phosphorus concentration [46–48].

As will be shown, real-time control of distributed sewer assets presents the exciting opportunity to augment and shape influent dynamics, ideally to improve performance and efficiency of WRRF processes, among other objectives. While previous studies have evaluated operational and control strategies at the plant [46–48], interaction of sewer control, influent conditions, and WRRF dosing strategies remains an open question. The extent to which improvements in operation and performance can be achieved across the urban wastewater system must be explored, which is the goal of the final chapter of this dissertation.

# CHAPTER 2

# An Automated Toolchain for the Data-Driven and Dynamical Modeling of Combined Sewer Systems

Published as: S. C. Troutman, N. Schambach, N. G. Love, B. Kerkez. An automated toolchain for the data-driven and dynamical modeling of combined sewer systems. *Water Research*, 126: 88–100, 2017. doi:10.1016/j.watres.2017.08.065.

## 2.1 Introduction

Combined sewers convey large quantities of wastewater and stormwater to downstream treatment facilities. The delivery of these waters is highly dynamic, being dependent not only on diurnal wastewater patterns, but also on highly uncertain precipitation inputs. The latter is also true in separated sewer systems, which often become susceptible to infiltration due to aging [8, 49–51]. The sheer size and complexity of these systems makes it nearly impossible for operators to anticipate transient changes and optimally control every field-deployed asset, especially during spatially variable storms. These assets include, but are not limited to, pumps, gates, inflatable pillows, and large storage basins, which store, divert, and discharge excess flows during large storms. Improving how all of these assets are controlled and coordinated in real-time will not only reduce harmful combined sewer overflows (CSOs) [41, 52], but will also minimize variability of the wastewater inflows that impact treatment operations and performance [17, 53–55]. To that end, autonomous

and coordinated real-time control stands to change how sewer networks are operated across the scale of entire cities [16, 56–58].

The efficacy of any system-scale control must be underpinned by accurate estimates of field conditions, such as water flow, levels, and quality. The recent availability and affordability of wireless sensing technologies will lead to highly instrumented water systems in the near future [21, 59]. Once sensors become dispersed throughout sewer networks, the data obtained will form the backbone for real-time management and decision-making. However, it will not be sufficient to just use the latest measurements for decision making. Depending on the size and complexity of infrastructure, once a problem is detected in the field, it may already be too late to respond. In many instances, the combined sewer system or treatment plant will need to be prepared hours or days in advance of storms to ensure that existing assets are maximally leveraged in anticipation of any given input scenario; e.g., releasing flows from basins or in-line storage to make room for an incoming storm, or rerouting flows during a storm to maximize system-wide storage. Akin to steering a large ship around an obstacle, control actions in large sewer networks will need to be proactive rather than reactive. In a control theoretic context, this brings up the important need for model predictive control (making decisions based on predicted future outcomes) [60], rather than strict feedback control (making decisions based just on real-time conditions). Effective control strategies will require the most up-to-date knowledge of system dynamics, which may change over time and require model re-calibration. A reliable forecast of future flow thus becomes imperative.

Once calibrated, a water model does not remain calibrated indefinitely. Many water systems exhibit *uncertainty*, which is driven by short-term shifts in wastewater patterns, seasonal runoff dependencies, or long-term climate and land use changes [13–15]. Thus, a vision for smart water infrastructure, which adapts itself in real-time to human and natural inputs, demands the development of a new generation of adaptive models, which will ingest unprecedented quantities of streaming sensor feeds to provide the best possible estimates of current and future conditions. The development of such flexible modeling toolchain will, however, require a holistic approach that combines our domain knowledge of water systems with modern advances

in real-time data processing.

To this end, the goal of this paper is to enable a fully automated and data-driven approach for the dynamical modeling and prediction of dry- and wet-weather flows in a combined sewer system. The core innovation behind our toolchain relates to its automated identification, whereby the toolchain continually re-calibrates the underlying model using real-time sensor feeds to ensure the best possible forecasts of future system flows. The reliance on real-time measurements ensures that system operators and future control algorithms will always be informed by the most up-to-date understanding of system dynamics, especially as these dynamics evolve due to changing weather or land uses. While this paper does not explicitly address control strategies, the toolchain is inherently structured to support predictive control in the future. The specific contributions of this paper are:

- A new data-driven identification toolchain for combined sewer and stormwater systems, based on Gaussian Processes and dynamical System Identification,
- A characterization of system uncertainty, which guides how often components of a model need to be re-calibrated to reflect the uniquely changing nature of urban water systems.

To justify the need for this approach, we begin by providing an overview of existing models for combined sewer systems. The proposed toolchain will then be introduced and evaluated using a novel cloud-based data architecture. Finally, this entire end-to-end solution will be evaluated on sensor data collected in a large, real-world combined sewer system.

### 2.1.1 Existing Approaches

#### 2.1.1.1 Physical Modeling

The most longstanding approach for the modeling of sewer networks has been the physical model. These models seek to characterize the entire sewer collection system, including the drainage subcatchments, the wastewater generation patterns, the pipe

network, and many other physical components. Due to this large degree of characterization, physical models have greatly added to our understanding and management of urban water systems. Such a high level of detail requires a correspondingly high level of parameterization including land use, soil types, and pipe characteristics (e.g., slope, diameter, roughness), as well as less well-defined information (e.g., roof downspout connections). Maintaining these models at the city-scale is laborious and expensive, especially when considering the need to update model parameters in response to urban development, urban contraction, and the implementation of new distributed stormwater solutions [18–20]. As such, uncertainty in the dynamics of the system limits the useful life of physical models. Additionally, the most common physical models are constructed using systems of partial differential equations, such as the Saint-Venant equations, requiring advanced analytic or numerical techniques to generate solutions [16], and demand significant computational effort for model simulations. Hence, the challenge of using large and high-resolution physical models for real-time control concerns the computational expense and complexity related to re-calibration [16, 17].

#### 2.1.1.2 Data-Driven Modeling

The development of data-driven approaches has been increasing in the modeling of urban water systems. This is most evident in the use of Neural Networks (NNs), a form of *black-box* model in which hidden parameters, or weight layers, are adjusted to *"learn"* the relationship between measured input and output data [61]. Most often, the input data comprise a rainfall time series and the NN is trained to predict the corresponding flows [25, 27–31]. This approach relies only on data, which has made it a popular and powerful tool across many disciplines beyond water resources. Unlike in physical models, characterization of the actual water system is not required. The application of neural networks for the modeling of hydrologic and hydraulic systems has generally reported good model performance [26, 28–30]. In part, this can be explained by the ability of NNs to model highly non-linear and nuanced relationships between input-output data sets [26, 32, 61]. Furthermore, once trained, NNs are

highly computationally efficient in making fast predictions of future system states [28–30].

Unlike physical models, however, the parameters of NNs often lack physical interpretation [29, 32, 33, 62]. Since the majority of optimization and control approaches depend on an explicit description of system dynamics [63], this limits the use of NNs in robust management and safety-critical control approaches. Most importantly, perhaps, requirements pertaining to data quality and measurement or model uncertainty have yet to be clarified, which limits the extent to which these models can be transferred between study areas or accommodate changing conditions.

## 2.2 Toward a Holistic Real-Time Modeling Toolchain

More so than just a model, the real-time forecasting in sewer networks demands an end-to-end toolchain. While a model represents the underlying dynamics of the system, it is only one part of a more complex processing chain, which must ingest noisy sensor data and convert it to actionable forecasts. The complexities associated with such a task are best illustrated visually, as shown in Figure 2.1, in which rain and flows in a combined sewer system are plotted. Real-world sensor data is inherently noisy, often to a degree beyond which it is difficult to visually interpret. Once filtered, however, the underlying dynamics become more apparent, such as stormwater inputs or the diurnal wastewater inputs generated by households. Since these diurnal dynamics and wet-weather flows are described by fundamentally separate dynamics, calibration of the model becomes challenging because the two input data streams must first be decoupled.

Furthermore, depending on the location of the sensors in the collection network, the magnitude of the underlying flows differs, making it impractical to translate model parameters of one site to another. System-based uncertainty in the measured signals also introduces significant challenges, as a set of model parameters that were calibrated in the past may not adequately describe present dynamics due to changing climate, baseflows, or human inputs. While many more challenges exist, for instance deploying sensors for water quality as in Banik et al. [64], a set of core requirements

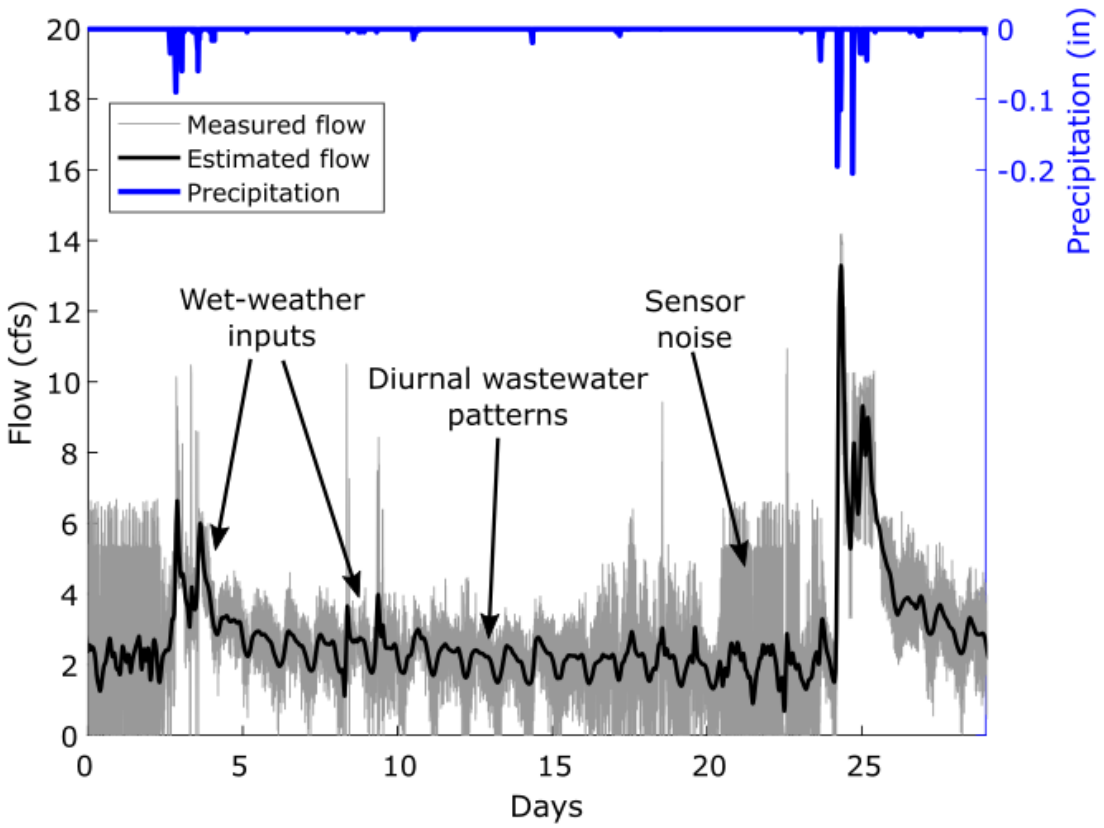


Figure 2.1: Example of sensor signal in a combined sewer system, sampled at five-minute resolution, highlighting the complexities that are present in real-world measurements (Site Q05). The estimated flow was determined using a low-pass Butterworth filter to remove high frequency sensor noise. More information about sensor measurements is included in Section 2.3.3.1.

arises in the development of a robust real-time modeling toolchain:

- Streaming sensor data must be ingested, quality-controlled, and decoupled (dry-weather flows, wet-weather flows, etc.) rapidly before they can be used to calibrate or re-calibrate the underlying model.
- The approach should be automated and readily transferable between sites, requiring only data as an input.

- The underlying model must be computationally efficient to ensure that forecasts can be made within time windows that are suitable for decision-making and control.
- Ideally, the model dynamics should be structured in a way to interpret the physical meaning of parameters and enable the use of formal control theoretic or optimization approaches.

In order to meet these requirements, our approach is data-driven, yet aims to preserve intuition by decoupling the signal into physically-meaningful flow components (i.e., dry- and wet-weather) — that is, rather than being fully abstracted as a black-box, the underlying models are of a structure that should be familiar and interpretable to those working in the water domain.

## 2.3 Methods

Given a rainfall measurement or weather forecast $p$, our problem is framed by the need to predict the flow $q$ at time $t$ in a combined sewer or stormwater conduit. In this section, we first begin by introducing the model structure. We then describe the core contribution of the paper: an automated identification toolchain used to continually re-calibrate the underlying model in response to streaming sensor data.

### 2.3.1 Model Structure

The instantaneous flows in a combined sewer are described by the sum of wet-weather flows (rainfall runoff) and dry-weather inputs (domestic wastewater). Specifically, we assume that

$$q(t) = h(t) + d(t), \tag{2.1}$$

where $q$ is the combined flow, $h$ is the wet-weather flow, and $d$ is the dry-weather or wastewater flow. The flexibility of this representation permits it to be used for a number of models. For example, a stormwater network can be represented when the dry-weather flows are not modeled, while a non-combined sewer network can

be represented without accounting for wet-weather flows. Our approach does not explicitly quantify groundwater infiltration into the network since this component is implicitly included in the "dry-weather" estimates. Infiltration can be a significant and important component in many systems, and could be estimated, if needed, by further segmenting the flows.

The dry-weather flows $d(t)$ are governed by a repeating probabilistic process, which must be *learned* from the data. The wet-weather flows $h(t)$ are approximated by an $n$-th order linear differential equation

$$\begin{aligned} &\frac{d^n h}{dt^n} + a_1 \frac{d^{n-1} h}{dt^{n-1}} + \cdots + a_{n-1} \frac{dh}{dt} + a_n h(t) \\ &= b_0 \frac{d^n p}{dt^n} + b_1 \frac{d^{n-1} p}{dt^{n-1}} + \cdots + b_{n-1} \frac{dp}{dt} + b_n p(t), \end{aligned} \tag{2.2}$$

where $a_1, \cdots, a_n$ and $b_0, \cdots, b_n$ are parameters. When $n = 1$ the model presents the familiar and physically-intuitive *unit hydrograph*, which is used in the hydrologic sciences to conceptualize the hydrograph resulting from one unit of rainfall (e.g., $m^3/s/mm$). Increasing the order of the model permits for more nuanced dynamics to be represented. The biggest benefit of this representation relates to the ability to rewrite the model as the impulse-driven system or transfer function [65], enabling the application of powerful parameter identification tools, which have been developed in the dynamical systems community [66]. Furthermore, this formalism allows for feedback control and model predictive control methods to be applied to the system [63], thus opening the door to future real-time control applications.

### 2.3.2 Toolchain to Identify and Predict Dry- and Wet-Weather Flows

Given sensor measurements of flow $q$ and rainfall $p$, our problem is framed by the need to identify the model order and the parameters describing the wet-weather flows, as well as the parameters of the dry-weather flows. Once the model parameters are identified or *learned*, the resulting model can then be used in a predictive fashion by taking the measured state $q$ and forward-modeling it using the forecasted or measured rainfall $p$.

For a given sensor pair (flow and rain), our toolchain (Figure 2.2) identifies the model parameters by *training* the full model on a set of historical observations of flows and corresponding rainfall measurements. The first step in our processing chain involves the *learning* of the dry-weather flows using a Gaussian Process (Section 2.3.2.2). The full time series of historical dry-weather flows is then estimated and subtracted from the original flows to derive an estimate of the wet-weather flows, which are then used along with measured rainfall to identify the parameters of the wet-weather model (Section 2.3.2.3). This step is very important, as it is particularly difficult using frequency-based filtering, for example, to separate a storm from the dry-weather flows when the two have similar magnitudes or occur across the same timescale. The approach is inherently flexible, as it can be re-calibrated continuously, or as needed, when more measurements become available. As will be shown, given our dual identification and estimation formulation, the approach is also highly resilient to missing or incomplete measurements. The only input requirements are pairs of flow and rainfall measurements.

#### 2.3.2.1 Flow Separation and Pre-Processing

The first step in the processing chain involves the separation of the dry-weather flow from the measured signal (Figure 2.2a–b). The observed dry-weather diurnal patterns display daily repetition ($1\ \frac{1}{day}$) and approximate semi-daily peaks ($2\ \frac{1}{day}$). Thus, to achieve this separation, a *Butterworth* bandpass filter [67] parameterized with a range of 0.5 to 3 $\frac{1}{day}$ is applied. This has the immediate impact of removing high-frequency sensor noise and low-frequency flows (Figure 2.2b). The outputs of this operation clearly exhibit the familiar wastewater diurnal pattern, with distinct dynamics for weekdays and weekends. However, since the filter allows daily components through its pass band, daily fluctuations in wet-weather flows are still very apparent in the output and must be removed before the dry-weather diurnals can be characterized. To remove the diurnal wastewater patterns distorted by rain storms, the precipitation input is used to delineate times of "dry" weather. As an additive step, the filtered signal is separated into daily bins. Simple threshold criteria for

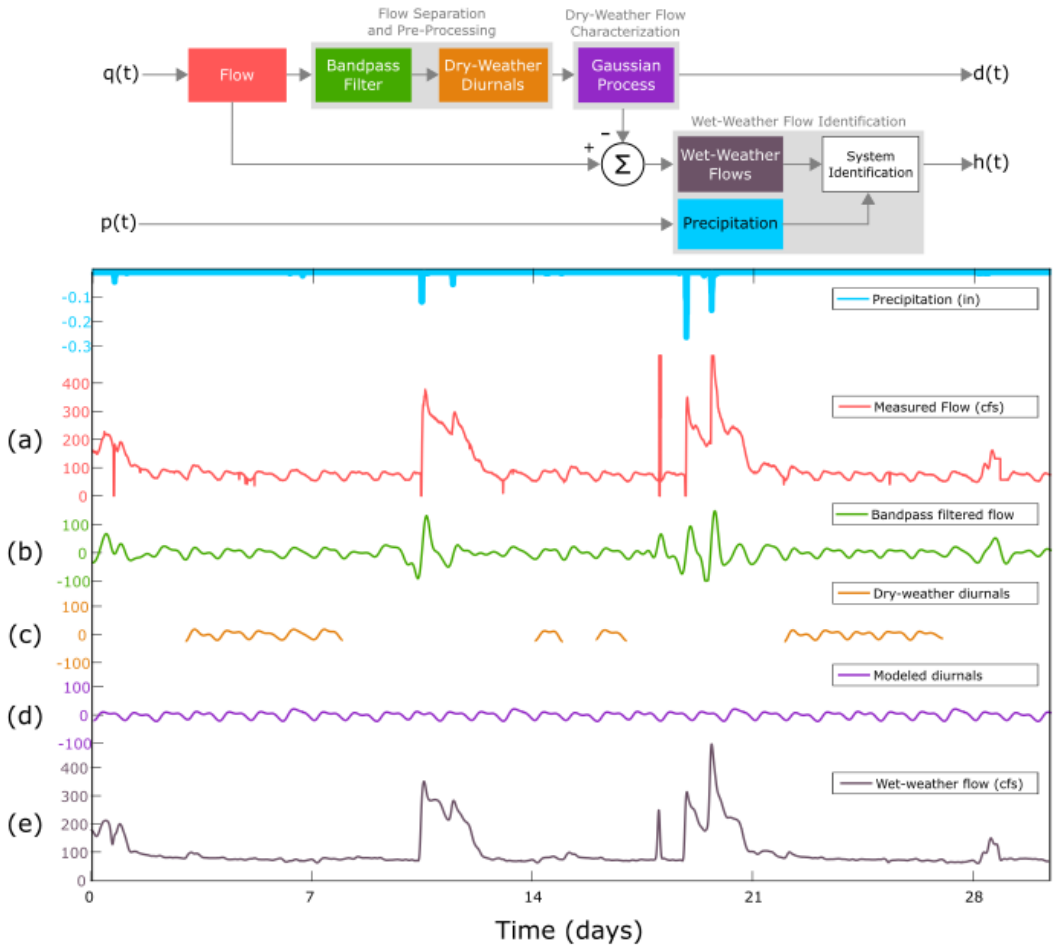


Figure 2.2: Proposed identification toolchain applied to measured combined sewer flows.

magnitude and length of the diurnal pattern for each site are used to remove daily signals influenced by wet-weather flows. This may occur when a rain gauge does not measure rainfall, but wet-weather flows are still evident. The result of these operations is a sparse dry-weather time series, which only contains those portions of the flow that are not impacted by wet-weather inputs (Figure 2.2c). This series is then used to characterize the dry-weather model (Section 2.3.2.2). Most importantly, perhaps, the dry-weather model can be used to estimate historical dry-weather flows

(Figure 2.2d), which can then be subtracted from the measured flows to derive a historical estimate of wet-weather flows (Figure 2.2e).

#### 2.3.2.2 Dry-Weather Flow Characterization

As evident in Figure 2.2, the task of characterizing dry-weather diurnal patterns in an arbitrary sensor signal is non-trivial due to daily uncertainty in wastewater generation and other factors. If accuracy is desired, there is a need to characterize individual dynamics for each day of the week, and especially the weekends. Furthermore, measurements may not be available on some week days if they have been obscured by wet-weather flows. As such, the approach has to be robust to missing measurements. The high level of non-linearity in the dry-weather diurnal dynamics, as well as their repeating pattern makes them particularly difficult to model as a function of simple inputs. This likely explains why dry-weather signals are often modeled in literature as simple static functions [68], rather than the dynamically changing systems that they really are. Physical models have been proposed as an alternative, but are highly parameterized [69, 70].

To address these challenges, our approach represents the dry-weather signal using a non-parametric probability model, which is conditioned on the incomplete dry-weather data received from the first stages of our processing chain. Specifically, we assume that for a measured dry-weather signal $y$ at time $t$,

$$y(t) = f(t) + \varepsilon, \tag{2.3}$$

where $f(t)$ is the modeled dry-weather and $\varepsilon \sim \mathcal{N}(0, \sigma_n)$ represents the underlying model and measurement uncertainty, which is normally distributed with a variance $\sigma_n$. A powerful model can be obtained by representing the above relation as a Gaussian Process (GP) [71]. Specifically, rather than learning an explicit mapping for $f(t)$, it is possible to characterize the distribution over all (possibly infinite) dry-weather diurnals that describe the observed data. In this setting, the distribution

over all dry-weather models is given by the Gaussian Process

$$f(t) \sim \mathcal{GP}\left(d(t), k(t, t')\right), \tag{2.4}$$

which is fully characterized by its mean function $d(t)$ and covariance function

$$k(t, t') = \mathbb{E}[(f(t) - d(t))(f(t') - d(t'))]. \tag{2.5}$$

Due to their cyclical patterns and irregular shapes, dry-weather diurnal signals are difficult to model using standard linear regression techniques, since the underlying basis functions that describe the model are unknown. Rather than defining an explicit relation that depends on just time, our implementation relies on using the covariance function $k(\cdot, \cdot)$ to determine the degree of *similarity* between points in the dry-weather signal. When making predictions of dry-weather signals at times when no measurements are available, this logic dictates that the missing measurements is most likely similar to its nearest neighbors or to those points that have been observed on the same day during a different week.

This notion can be encoded through the use of specific covariance functions, or *kernels*. Specifically, our models make use of two *kernels*, which are added together to model the covariance of the dry-weather signal. The first is a sinusoidal or *periodic* kernel

$$k_{per}(t, t') = \sigma_p^2 \exp\left[-\frac{2\sin^2\left(\frac{\pi|t-t'|}{p}\right)}{\ell_p^2}\right]. \tag{2.6}$$

This kernel is characterized by its hyperparameters $\sigma_p, p$, and $\ell_p$, which must be *learned* before predictions can be made. Given two points $t$ and $t'$ in time, this kernel embeds the notion that similarity between observations is determined according to a repeating pattern. Simply stated as an example: an observation on a Wednesday more closely resembles that made during the same time during another week, rather than a measurement made on a Saturday morning. This also implies that the parameters of the kernel embed meaning about the physical and hydrologic nature of the diurnal wastewater flows, such as periodicity and magnitude, unlike black-box

models. The $p$ parameter, for example, encodes how often a signal repeats (daily in our case), while the length-scale parameter $\ell_p$ determines how closely points are related throughout the day.

Recognizing that the day and time of the week are not the only factors describing the dry-weather wastewater pattern, we also use a rational quadratic kernel $k_{RQ}(\cdot,\cdot)$, which is given by

$$k_{RQ}(t,t') = \sigma_r^2 \left[1 + \frac{|t-t'|^2}{2\alpha\ell_r^2}\right]^{-\alpha}. \tag{2.7}$$

Once the the hyperparameters $\sigma_r, \alpha$, and $\ell_r$ are *learned*, the use of this kernel captures variations in the magnitude of the dry-weather signal that cannot be explained by simple periodicity, but rather by a proximity to neighboring points in time. This includes, but is not limited to, seasonal variations in magnitude or short-term fluctuations (e.g., holidays, sporting events).

While the hyperparameters of these kernels could be manually calibrated, the major task in the use of this probabilistic model relates to using the sensor data to automate this task. This can be accomplished by storing the observed dry-weather measurements and their corresponding weekly time stamps in the vectors $\mathbf{y}$ and $\mathbf{t}$. It can be shown that the posterior distribution over all the dry-weather functions that describe this data is given by applying Bayes' Rule

$$P(f|\mathbf{t},\mathbf{y}) = \frac{P(f)P(\mathbf{y}|\mathbf{t},f)}{P(\mathbf{y}|\mathbf{t})}, \tag{2.8}$$

which, given our assumptions, simplifies to

$$\begin{aligned} P(f|\mathbf{t},\mathbf{y}) \sim \mathcal{N}\Big(&k(t,\mathbf{t})\left[K(\mathbf{t},\mathbf{t}) + \sigma_n^2 I\right]^{-1}\mathbf{y}\,, \\ &k(t,t') - k(t,\mathbf{t})\left[K(\mathbf{t},\mathbf{t}) + \sigma_n^2 I\right]^{-1} k(\mathbf{t},t')\Big)\,. \end{aligned} \tag{2.9}$$

The hyperparameters can be learned by maximizing the marginal likelihood $P(y|t)$. Unlike in the predictive distribution, no closed form solution exists for this relation. However, a gradient-based optimization algorithm can be used to find the optimal (or near-optimal) hyperparameters by maximizing the log-likelihood, which is given

by

$$\log P(\mathbf{y}|\mathbf{t}) = -\frac{1}{2}\mathbf{y}^T\mathbf{K}^{-1}\mathbf{y} - \frac{1}{2}\log|\mathbf{K}| - \frac{n}{2}\log 2\pi. \tag{2.10}$$

Once model is *learned*, Equation 2.9 can then be used to make a prediction $y^*$ at a time $t^*$ via

$$\begin{aligned} P(y^*|t^*, \mathbf{t}, \mathbf{y}) \sim \mathcal{N}\Big(&\mathbf{k}(t^*, \mathbf{t})^T \left[K + \sigma_n^2 I\right]^{-1} \mathbf{y}\ , \\ &k(t^*, t^*) + \sigma_n^2 - \mathbf{k}(t^*, \mathbf{t})^T \left[K + \sigma_n^2 I\right]^{-1} \mathbf{k}(t^*, \mathbf{t})\Big)\ . \end{aligned} \tag{2.11}$$

#### 2.3.2.3 Wet-Weather Flow Identification

Once the full historical dry-weather flows are estimated, they are subtracted from the original measurement to derive an estimate of historical wet-weather flows (Figure 2.2). This estimate can then be used to identify the input-output relationship between precipitation and wet-weather flow, which our toolchain accomplishes through the use of *System Identification* [66]. In short, System Identification is a form of inverse modeling, where input and output data are provided, a model structure is specified, and the parameters of the model are learned from the data.

In our toolchain, the structure takes the form of a transfer function model [65, 72], which represents the frequency ($s$) response of the flow model (Equation 2.2) as

$$G(s) = \frac{H(s)}{P(s)} = \frac{b_0 s^n + b_1 s^{n-1} + \cdots + b_{n-1}s + b_n}{s^n + a_1 s^{n-1} + \cdots + a_{n-1}s + a_n}; \tag{2.12}$$

the input is precipitation data $P(s)$ and output is wet-weather flow data $H(s)$.

The parameters of the differential equation $a_1, \cdots, a_n, b_0, \cdots, b_n$ are placed into the vector $\theta$. For parameter identification, let $Z^N$ denote the $N$-dimensional measured data set, $h(t)$ denote the measured system output, and $\hat{h}(t|\theta)$ denote the predicted system output given system parameters $\theta$. The prediction error is given by

$$\varepsilon(t, \theta) = h(t) - \hat{h}(t|\theta). \tag{2.13}$$

The desired parameters maximize the fit between observed and modeled dynamics.

Mathematically, we seek to minimize a norm of the prediction error, given as

$$V_N(\theta, Z^N) = \frac{1}{N}\sum_{t=1}^{N} l(\varepsilon(t,\theta)), \tag{2.14}$$

where $l(\cdot)$ is a scalar-valued norm function. If the standard choice of $l(\cdot)$ as the quadratic norm is used

$$l(\varepsilon) = \frac{1}{2}\varepsilon^2, \tag{2.15}$$

an estimate of the system parameters $\hat{\theta}$ for the measured data set is given by

$$\hat{\theta} = \hat{\theta}(Z^N) = \arg\min_{\theta} V_N(\theta, Z^N). \tag{2.16}$$

To minimize $V_N$, parameters are iteratively changed using numerical strategies such that

$$\hat{\theta}_N^{(i+1)} = \hat{\theta}_N^{(i)} - \mu_N^{(i)} \left[R_N^{(i)}\right]^{-1} V_N'\left(\hat{\theta}_N^{(i)}, Z^N\right), \tag{2.17}$$

where $V_N'$ is the gradient of $V_N$, $R_N^{(i)}$ denotes a matrix to dictate the search direction, and $\mu_N^{(i)}$ is the step size to decrease $V_N$ with each iteration. For the quadratic norm,

$$V_N(\theta, Z^N) = \frac{1}{N}\sum_{t=1}^{N} \frac{1}{2}\varepsilon^2(t,\theta), \tag{2.18}$$

which implies that

$$V_N'(\theta, Z^N) = -\frac{1}{N}\sum_{t=1}^{N} \psi(t,\theta)\varepsilon(t,\theta), \tag{2.19}$$

where $\psi(t,\theta)$ denotes the gradient of $\hat{h}(t|\theta)$ with respect to $\theta$.

To estimate the parameters, during each numerical iteration, the search direction is calculated using each using a Gauss-Newton method. Specifically, the search direction is calculated

$$R_N^{(i)} = V_N''(\theta, Z^N) = \frac{1}{N}\sum_{t=1}^{N} \psi(t,\theta)\psi^T(t,\theta) - \frac{1}{N}\sum_{t=1}^{N} \psi'(t,\theta)\varepsilon(t,\theta), \tag{2.20}$$

where $\psi'(t,\theta)$ is the Hessian of $\varepsilon(t,\theta)$. However, determining $\psi'$ may be computationally expensive for each iteration. Rather, we assume that there exists $\theta_0$ such that the prediction errors are independent (i.e., $\varepsilon(t,\theta_0) = e_0(t)$). Near $\theta_0$, Equation 2.20 can be approximated as

$$V_N''(\theta, Z^N) \approx \frac{1}{N}\sum_{t=1}^{N} \psi(t,\theta)\psi^T(t,\theta) \triangleq H_N(\theta). \tag{2.21}$$

This ensures the Hessian estimate ($H_N$) is positive semidefinite and thus converges to a stationary solution (i.e., the global minimum).

### 2.3.3 Implementation

The entirety of the toolchain developed in this paper, which includes the full source code, how-to documentation, and implementation details has been made available on an open-source public web repository (github.com/kLabUM/DRIPS). While the authors are not at liberty to share all of the raw sensor data used in this study due to privacy considerations, an anonymized example data set (precipitation and corresponding flow) has been included in the web repository to allow others to evaluate our approach and implementation. Users should also be able to apply the model to their own datasets of rainfall and flows.

For this study, all analyses were carried out on a Windows OS laptop and the software is written in *MATLAB* (2016b edition). The implementation of the real-time system is executed on *MATLAB* as well, but is hosted on a cloud server, specifically an Amazon Web Services (AWS) Linux instance. The low computational overhead of the proposed toolchain does not require large server resources, which permits it to run on a low-cost or free cloud instance.

#### 2.3.3.1 Data Architecture and Study Area

The study was provided with access to observations from 10 flow measurement sites and 18 precipitation measurement sites, spanning three years (2013–2016) at 5 minute measurement resolution. Precipitation data were measured using tipping

bucket rain gauges and flow sensors varied across the sewer network, including magnetic, Parshall flume, and ultrasonic flow meters. The extent of study area and location of sensors is shown in Figure 2.3, with geographic and infrastructure identifiers removed in compliance with the data agreement. The data were retrieved in real-time using software written in the *Python* language and stored in the *InfluxDB* time series database system [73]. This database architecture is optimized for time series data, permitting large series to be seamlessly searched and retrieved using web services and interfaces to popular programming languages, such as *Python* and *MATLAB*. This was particularly important in our approach, which presents an end-to-end, functional, and real-time data process chain. The toolchain was deployed on an AWS instance. A visualization interface was also developed on top of the *Grafana* time series visualization package [74] and *Google Maps* [75]. The deployed system not only permits for data to be visualized, but also executes underlying flow models and re-calibrates them based on intervals deemed appropriate in our identification study.

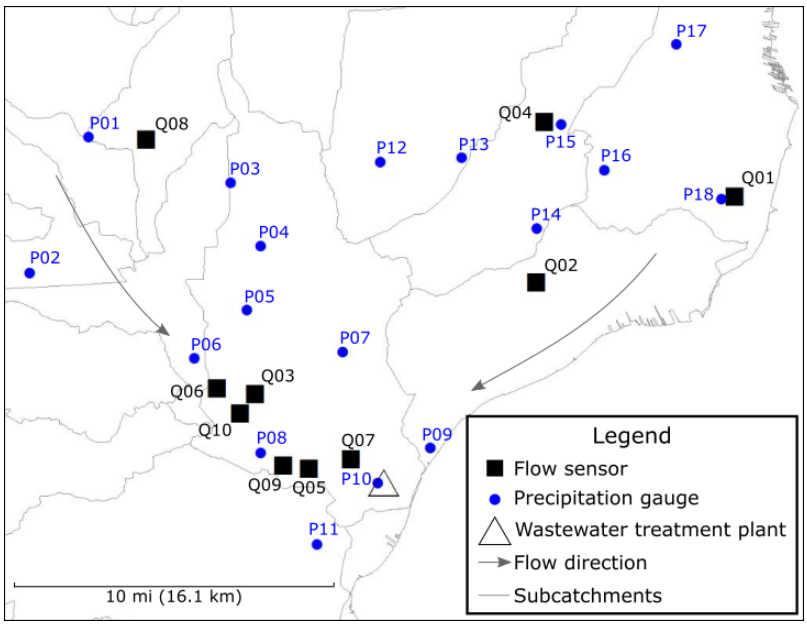


Figure 2.3: Study area extent and location of sensors used in toolchain analysis. Subcatchments were delineated based on contributing runoff areas and the pipe system.

#### 2.3.3.2 Evaluation

While automated, the processing chain (Figure 2.2) for the dry-weather and wet-weather model still depends on input data, which raises two challenges. Firstly, the computational complexity of the GP algorithm scales cubically with the number of input data [71], while the Gauss-Newton method within System Identification typically has quadratic local convergence rates [76]. As such, to improve computational efficiency it is generally in the interest to reduce the number of historical observations that are used to train the models. Secondly, and more importantly, just like all other models, the proposed toolchain is challenged by system uncertainty, which means that the age of the data used to calibrate the model may play a large role in model performance. This is particularly important when considering changing climate patterns, land use, or human inputs, which may operate on unique timescales.

To determine the impact of the size and age of calibration data, various *lookback* periods were evaluated. Wet-weather models were calibrated using one to 24 months of lookback training data. For each site, the three nearest rain gauges were used as inputs into the System Identification procedure. A cross validation was then carried out across a lookback period, whereby System Identification was used on each rain gauge and flow measurement. The model that most accurately predicted the wet-weather response of the remaining storms in the lookback period (*training data*) was then used to make a prediction on a future storm (*testing data*). The decision to train the model on the three closest gauges and then choose the best performing rain-flow pair was guided by a number of factors. Firstly, the choice was motivated by practicality, since in most cases the three closest rain gauges were either located in the same subcatchment as the flow sensor or were close enough to assume some level of rainfall uniformity. Secondly, this specific pairing of gauges with flow meters is actually what the city staff had assigned through their judgment, so it provided a good starting point to begin evaluating the proposed toolchain. It is, of course, possible to train the flow model on every rain gauge, which proved to be out of the scope for our initial evaluation and will be reserved for future studies. The model calibration/identification for each site is carried out in a rolling fashion, whereby

the approach automatically re-calibrates or re-trains the wet-weather model based on new measurements. A similar procedure was used to evaluate the dry-weather model performance. To predict dry-weather flows one month in advance, the model was trained across one to 24 month lookback periods.

To evaluate the performance of each model, the fit was quantified using the normalized root mean square error (NRMSE)

$$NRMSE = 1 - \frac{\|x_{ref}(t) - x(:t)\|_2}{\|x_{ref}(t) - avg(x_{ref}(t))\|_2}, \tag{2.22}$$

where $x_{ref}$ denotes the measured data, $x$ denotes the modeled data, and $\|\cdot\|_2$ denotes the 2-norm. Since flow magnitudes vary drastically from site to site, this formulation permits for a relative comparison across the study area. Using this metric, a perfect fit receives a value of one and increasingly poor fits approach a value of negative infinity. An NRMSE of zero would indicate that a mean model (simply taking the average of all historical training data) performs as well as the proposed model.

## 2.4 Results

### 2.4.1 Dry-Weather Flow Model

When tested against future data, the GP-based approach accurately modeled the dry-weather diurnal patterns in the conduits, as evidenced by NRMSE metrics (Table A.1), as well as a visual inspection (Figure 2.4). In particular, the modeled dynamics closely resembled those of the measured values. The approach even captured the nuanced dynamics of individual days, such as weekends (one diurnal peak) and weekdays (two peaks). The GP model also provided estimates during times of wet weather (middle section of Figure 2.4), during which measured values were not available. While the accuracy of these wet-weather diurnals can thus not be calculated, the modeled dynamics did reflect what could intuitively be expected on those days.

The impact of lookback periods (how much data was used to train the model)

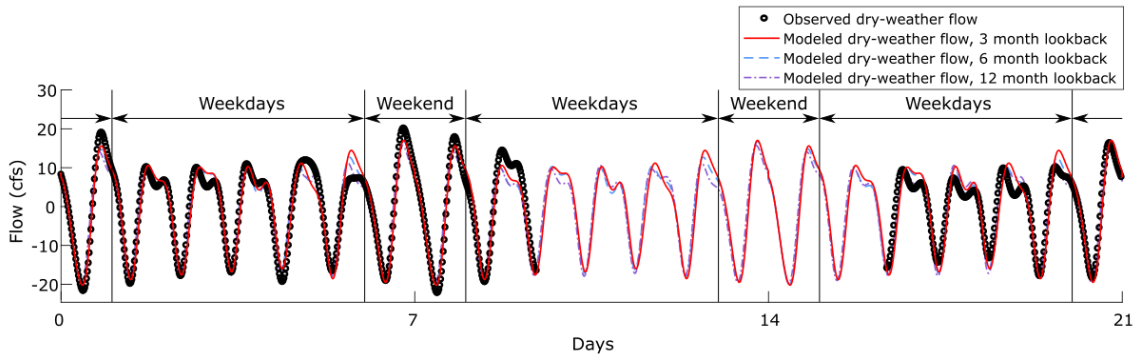


Figure 2.4: Predicted dry-weather flow using GP, compared to the observed dry-weather flow (Site Q02) (average NRMSE value of predictions is 0.7427).

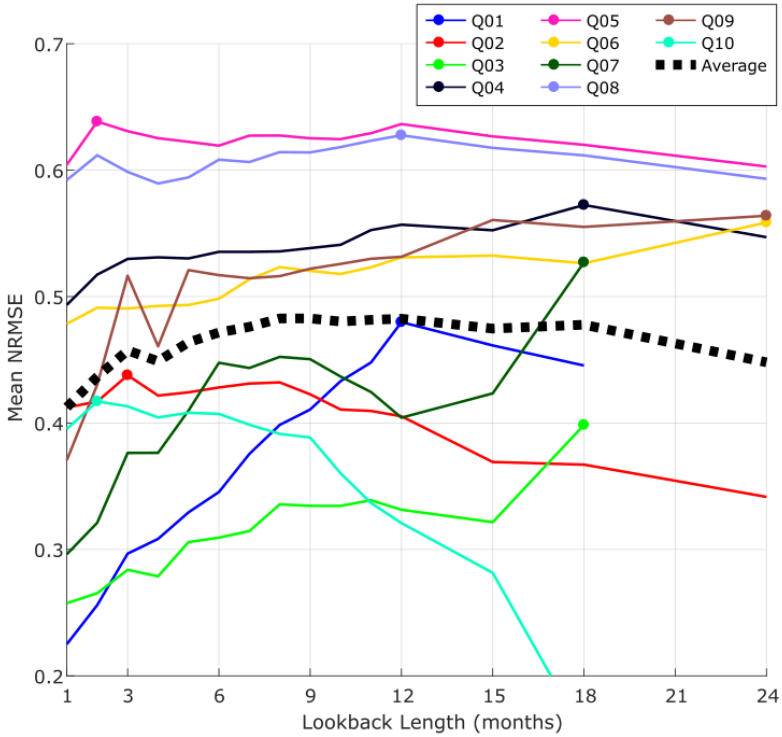


Figure 2.5: Dry-weather prediction performance of GP using different training lookback windows. Dot on each curve indicate the lookback period that resulted in the best performing model. Dashed line indicates average model performance.

was unique to each site (Figure 2.5 and Table A.1). For most sites (Q02, Q04, Q05, Q06, Q08, Q09), model performance did not drastically improve with longer lookback periods, showing only marginal improvements when more data was used to train the model. This is also apparent through visual inspection of the modeled dynamics (Figure 2.4), which showed very similar model predictions regardless of the duration of measurements used to train the model. One site (Q10) yielded notably better performance for short lookback periods, while the remaining sites (Q01, Q03, Q07) required longer lookback periods for satisfactory model performance. On average, a lookback period of 6–9 months yielded the best performing dry-weather model. Beyond this point, the use of longer periods of historical training data actually resulted in a worse model performance on average.

### 2.4.2 Wet-Weather Flow Model

For all sites, a third order wet-weather model structure exhibited the best NRMSE performance. Visual inspection revealed that the System Identification procedure accurately parameterized the wet-weather model, as seen in the predicted dynamics when given a measured rainfall input (Figure 2.6). Generally, the fit of the model improved as the lookback period increased (Figure 2.7 and Table A.2). In other words, when the model was trained using more historical storms, it generally performed better at predicting future events. At some point, however, increasing the lookback period yielded marginal or worse performance. On average, peak model performance was achieved when using 15 months of training data (Figure 2.7), after which using more data to train the model actually yielded worse NRMSE performance. For a few sites, the model performed best when using even shorter lookbacks (Q10, Figure 2.7 and Table A.2).

Rainfall dynamics played one of the largest roles in explaining differences in modeled and measured wet-weather flows. In particular, relatively worse model performance often connected to storms during which measured rainfall dynamics and measured flows did not correlate. For example, in Figure 2.8a, a storm with distinct rainfall peaks is shown. While the modeled flows also revealed these peaks,

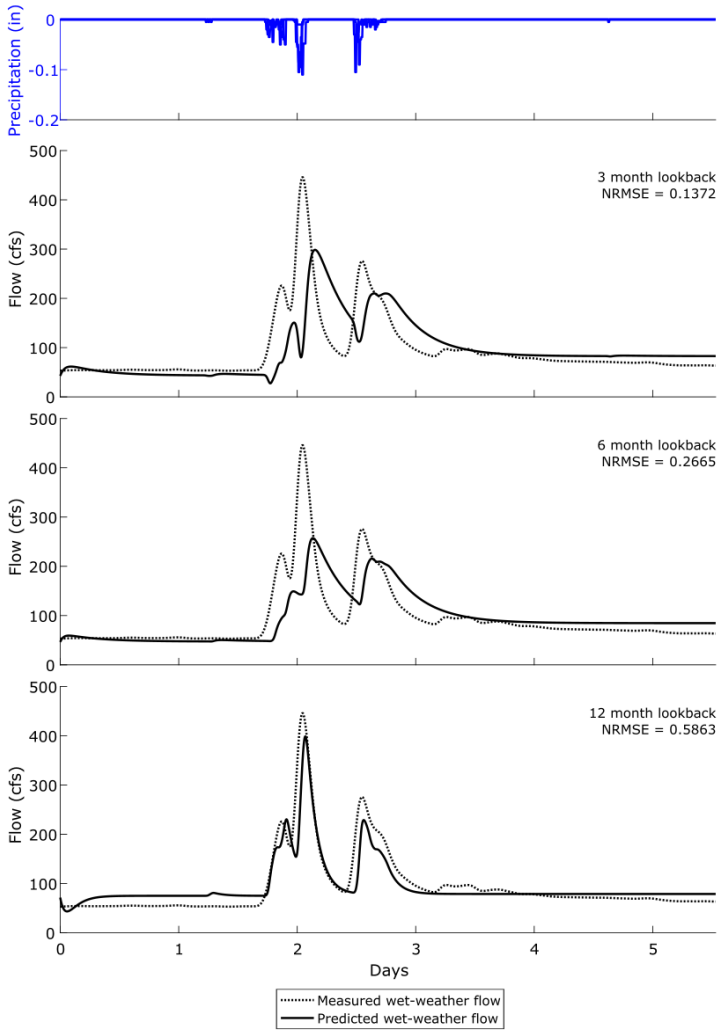


Figure 2.6: Predicted wet-weather response during a storm event using System Identification and various lookback windows for model learning, compared to the measured wet-weather flow (Site Q03). The plotted rainfall measurements are those of the gauge that was selected for the model (Section 2.3.3.2).

the actual measured flows did not exhibit one of the major flow episodes (i.e., approximately mid-way through the third day). While not shown here, the converse was also observed at times, where no rainfall was measured but a wet-weather flow was measured. This is likely due to the rain gauge being outside of the contributing

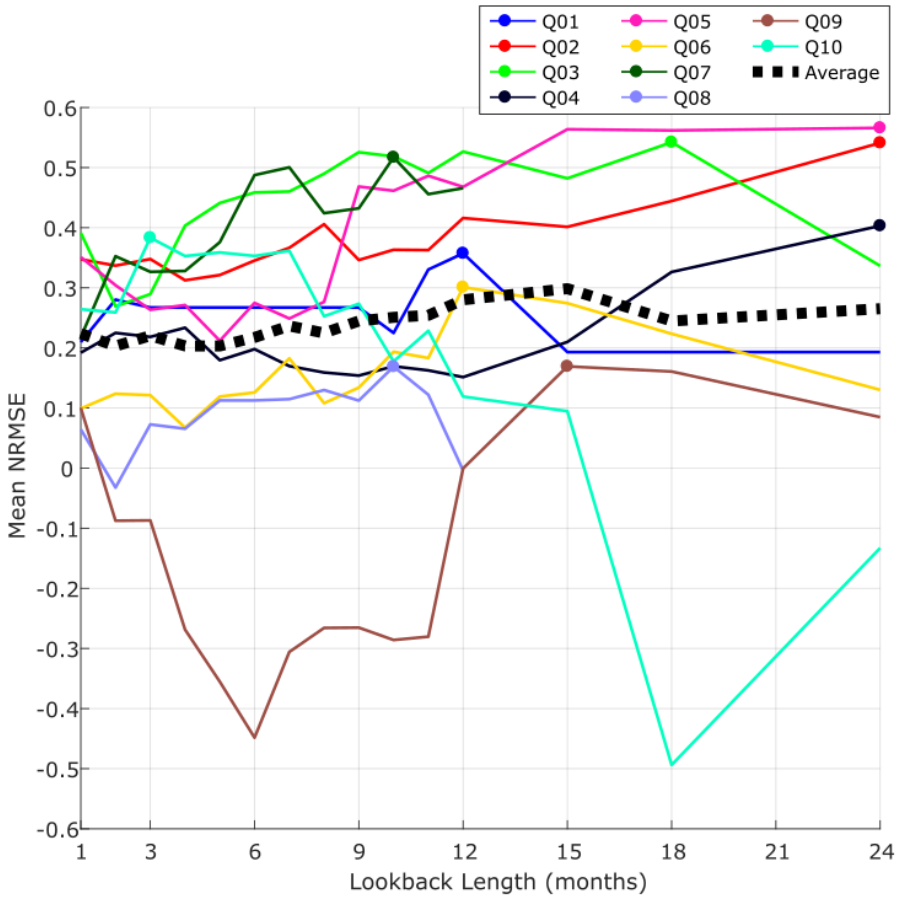


Figure 2.7: Impact of model learning lookback window on wet-weather response prediction performance for each site. Dot on each curve indicate the lookback period that resulted in the best performing model. Dashed line indicates average model performance.

watershed and underscores the significance of spatially variable storms. As expected, the model did not predict these flows during these isolated instances.

Models for five of the ten sites also showed a behavior wherein the modeled dynamics agreed with measurements for most storms, except during large rain events (example Figure 2.8b). In these cases, the measured values showed a distinct leveling-off, whereas the model predicted a sharp hydrograph peak. These dynamics could be caused by pipe capacity exceedance or, given the interconnected nature of sewer net-

works, control actions at upstream infrastructure assets, such as pumping stations, storage dams, and weirs. In this study, it was, however, determined through confirmation with the city that these instances corresponded with flows that exceeded pipe conveyance capacity.

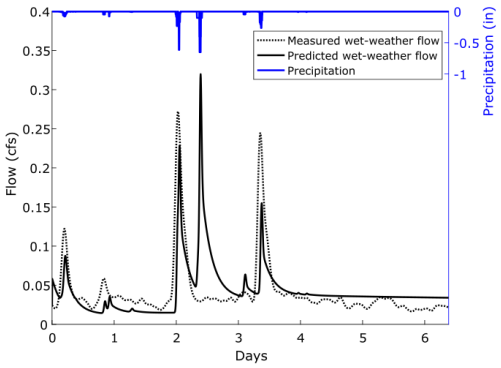


(a) Example of measured rainfall that does not result in wet-weather response (Site Q06). The precipitation data shown here is the rain pair for the given flow site.

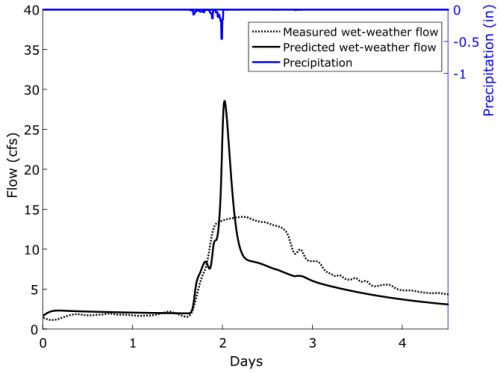


(b) Instance of pipe capacity exceedance caused by a large storm event (Site Q05). The precipitation data shown here is the rain pair for the given flow site.

Figure 2.8: Wet-weather artifacts of the System Identification procedure.

### 2.4.3 Combining Flows

Once the dry-weather and wet-weather flow models are identified using the proposed toolchain, the combined flows are modeled for a given precipitation input by summing the two components. While the performance of the final model is thus clearly underpinned by the performance of the respective sub-models, it is nonetheless worth noting that the final model exhibited good performance in predicting combined flows. For example, as shown in Figure 2.9 for site Q05, the combined model closely adhered to the measured flow both during dry weather and wet weather periods, aside from a small deviation measured on day five, where a change in flow was measured but not accompanied by a change in measured rainfall.

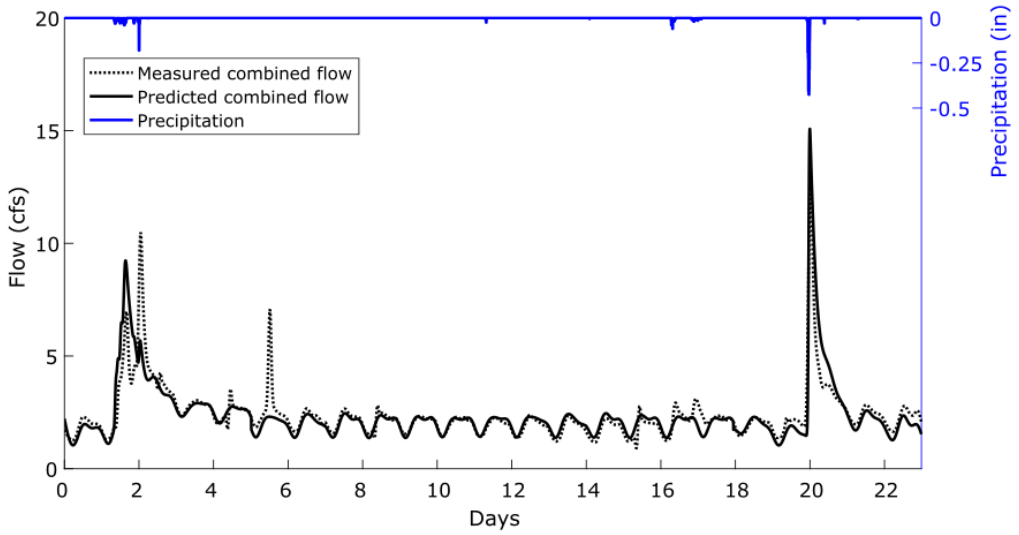


Figure 2.9: Measured and predicted combined flow (Site Q05), obtained by combining the forecasts made by the dry-weather and wet-weather models. The precipitation data shown here is the rain pair for the given flow site.

## 2.5 Discussion

### 2.5.1 Dry-Weather Identification

As indicated by the results, the GP-based model provides a powerful tool by which to predict and describe dry-weather diurnal patterns in urban sewer networks. This is especially evident when considering the complexity of dry-weather dynamics, which not only vary across time, but also between sites. The GP approach accurately reflected diurnal dynamics of each site using a sparse set of dry-weather observations. This included the nuances of dry-weather diurnal shapes, magnitudes, and weekly trends. This should make it a very powerful tool for modeling and predicting components of sewer flows that have generally been very difficult to model due to variability of the wastewater generation patterns. It also underscores the need for a flexible modeling approach that is able to learn from the site-specific data, rather than being confined to assumed shapes or dynamics. While outside of the scope of this study, future work will include explicitly quantifying groundwater infiltration

or baseflows from the dry-weather signal. This can be accomplished by subtracting the diurnal estimates of the Gaussian Process from the overall flow signal during dry-weather periods.

The major take-away from the dry-weather analysis relates to the role of the training data: generally speaking, the best model performance will be achieved when the model is trained on enough, but not too many historical observations. As expected, an insufficient amount of training data (in our case fewer than three months, on average) may lead to relatively poor model performance due to overfitting. Once enough training data are obtained, however, increasing the length of the lookback period did not result in drastically improved modeling performance. The notion of "enough" data will ultimately be guided by practical considerations and modeler judgment. Nonetheless, for the sites studied in this paper a clear guideline would focus on choosing the lookback period with the best NRMSE criterion, or the point at which NRMSE improves only marginally with longer lookback. This underscores the need to acknowledge uncertainty in the dry-weather diurnal dynamics, which may be driven by changing wastewater generation patterns, seasonal impacts, or new connections or repair to the system, indicating that older dry-weather flow signals no longer represent the current dry-weather diurnal patterns. While the best performing dry-weather models required about 3–6 months of training data, there was significant variability around this average, suggesting that changes in long-term diurnal patterns are unique to each site. As such, this underscores the importance of a flexible calibration/identification chain, such as the one presented in this paper, which will continually tune the dry-weather model to ensure that the most relevant measurements are used to inform forecasting.

One benefit of this dry-weather model is the ability to *hindcast*, wherein the dry-weather model is used to project historical estimates of dry-weather flows. These estimates can then be subtracted from the time-series of historical flows to reconstruct the series of wet-weather flows. Without a good dry-weather model, the reconstruction of wet-weather flows becomes very difficult, if not impossible. This is especially true for sites at which dry-weather and wet-weather flows share similar timescales and magnitudes. As was shown (Figure 2.2), the resulting wet-weather

signal becomes much more clear after this operation, especially during small storm events, which would have otherwise been obscured in the original time series. While improved historical estimates of dry-weather flows are useful in practical applications, such as billing, they are perhaps even more valuable because they can then be coupled with the System Identification procedure to reliably learn the underlying wet-weather model.

### 2.5.2 Wet-Weather Identification

The performance of the wet-weather model was highly underpinned by the availability of training data. The wet-weather lookback period is a proxy for the number of storms used for training. Given the extent of the analysis area, this number was the same for all sites. Unlike in the case of the dry-weather model, which depends on readily-available dry weather observations, the number of available storms to train the wet-weather model can often be limited, which explains why the wet-weather model requires longer periods of training data compared to the dry-weather model. In fact, the number of storms in a particular time period can vary widely based on the time of year; for instance, for a nine month period, the number of storms included varied from 5 to 17 storm events. There appears to be a minimum data requirement for the procedure to yield satisfactory results. For most sites, the System Identification procedure required at least nine months of data to result in the best relative performance, which suggests that the value of sensor data increases with the deployment period. As such, investments into sensor networks should be cognizant of this requirement, especially if prediction of wet-weather flows is desired.

As in the case of the dry-weather flows, the biggest take-away relates to the discovery that including more data beyond a certain lookback point can actually degrade the performance of the model. While this optimal period varied for each site, this feature was evident across almost all sites. In our study, no physiograhic features of the urban environment or storm characteristics revealed why some sites require more or less training data than others. These features included position of sensors in the watershed (i.e., upstream, downstream), size of the noncontributing

sewersheds, as well as the precipitation intensity and peak rainfall of storm events. This again suggests that system uncertainty plays a large role in model performance, even when forecasting wet-weather flows. As such, the ability to predict future flows depends on re-calibration of the model. The toolchain presented herein offers the opportunity to autonomously adjust this optimal lookback period for each site, and thus ensure that each future forecast is based on the most relevant time record of historical measurements. The approach thus implicitly addresses the need to re-calibrate and adapt the model as the overall collection system changes due to changing land uses, climate, or infrastructure upgrades. This will be particularly important in locations where changes in climate, storms, and infrastructure need to be accounted for to ensure longevity and accuracy of a model.

Beyond sensor data availability, knowledge of the physical system will also play a large role in the long-term efficacy of the proposed toolchain. Large storms that cause pipe capacity exceedance will result in non-linear system behavior that may not be fully represented by our wet-weather model. As illustrated in Figure 2.8b, if the wet-weather model is trained on a smaller storm, the linear transfer function will result in a predicted hydrograph that may exceed the capacity of conduits or sensing limits. In such rare instances, the model will still have utility, as it will be able to predict instances of overflows. Also, as mentioned in Section 2.4.2, the impact of control actions on flow dynamics must be considered in some systems. The identification approach used here provides the flexibility to learn a dynamical model with exogenous inputs [66], which will be explored in future work.

As with all modeling approaches, sensor quality will play a large role in predictive outcomes. Sensor background noise will likely not be the major challenge, as our toolchain addresses noise via filtering and probabilistic estimation. Extensive studies on real-time data quality evaluations are available in literature [36, 77, 78]. Beyond formal methods there will still be a need to subjectively evaluate, on a case-by-case basis, whether data quality is sufficient for the model to provide adequate forecasts, especially for critical operations. Ultimately, the quality of the forecasts will be implicitly determined by the quality of the input data. Once calibrated on reliable data, if measurements deviate too much from forecasts, as measured by specific

magnitude or probabilistic bounds, alerts could be sent to operators to maintain or repair field-deployed sensors.

Additionally, if the toolchain is to be entirely automated across large systems, a degree of sensor redundancy may be required, which will allow for a more accurate assessment of any given situation (e.g., broken sensor vs. clogged pipe). Redundancy will be critical across inputs (rain gauges) as well as outputs (flows), with the latter offering more flexibility because short-term flow forecasts can still be made given rainfall alone. Practical guidelines regarding the challenge of sensor quality will be best learned over time by observing how operators trust, interpret, and use the forecasts offered by toolchains such as the one presented here.

The need to understand urban rainfall variability will play, perhaps, the largest role in improving model predictions. This is not only true for the models presented in this paper, but for any modeling toolchain. This will be particularly true for large collection systems, such as the one studied in this paper. Since there was no clear correlation between model performance and the distance of a flow measurement to its corresponding rain gauge, the role of micro-climate thus needs to be accounted for as we develop the next generation of high-resolution urban water models. Much of this is expected to improve as more rain gauges are deployed and as high-resolution radar data become available.

## 2.6 Conclusions

Our study underscores the need to understand the uncertain and dynamic nature of urban water systems. The various components that drive flows in urban sewer and storm networks change across their own unique timescale. To capture these changes more measurements are needed to characterize the spatiotemporal variability in flows. This will be enabled by the rapid rise in sensors that are now being deployed throughout cities. Sufficient historical observations must be available to train the models, while also ensuring that data that are *"too old"* are not used in the identification of the model. More importantly, the duration of the training periods was unique for each site and each sub-model. The need to train the dry-weather model on a

different amount of data than the wet-weather model suggests that a conventional, broad-sweeping calibration approach would struggle to accomplish such a task. As such, individual models of each flow component should be uniquely calibrated and re-calibrated for each site, which is well within the flexibility and computational efficiency of the proposed toolchain. The accuracy of predicted flows may thus depend on the ability to autonomously re-calibrate a model, perhaps more so than the model itself. This may permit the use of simpler models to predict flows, as opposed to more complex models that try to capture higher degrees of complexity.

The proposed toolchain has the potential to serve as an operational tool for sewer system control, overflow prediction, and treatment control. Since the model explicitly separated dry-weather and wet-weather flows, it will also be applicable in the modeling of separated stormwater or sewer systems. More importantly, the formulation of the toolchain as a dynamical system opens up the possibility of applying a suite of robust control algorithms that could be used to guide the real-time operation of the sewer system. While this is beyond the scope of this paper, it was a major motivation for the specific formulation presented herein. Future work will thus focus on extending the utility of our proposed models into a holistic and real-time control toolchain.

# CHAPTER 3

# Balancing Water Quality and Flows in Combined Sewer Systems Using Real-Time Control

Published as: S. C. Troutman, N. G. Love, B. Kerkez. Balancing water quality and flows in combined sewer systems using real-time control. *Environmental Science: Water Research and Technology*, 2020. doi:10.1039/C9EW00882A.

## 3.1 Introduction

New technologies and data algorithms show promise of enabling a new generation of smart and connected stormwater and sewer systems. These systems process distributed sensor data to predict flows, levels, and other relevant states to control valves, gates, and pumps. This enables entire collection systems to be adapted to changing storms and inputs in real-time, promising to reduce flooding and improve water quality by making more effective use and achieving high performance out of existing infrastructure. Most studies evaluating real-time control technologies have focused on water quantity objectives, in particular the reduction of overflows and flooding. Comparatively little emphasis has been placed on the role of smart stormwater systems in controlling water quality. While not regulated explicitly, controlling water quality within the collection system stands to reduce effluent loads at WRRFs by improving treatment operations, which should ultimately lead to improved water quality in receiving waters.

In the case of combined sewer systems, the same pipes are used to convey stormwater and wastewater. Water Resource Recovery Facilities (WRRFs), also known as wastewater treatment plants (WWTPs), receive these combined flows. This challenges treatment efficiency due to fluctuations in flows and pollutant loads during storm events. Given the advent of smart stormwater systems, there is an opportunity to begin viewing the collection system as a tool for assisting the treatment plant by providing desirable inflows. By dynamically controlling flows in these combined sewer systems, peak flows to the plant can be minimized, while solids loads to the plant, for example, can be controlled in response to real-time WRRF states, such as nutrient loading or treatment capacity. In this paper, we evaluate the potential benefits of such an approach by investigating how the collection system can be controlled methodically in a real-time and coordinated approach to shape inflows and loads going to a receiving WRRF.

The specific contributions of this paper are:

- The formulation of a real-time load-balancing algorithm to control distributed storage assets in the collection system, to improve wet-weather flows and water quality at a receiving point, and
- An evaluation of this algorithm under simulated conditions, with an analysis of trade-offs arising during the balancing of flows and total suspended solids (TSS) going to a WRRF.

We also provide a fully open-sourced implementation of the algorithm, with all code, model of the study, and results shared to promote transparency, reproducibility, and broader adoption.

### 3.1.1 Background

#### 3.1.1.1 Water Quality and Combined Sewer Systems

Combined sewers integrate stormwater and wastewater flows into the same pipe network, which is connected to the downstream WRRF. Thus, the WRRF often experiences abrupt wet-weather impulses on top of more regular dry-weather wastewater

inflows. WRRF treatment processes are sensitive to sudden changes in influent dynamics, as these can adversely affect treatment efficacy [9]. For instance, peak flows received at WRRFs can cause washout of settled solids and microorganisms present in preliminary, primary, and secondary treatment units [10]. Beyond wet-weather dynamics, variations in pollutant loads (mass of pollutant per time) received by the WRRF can be driven by seasonal and diurnal wastewater generation patterns, and other factors [9], further challenging efficiency of WRRF treatment processes [10, 79]. One of the most notable and variable pollutant loads includes particulates, such as total suspended solids (TSS). Highly variable TSS inflows can drastically affect treatment performance, either due to lack of treatment capacity or the time required to adjust to inflow variability [10]. It is not surprising, as such, that many research efforts have been dedicated to investigating WRRF resiliency under highly variable loads [80].

An ideal WRRF influent is one of constant flow and pollutant loads [81]. However, this is not trivial to achieve in the real world, even with the construction of a large equalization basin at the inlet of the WRRF [82], particularly with large and/or flashy storm events. These large storage structures receive inflow and pump it out at regulated rates so as to not overwhelm the WRRF [9, 79, 83]. Equalization basins often require extensive footprints (not to mention capital investments), which does not make them a viable option for many communities. In lieu of the construction of expensive storage assets at the inlet of the WRRF, we contend that there is an opportunity to look further upstream, by evaluating the feasibility of using storage capacity that already exists in the sewer network as a means of equalizing inflows to the WRRF. As already demonstrated, control of the collection system can be achieved by controlling already existing assets, such as storage basins, in-line storage dams, gates, valves, and pump stations [14, 54, 84–86].

Control of the collection system for broader water quality benefits, especially at the WRRF, poses a number of new challenges. It is critical to examine not only the potential of creating close-to-steady-state influent conditions (similar to an equalization basin) [10], but also to evaluate the impacts that these control actions have on the conveyance and performance of the combined sewer system itself. For

instance, the control of upstream combined sewer storage to achieve downstream objectives should not place the storage assets at greater risk of overflowing and local flooding. Further, the storage of combined sewer flows within sewer assets could promote the settling of solids across the collection system [10, 87], a challenge for which many upstream assets are often not prepared. In particular, upstream assets are not traditionally designed to accumulate solids, which can require significant effort to resuspend, flush, or remove, and often have no on-site mechanism for solids removal, handling, or treatment. As such, any local benefits of real-time control must consider the system in which it is being deployed and weigh against potential drawbacks, which is a core motivation of this paper.

#### 3.1.1.2 Benefits of Real-Time Control

Given the recent ubiquity of sensors and connected technologies, the real-time control of urban stormwater systems has witnessed a surge in studies and adoption [22, 36]. The idea of autonomously controlled stormwater systems is not necessarily very recent itself; indeed, real-time control for sewer systems has been investigated for some time [54, 88–91]. Many of these important studies have laid the groundwork for today's ideas — especially for the control of flooding and overflows — and it is arguably the emergence of readily-available and cost-effective technologies that is fueling efforts to deploy and study smart stormwater systems. Presently, a number of operational systems and test beds exist, including model predictive control (MPC) implementations in Spain [92–94] and Denmark [95], as well as notable market-based approaches in the USA [96]. The control of separated stormwater systems has also been evaluated, including the deployment of new open-source technologies that can be used to retrofit existing stormwater sites with internet-connected valves [23, 97]. These and other studies highlight the potential of real-time control to reduce flooding and overflows. However, much more research is needed to close knowledge gaps underpinning scalable and reliable control algorithms.

Despite progress on real-time flow-based monitoring and control, only a few studies have investigated the benefits of real-time control on water quality. Studies of

individual stormwater basins have shown that TSS can be captured in retention basins by strategically controlling retention time using a valve [98–100]. Similar results have been obtained for dissolved pollutants [101] and bacteria [102]. While highly promising, existing studies have focused on site-scale benefits and were not carried out in the scope of system-scale analysis, which leaves much to be discovered with real-time water quality control of entire systems. As a first step toward a bigger goal, we address this knowledge gap in this paper by formulating a control methodology that coordinates an entire network of storage assets to achieve desired downstream TSS objectives.

#### 3.1.1.3 Existing Control Methodologies

A number of system-level control methodologies have risen to prominence for the real-time control of stormwater systems. One of the most studied involves MPC, a mathematical approach grounded in dynamical systems theory [37–40, 85, 103, 104]. MPC approximates the flows in a collection system using linearized dynamical equations, which often take the form of mass-balance reservoirs. It has shown great potential to reduce overflows and flooding in combined sewer systems [37–40]. However, given that the approach assumes linear dynamics both for flows and water quality — which is a considerable simplification of nonlinear water quality dynamics — this approach has been applied to the control of water quality in a limited capacity [37]. Further, there has still been little focus on the influence of weighting between water quantity and quality objectives.

An alternative to MPC is provided in the form of market-based control methods [96]. These approaches treat storage assets in a system (e.g., basins, pipes) as buyers and sellers of a commodity (e.g., pipe or storage capacity). In these formulations, agents trade the commodity as part of a market, where the most stressed assets are allowed to release water via "purchases" of capacity. An appealing aspect of this approach is its lack of reliance on explicit system dynamics for the determination of control actions. Rather it only requires measurements of system states (e.g., water level, flow, pollutant concentration). While this does not allow it to be analytically

studied like MPC, it does allow for easier implementation and decentralized application. A market-based approach can be viewed as an extension of the "Equal Filling Degree" approach [41, 105–108], which seeks to balance the filling degree, defined as the actual stored volume relative to the maximum storage volume in a storage structure, among all storage assets in a collection system. This is done at each time step by triggering control actions that increase (or decrease) the stored volume in a particular asset if it is below (or above) the average filling degree among all assets. Borsányi et al. [41] extended and compared Equal Filling to include a downstream structure with a capacity related to the WRRF. The control of all other structures was inversely related to the filling degree of this downstream asset. For example, if the filling degree of this downstream asset increases, the upstream assets decrease their releases to the downstream. Other approaches, such as dynamical systems, neural network-based, and reinforcement learning-based controls have also been proposed as intermediate complexity alternatives to MPC and market approaches, showing good potential to remedy flooding and overflows [109–111].

Given the general emphasis of these methods on controlling flows and flooding, it is unclear — regardless of actual control methodology — what water quality benefits can be achieved with them when applied with real-time control at the scale of the collection system. Integrating water quality optimization into existing real-time flow control approaches requires significant computational overhead, especially when considering the need to formulate, linearize, and analyze dynamics with approaches such as MPC. We contend that before exploring more complex control implementations, a more general analysis of the trade-offs and benefits of controlling system-level water quality is warranted. To that end, we introduce a control technique — coined Load Balancing — of relatively low complexity but of high flexibility to simulate a broad range of conditions focused on controlling drainage systems for water quality. We formulate the technique in a model-free context that allows us to specify flow and water quality objectives by tuning a small number of intuitive parameters. By evaluating the range of trade-offs that exist when both water flows and water quality are controlled, this study provides an assessment of real-time control benefits that can be expanded in the future using more complex control formulations.

## 3.2 Methods

We present a load balancing control methodology built around a set of core parameters, the analysis of which will provide insight into upstream and downstream trade-offs when controlling a system in real-time. The control algorithm is evaluated on an established case study [112], based on a real world-inspired combined sewer system.

### 3.2.1 Load Balancing Control Algorithm

Consider a collection system with $n$ total network storage assets (e.g., tanks, in-line storage facilities) distributed into a set of controllable assets, $I_C$, and a set of uncontrollable assets $I_U$. At time step $t$, each asset $i$ is described by a vector of states of interest

$$S_i(t) = \begin{bmatrix} S_i^1(t) \\ \vdots \\ S_i^d(t) \end{bmatrix}, \tag{3.1}$$

where the $d$ elements of the vector include relevant states that describe the asset (e.g. water level, outflows, TSS concentration). Each asset also has a corresponding setpoint vector $S_i^*(t)$, which describes the desired states of the asset (e.g. overflow conditions, maximum desired flows, desired loads). The state vector for each asset is user-specified and includes those states that are most relevant to any given application. In simple applications, one may only seek to control water levels (e.g. flooding), but in more complex scenarios one can expand the state vectors to include water quality or other factors.

Some assets may be considered more critical in the system than others. For example, operators may want to release water sooner or avoid overflows at one location more than others due to specific preferences or regulations. To capture this user

preference, we introduce the system importance factor $\alpha_i$ for each asset and state

$$\alpha_i = \begin{bmatrix} \alpha_i^1 \\ \vdots \\ \alpha_i^d \end{bmatrix}. \tag{3.2}$$

This captures a relative weight of one asset's state over another in the system — with a higher number reflecting relatively larger importance in the system. For controllable assets ($i \in I_C$), the importance of each asset is also extended to include an instantaneous component. For example, a storage tank that is close to capacity or overflowing, should be considered briefly more important than those that are not full, so as to minimize overflows or flooding. To capture this notion, we introduce an instantaneous, or short-term, importance for each asset and state

$$\gamma_i(t) = \begin{bmatrix} \gamma_i^1(t) \\ \vdots \\ \gamma_i^d(t) \end{bmatrix}, \qquad \gamma_i^1(t) = \frac{e^{\rho S_i^1(t)} - 1}{e^{\rho} - 1}. \tag{3.3}$$

This exponential factor is computed element-wise for each time step and state within the state vector $S_i$ and can be tuned to reflect user preferences. Given the state of the asset, the instantaneous importance weight $\rho$ can be tuned to reflect how stressed an asset is at any given point in time. By analogy, $\rho$ could encapsulate the comfort level of an operator (e.g., release proportional to water level vs. prioritize an asset only if it is close to full). For example, if storage capacity is used as an indicator of importance, with $\rho = 1$ the instantaneous importance of the asset increases nearly linearly with water level (Figure 3.1). With $\rho = 100$ the asset would be considered important only if it is close to capacity. If asset $i$ is uncontrollable ($i \in I_U$), its importance is not discounted in this state-dependent manner because, regardless of state, uncontrollable assets will passively release flows (thus $\gamma_i = 1$). Finally, the overall importance $\beta_i(t)$ is calculated by simply multiplying the system importance

with the instantaneous importance of each asset:

$$\beta_i(t) = \alpha_i \odot \gamma_i(t), \tag{3.4}$$

where $\odot$ indicates the Hadamard, or entrywise, product between $\alpha_i$ and $\gamma_i(t)$ (that is $\beta_i^1(t) = \alpha_i^1 \gamma_i^1(t)$, etc). At any point in time, this overall importance factor is used to determine how much water is released from each controllable asset. This is accomplished by computing the importance-weighted average, which compares the state of each asset to its desired setpoint

$$\bar{C}(t) = \frac{1}{n} \sum_{i=1}^{n} \beta_i(t)^\top \left( S_i(t) - S_i^*(t) \right). \tag{3.5}$$

Note that this $\bar{C}$, the importance-weighted average, includes all $n$ assets, both controllable and uncontrollable. At each time step $t$, the set of controllable assets that will release water, $J \subseteq I_C$, is determined as those whose importance-weighted deviation is greater than the average; that is,

$$J = \left\{ j : \beta_j(t) \cdot \left( S_j(t) - S_j^*(t) \right) > \bar{C}(t) \right\}. \tag{3.6}$$

Assets below this average (e.g., storage tanks with available capacity) do not release flows. Furthermore, the amount of water released from each of these assets in set $J$ is computed as a relative allotment factor $R_j(t)$ for asset $j$. This relative allotment factor is defined as the importance-weighted deviation normalized within set $J$; that is,

$$R_j(t) = \frac{\beta_j(t)^\top \left( S_j(t) - S_j^*(t) \right) - \bar{C}(t)}{\sum_{k \in J} \left( \beta_k(t)^\top \left( S_k(t) - S_k^*(t) \right) - \bar{C}(t) \right)}, \tag{3.7}$$

where $\sum_{k \in J}$ is the summation of the importance-weighted deviation over all assets that will release water (i.e., each asset $k$ in set $J$). This allotment factor $R_j$ simply assigns the fraction of a downstream asset's capacity that will be allotted to an upstream asset $j$ and is then multiplied by available downstream capacity to determine how much to release from each upstream storage asset.

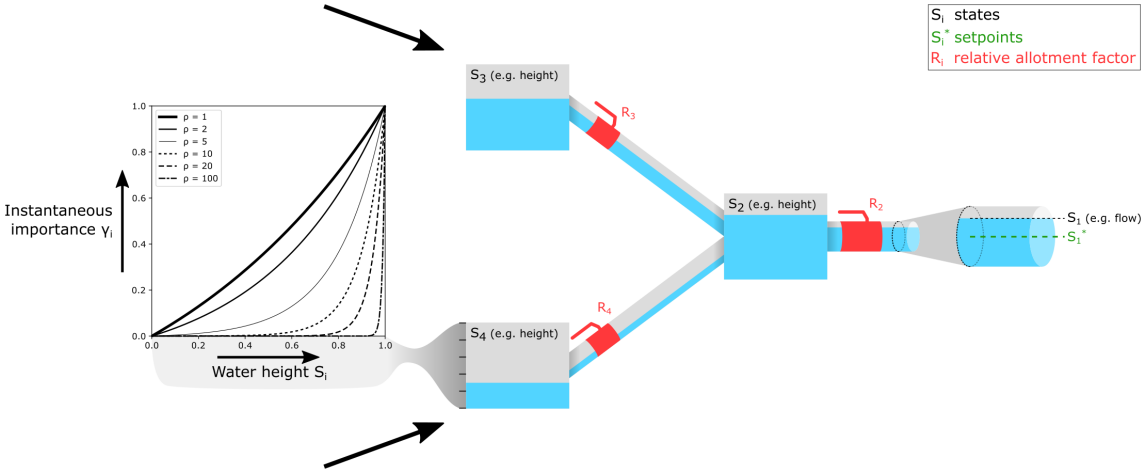


Figure 3.1: Graphical representation of control procedure. Valves are controlled to release water from controlled assets, relative to an allotment factor that is assigned to each controlled asset. The instantaneous importance weight $\rho$ can be tuned to determine when water is released from each asset.

This procedure is summarized in Algorithm 1 (Figure 3.2).

**Algorithm 1** Load balancing control

**Inputs:** $S_i$ (states), $S_i^*$ (setpoints), $\alpha_i$ (system importances), $\rho$ (instantaneous importance weight), $I_C$ (controllable assets), $I_U$ (uncontrollable assets)

**for** $t \in T$ **do**
  **for** $i \in (I_C \cup I_U)$ **do**
    **if** $i \in I_C$ **then**
      $\gamma_i(t) \leftarrow \frac{e^{\rho S_i(t)} - 1}{e^{\rho} - 1}$
    **else**
      $\gamma_i(t) \leftarrow 1$
    $\beta_i(t) \leftarrow \alpha_i \odot \gamma_i(t)$
    $\bar{C}(t) \leftarrow \frac{1}{n} \sum_{i=1}^{n} \beta_i(t)^\top \left(S_i(t) - S_i^*(t)\right)$
    **if** $i \in I_C$ **and** $\beta_i(t)^\top \left(S_i(t) - S_i^*(t)\right) > \bar{C}(t)$ **then**
      $J \leftarrow J \cup \{i\}$
  **for** $j \in J$ **do**
    $R_j(t) \leftarrow \frac{\beta_j(t)^\top \left(S_j(t) - S_j^*(t)\right) - \bar{C}(t)}{\sum_{k \in J} \left(\beta_k(t)^\top \left(S_k(t) - S_k^*(t)\right) - \bar{C}(t)\right)}$

Figure 3.2: Load balancing control algorithm.

### 3.2.2 Case Study

#### 3.2.2.1 Scenario and Implementation

All code for implementation of the above algorithm is provided open-source in a public web repository (github.com/stroutm/LBCsewer). The algorithm is applied to Scenario `epsilon` of the Open-Storm.org `pystorms` Python package (`open-storm.org/pystorms`) (Appendix D) [112]. This package uses `PySWMM` [113], a Python wrapper for the popular U.S. Environmental Protection Agency Stormwater Management Model (SWMM), to run and dynamically control a sewer model throughout a simulation. In `PySWMM`'s step-by-step execution, specified states (e.g., depths, inflows, pollutant concentrations) are collected, calculations for control actions can be performed in Python, and control asset settings (e.g., gate positions) are set before the next simulation step is run.

The case study used for this paper is Scenario `epsilon` of the `pystorms` package (Appendix D) [112]. It represents a combined sewer network with a subcatchment area of 67 $km^2$ (26 $mi^2$) and eleven in-line storage assets with controllable orifices (Figure 3.3). This scenario was selected due to network topology (i.e., storage assets in series and parallel) and multiple objectives: regulation of flow and TSS load at the network outlet (WRRF inlet) and the need to reduce flooding at each of the upstream storage assets. The collection system receives rainfall runoff, as well as steady, dry-weather inputs to reflect wastewater diurnal patterns (Figure B.1). More information regarding this network can be found in the `pystorms` package documentation (`open-storm.org/pystorms`) [112].

There is one downstream WRRF (node 1 in the network) ($I_U = \{1\}$), which receives flows from the entire upstream network. Applying the control procedure described above, for this WRRF we are interested in flow ($q$) and TSS load ($tss$) inflow states:

$$S_1(t) = \begin{bmatrix} S_1^q(t) \\ S_1^{tss}(t) \end{bmatrix}, \qquad S_1^*(t) = \begin{bmatrix} S_1^{q*}(t) \\ S_1^{tss*}(t) \end{bmatrix}, \qquad \alpha_1 = \begin{bmatrix} \alpha_1^q \\ \alpha_1^{tss} \end{bmatrix}. \tag{3.8}$$

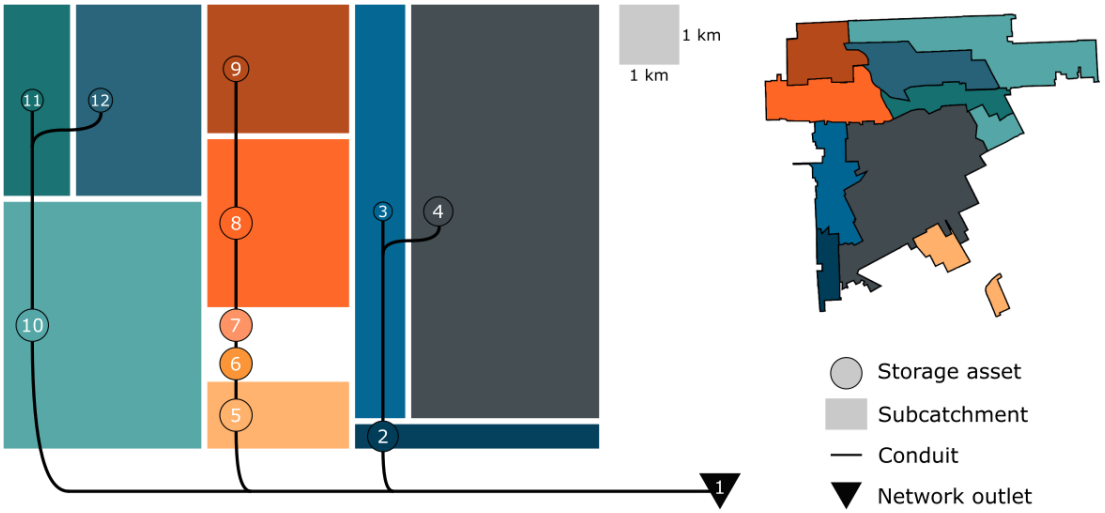


Figure 3.3: System subcatchments and network topology of the case study collection system. Numbered, circular nodes in network topology represent upstream storage assets; relative size of circles indicate the diameter of the in-line conduit. Relative areas of the rectangles represent subcatchment areas that directly contribute to the corresponding storage asset. System physical dimensions are provided in Table B.1.

The flow and TSS load states are normalized to the dry-weather flows in the system. The goal is to maintain all controlled inflows (volume per time) or loads (pollutant mass per time) (both wet and dry) at the WRRF below the average dry-weather flow. This is an aggressive strategy that may not be realizable, but it presents an upper bound on performance. Striving for dry-weather inflows during wet-weather conditions should results in benefits compared to the baseline.

The collection system also contains eleven controllable in-line storage assets ($I_C = \{2, ..., 12\}$). Each storage asset is a conveyance pipe, whose outlet is controlled through a valve or inflatable dam. When closed, the water level in the pipe rises and the available in-line storage capacity is used to keep flow from going downstream. The state for each of these assets is the water level ($h$), which is normalized to the maximum water depth in each controlled pipe. The setpoint for these assets is set to zero

$$S_i(t) = \left[S_i^h(t)\right], \qquad S_i^*(t) = \left[S_i^{h*}(t)\right] = \left[0\right] \tag{3.9}$$

to reflect the desire to empty the pipes and not keep water in the system, if possible. The case study considers each of these in-line storage assets as equally important within the system (the system importance for each asset $i \in I_C$ is $\alpha_i = \Big[1\Big]$).

The load balancing control algorithm provides the proportion of downstream capacity to be allocated to each controllable upstream storage asset $j$ via the relative allotment factor $R_j$. To translate this factor into control decisions (e.g., gate positions), the flow to be released from each upstream asset is determined as a balance between the downstream objective setpoints, $S_1^{q*}$ and $S_1^{tss*}$, weighted by the system importance values, $\alpha_1^q$ and $\alpha_1^{tss}$. In this study, since $\alpha_1^q$ and $\alpha_1^{tss}$ are the weights assigned to the downstream states, larger values of $\alpha_1^q$ and $\alpha_1^{tss}$ indicate higher importance for these downstream objectives relative to upstream. Note that for implementation with water quality-based control, measurements representative of average TSS concentrations in each upstream storage asset would be required to ensure that recommended TSS loads are released. The gate position is then calculated from the desired flow at each upstream asset via orifice and weir equations [114]. More details for this implementation can be found in the public web repository (github.com/stroutm/LBCsewer).

#### 3.2.2.2 System Water Quality Model

In the SWMM model, TSS is modeled using built-in pollutant model structures [115]. The build-up of TSS on subcatchments follows a power structure:

$$B = \min\left(C1, C2 \cdot t^{C3}\right), \tag{3.10}$$

where $B$ is the pollutant build-up (mass per unit area), $C1$ is the maximum possible build-up (mass per unit area) (16 kg/ha, 14.275 lbm/ac), $C2$ is the build-up rate (mass per unit area per day) (7 kg/ha/day, 6.245 lbm/ac/day), $t$ is the antecedent dry period length ($t^{-C3}$), and $C3$ is the exponent. The subcatchment wash-off function is exponential:

$$W = E1 \cdot q^{E2} \cdot B, \tag{3.11}$$

where $W$ is the pollutant wash-off (mass per area per hour), $E1$ is the wash-off coefficient (0.5 1/mm, 12.7 1/in), $E2$ is the wash-off exponent (1.5), $q$ is the runoff rate (in/h), and $B$ is the pollutant remaining build-up (mass per area). TSS model structure was taken from [115, 116] and parameter values from [116]. TSS removal at each upstream asset considered both settling, as a function of depth in the storage pipe, and resuspension, as a function of flow through the storage pipe:

$$R = 1 - \exp\left(-\frac{v_s \cdot \Delta t}{DEPTH}\right) - \exp\left(-\frac{a \cdot b}{FLOW}\right), \tag{3.12}$$

where $R$ denotes the percent removal of TSS concentration, $v_s$ is the settling velocity (determined by aggregating the solids classes in Gaborit et al. [116] to yield 0.00419 ft/s), $\Delta t$ is the time step, $DEPTH$ is the water depth in the storage pipe, $a$ is a ratio between velocity and TSS resuspension to result in 100% resuspension for the maximum velocity through the storage pipe, $b$ is a linear approximation of the ratio between flow and velocity computed for each upstream in-line storage asset, and $FLOW$ is the flow through the storage pipe. The assumption of a single settling velocity for all particles is a simplification made here to narrow the focus of this study. Note that this is a simplification of the representation of the underlying physical system; it merely serves as a simulation choice. The control approach described above requires only measured states from the system, not an entire model. Thus, whether implemented on a more complex simulation model or on a real-world system with sensors, this control algorithm would remain the same in structure and implementation.

#### 3.2.2.3 Performance Evaluation

The performance of the control algorithm was evaluated across an entire year, using the precipitation time series in Appendix B (Figure B.2). The dynamic behavior was evaluated by plotting the time series of controlled and uncontrolled scenarios. The aggregate performance was also summarized across the whole year, using a set of performance metrics while varying the control parameters ($\rho$, $\alpha_1^q$, and $\alpha_1^{tss}$). To

reflect real world implementation, control decisions were constrained to a 15 minute window.

Specifically, six performance metrics are evaluated: WRRF flow and TSS load variance during dry-weather periods, comparison of controlled and uncontrolled WRRF flow and TSS load peaks, TSS mass remaining in the sewer network, and flooding volume. Dry-weather periods are defined by the precipitation data as being a full 24 hours after the last occurrence of rain to simplify evaluation. During these periods, flow variance is computed by

$$\frac{1}{T}\sum_{t=1}^{T}\left(S_1^q(t) - \bar{S_1^q}\right)^2, \tag{3.13}$$

where $S_1^q(t)$ is the WRRF flow at time step $t$, $\bar{S_1^q}$ is the average WRRF flow over the dry-weather periods, and $T$ is the total length of the dry-weather periods [117]. The WRRF TSS load variance is computed similarly. Note that these are computed with respect to absolute, not normalized, flow and TSS load values and so scale will be indicative of respective units. This dry-weather variance provides a measure of deviation from the mean dry-weather flow or TSS load, indicating how "flat" inflow dynamics are, that is a variance of zero indicates perfect steady-state inflow conditions during dry-weather periods, which is beneficial for steady-state operation at the WRRF. To focus on wet-weather peaks, peak height is defined to be the amount of flow or TSS load *above* the maximum dry-weather flow or TSS load, respectively. While this would ideally be evaluated on a storm-specific basis, to automate this calculation the peak reduction is averaged across each week of the simulation period. Peak reduction is then computed as a normalized factor

$$1 - \text{peak}_{\text{controlled}}/\text{peak}_{\text{uncontrolled}}. \tag{3.14}$$

The TSS mass remaining in the sewer network is computed as the difference between the cumulative TSS load received by the WRRF, normalized against the uncontrolled

cumulative TSS load:

$$\text{TSS remaining } = \frac{\sum_{t=1}^{T} \text{TSS load}_{\text{uncontrolled}}(t) - \sum_{t=1}^{T} \text{TSS load}_{\text{controlled}}(t)}{\sum_{t=1}^{T} \text{TSS load}_{\text{uncontrolled}}(t)}. \quad (3.15)$$

The volume of flooding is calculated in the flow routing statistics by the simulation of the SWMM input file via `PySWMM`. This flooding volume is then expressed as a fraction of total volume that passes through the network.

## 3.3 Results and Discussion

This section is split into two parts. First, a number of specific control scenarios are carried out to evaluate the dynamic performance of the algorithm under a set of objectives and constant control parameters. The Scenario Analysis section is split into three scenarios, which compare parameterization of the algorithm to (1) attenuate flows, (2) attenuate TSS loads, and (3) jointly balance flows and TSS loads at the WRRF. Second, a parameterization analysis is carried out to determine how specific weight combinations of the control parameters affect the performance of the controlled system.

### 3.3.1 Scenario Analysis

#### 3.3.1.1 Scenario 1: Flow Attenuation

The control algorithm is first implemented with the sole objective of attenuating downstream flows, wherein the upstream storage assets are guided to hold water to reduce the peaks of dry- and wet-weather events. The normalized downstream flow setpoint $S_1^{q*}$ is 2.5, which was found to correspond with the maximum dry-weather flow. As such, the control algorithm tries to keep flow as close as possible to a steady-state without exceeding the maximum dry-weather flow. In this scenario $\alpha_1^q = 10.0$, meaning that the priority of the downstream flow objective is weighted as being 10 times more important than the desire to keep each upstream storage asset empty. For this scenario, $\alpha_1^{tss} = 0.0$ since there is no explicit consideration of water quality

load dynamics.

Since the assets are controlled, water levels in the upstream storage assets are higher than the uncontrolled case, both during dry- and wet-weather events (Figure 3.4a). This scenario is able to considerably attenuate wet-weather flow peaks and equalize dry-weather oscillations when compared to the uncontrolled case (Figure 3.4d). Furthermore, since flows are reduced, the TSS load exiting the combined sewer system is attenuated as well (Figure 3.4g). During the first two months of the simulation period, the wet-weather flow peaks at the outlet of the combined sewer system are reduced by an average of 94.17%, while wet-weather TSS load peaks are reduced by an average of 104.47% (controlled/uncontrolled peaks of 0.0583 and -0.0447, respectively; Table 3.1a). The dry-weather flow and TSS load oscillations are reduced as well; this can be quantified by flow and TSS load variance during dry-weather days, which is reduced by 78.7% and 78.8%, respectively, from the uncontrolled case (Table 3.1a).

Table 3.1: Summary of results in Figure 3.4 for the first two months of the simulation period; a summary of results for the one-year period is included in Figure 3.5. Ratio of peak flows and TSS loads are given as controlled peaks divided by uncontrolled peaks. Negative values for ratio of peak flows indicate that, on average, wet-weather peaks were reduced to below the maximum dry-weather levels. Variances are during dry-weather periods and the scales of values are indicative of their respective units.

| | **Uncontrolled** | **Attenuation Control Scenario** | | |
|---|---|---|---|---|
| | | **(a)** **Flow** $\alpha_1^q = 10.0$ | **(b)** **TSS** $\alpha_1^{tss} = 10.0$ | **(c)** **Flow & TSS** $\alpha_1^q = 5.0$ $\alpha_1^{tss} = 5.0$ |
| Ratio of Peak Flows | — | 0.0583 | 0.2176 | 0.1320 |
| Ratio of Peak TSS Loads | — | -0.0447 | -0.0361 | -0.0413 |
| Flow Variance | 364.7 | 77.7 | 48.0 | 44.2 |
| TSS Load Variance | $9.37 \times 10^{-2}$ | $1.99 \times 10^{-2}$ | $6.37 \times 10^{-3}$ | $1.20 \times 10^{-2}$ |

As expected, the control of storage assets reduces peak inflows at the WRRF (Figure 3.4d). The control not only attenuates peak storm flows, but also reduces

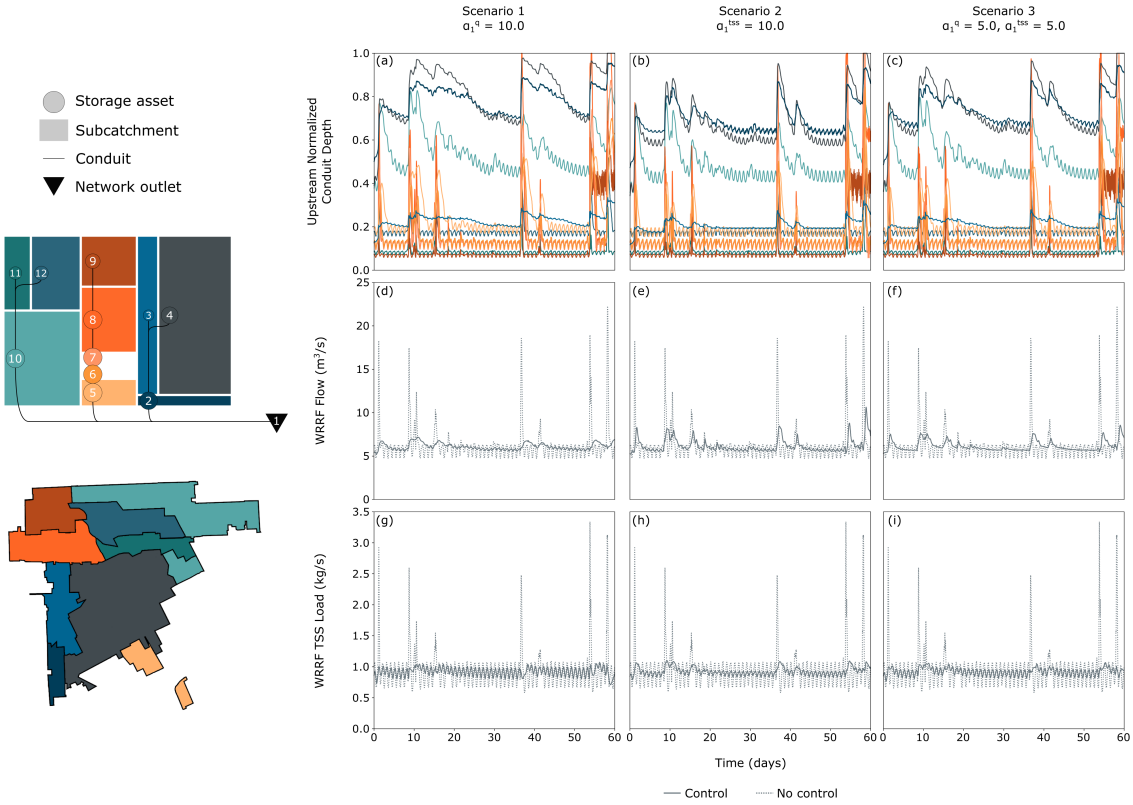


Figure 3.4: Comparison of three control scenarios during the first two months of the simulation period. Scenario 1 places an emphasis on flow control, Scenario 2 emphasizes TSS regulation, and Scenario 3 balances both flow and water quality. The top row shows the upstream normalized depth behind the controlled storage assets in the network. The flow and TSS load at the network outlet are shown in the second and third rows. Dashed and solid lines in Subfigures 3.4d–3.4i denote uncontrolled and controlled cases, respectively. Subfigures 3.4a–3.4c only show results from the controlled case for clarity.

the variability of the diurnal flows (Table 3.1a). This is due to the utilization of upstream assets, which now strategically hold back water. Overall, the storage assets with relatively higher water levels during storms are generally those with higher contributing and upstream subcatchment areas (in particular, subcatchments 2, 4, 10). Since these assets are more stressed during storms, the control algorithm holds water in the remaining assets to balance storage capacity across the system. While

this scenario does not explicitly control for TSS going to the WRRF, TSS loads are impacted positively because some TSS is held back in the upstream assets. As such, it can be expected that TSS peaks could be reduced even further by weighting TSS load, which is done in the next scenario.

#### 3.3.1.2 Scenario 2: TSS Load Attenuation

Compared to the prior scenario, the second scenario parameterizes the control algorithm to focus solely on attenuating TSS load dynamics ($\alpha_1^{tss} = 10.0$), without placing any weight on the flow dynamics ($\alpha_1^q = 0.0$). The normalized downstream TSS load setpoint $S_1^{tss*}$ is 2.5, to correspond with the maximum dry-weather TSS load. As would be expected, this formulation achieves similar TSS load attenuation relative to the formulation that focuses on flow only. Compared to the uncontrolled case, TSS load peaks that result from wet-weather events are reduced by an average of 103.61% over the first two months of the study period (controlled/uncontrolled peaks of -0.0361; Figure 3.4h and Table 3.1b.) Since water is held to regulate solids, flows are naturally attenuated as well, with average reductions of 78.24% (controlled/uncontrolled peaks of 0.2176; Figure 3.4e and Table 3.1b). This is a lesser degree of flow attenuation compared to Scenario 1 since, during wet-weather, TSS concentration is generally diluted by stormwater.

This scenario exhibits improved equalization of the dry-weather TSS load oscillations. During the first two months of the simulation period, there is a 93.2% reduction in TSS load variance, as well as an 86.8% reduction in flow variance, during dry-weather days (Figures 3.4e and 3.4h, and Table 3.1b). Thus, there is improved TSS performance compared to the first scenario.

While both scenarios perform better than the uncontrolled case, there is naturally a trade-off when comparing one to the other. Placing more emphasis on regulating TSS load peaks adversely impacts flow peaks, and vice versa. The equalization of TSS load is most notable during dry-weather, during which the control assets are used to buffer daily TSS load oscillations into the WRRF.

#### 3.3.1.3 Scenario 3: Balancing Flow and TSS Load

A natural extension of the prior two scenarios is to combine the flow and TSS attenuation objectives. This is accomplished by giving the two system importances equal values ($\alpha_1^q = \alpha_1^{tss} = 5.0$). In this formulation, wet-weather flow and TSS load peaks are attenuated with an average peak reduction of 86.80% and 104.13%, respectively, during the first two months of the simulation period (controlled/uncontrolled peaks of 0.1320 and -0.0413, respectively; Figures 3.4f and 3.4i and Table 3.1c). Further, similar to the above two scenarios, dry-weather diurnal wastewater oscillations are reduced; there is a reduction of 87.9% and 87.2% in flow and TSS load variance during dry-weather days, respectively (Table 3.1c). Overall, the equal weighing of flow and TSS objectives provides a middle ground relative to the first two scenarios, and perhaps a realistic strategy for real-world implementation. These weights do not have to be equal values of $\alpha_1^q$ and $\alpha_1^{tss}$, however; this is explored in the next section.

### 3.3.2 Parameterization Analysis

#### 3.3.2.1 Balancing Flow against TSS Loads

To assess trade-off sensitivity of weighing flow and TSS load objectives, reduction in wet-weather peaks and dry-weather variance are averaged over a one-year simulation time period across various combinations of $\alpha_1^q$ and $\alpha_1^{tss}$ values (Figures 3.5a and 3.5e). These plots can be interpreted through the ratio of $\alpha_1^q$ and $\alpha_1^{tss}$, which conveys how the relative magnitude of each parameter impacts system-wide performance. Furthermore, the absolute value of each parameter conveys how upstream assets are weighted against those downstream: as $\alpha_1^q$ and $\alpha_1^{tss}$ increase in magnitude, the downstream WRRF objectives are weighed more than those of upstream assets (Figure 3.5a). In general, the trend for wet-weather peak reduction and dry-weather variance reduction for both flow and TSS load at the sewer network outlet is similar: larger system importance values result in better downstream performance by way of greater peak reduction and damped dry-weather oscillations. This is due to increased priority on maintaining the downstream flow and/or TSS load below the

given thresholds as compared to the upstream objective of emptying storage assets. This implies that, when only considering downstream objectives, control with larger system importance values $\alpha_1^q$ and $\alpha_1^{tss}$ will result in smoother, more constant sewer network outflow and TSS load during both dry- and wet-weather periods compared to an uncontrolled case.

The flow system importance value $\alpha_1^q$ has more influence on both flow and TSS load peak reduction than the TSS load system importance value $\alpha_1^{tss}$ (Figures 3.5a and 3.5d). Further, the TSS load system importance $\alpha_1^{tss}$ has more impact than the flow system importance $\alpha_1^q$ on dampening the dry-weather TSS load oscillations (Figure 3.5e).

While the coordinated control of upstream sewer storage assets can be used to achieve flow and water quality objectives at the network outlet, this control must be sensitive to its impacts on other sewer dynamics that are important for the conveyance of water and pollutants through the network. First, the reduction of wet-weather flow and TSS load peaks at the combined sewer outlet can result in over-utilization of in-line storage assets, meaning that storage assets in the sewer will become fuller as capacity is allocated to the downstream outlet, and ultimately increase risk of network flooding. This is particularly pronounced during wet-weather events, as large volumes of water rapidly enter the sewer system as the contributing subcatchments drain. Thus, maintaining strict feedback control over storage assets can result in unanticipated flooding if upstream assets are used too liberally to hold water. Examples of this can be seen in Figures 3.4a–3.4c during wet-weather events. Figure 3.5c demonstrates how system importance values, $\alpha_1^q$ and $\alpha_1^{tss}$, impact this over-utilization and the volume of network flooding by the control algorithm. Both simulation and intuition confirm that lower system importance values for downstream objectives result in a reduction in flooding volume; this is particularly true for the flow system importance $\alpha_1^q$. As discussed above, due to the settling and resuspension of TSS within the storage assets and the dilution of TSS during wet-weather events, less upstream storage capacity is required to attenuate TSS load peaks when compared to flow peaks during wet-weather events. As a result, even the moderately high values of $\alpha_1^{tss}$ considered here result in minimal flooding volume when compared

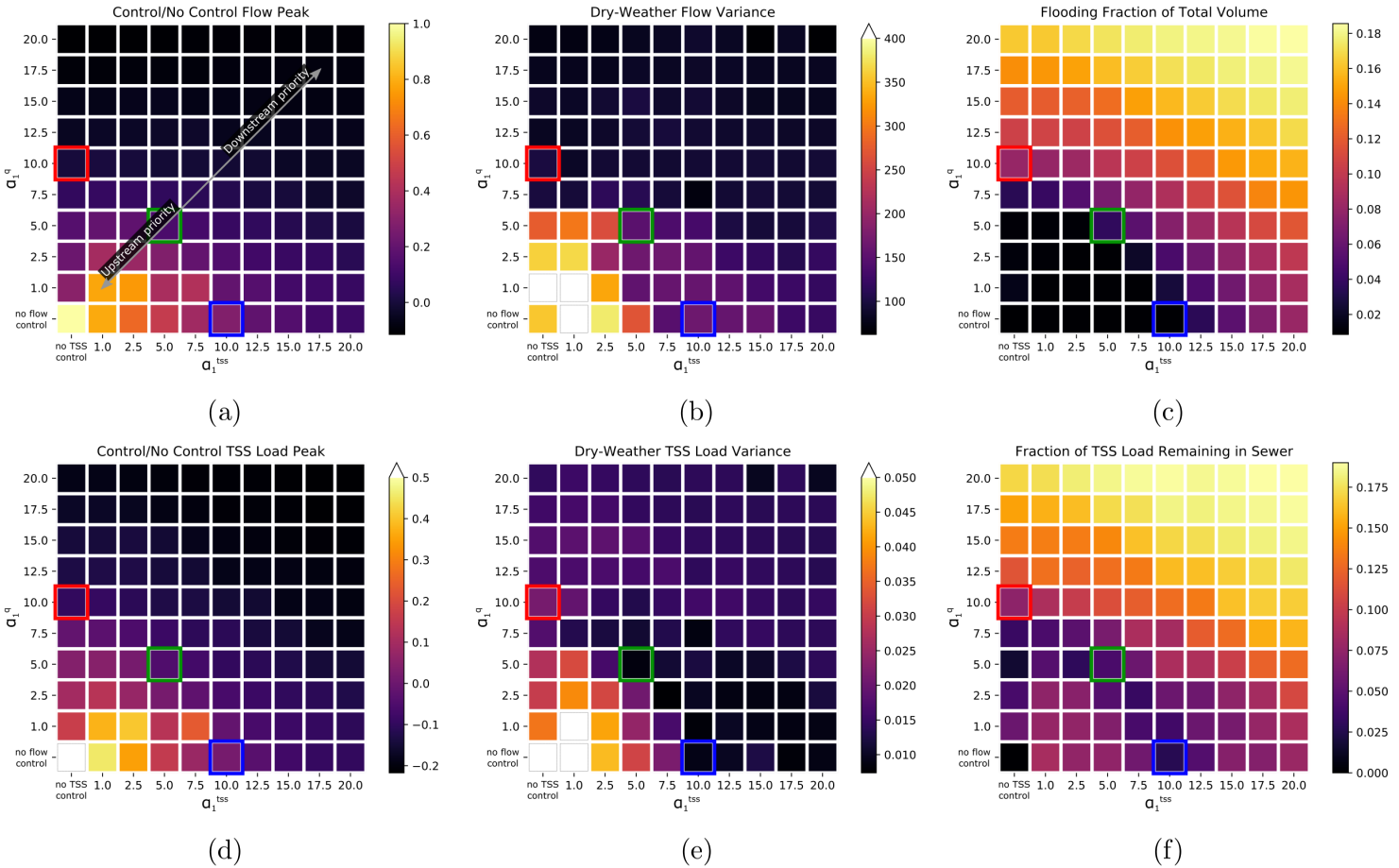


Figure 3.5: Impact of system importance values on performance metrics. Red, blue, and green boxes indicate selected parameter scenarios highlighted in Figure 3.4 for Scenarios 1, 2, 3, respectively. In all figures, a darker color indicates better performance in that particular metric. In Subfigures 3.5a and 3.5d, negative values for ratio of peak flows indicate that, on average, wet-weather peaks were reduced to below the maximum dry-weather levels.

to $\alpha_1^q$ values of a similar magnitude.

A second effect of control on the system is the accumulation of solids in the sewer system. Combined sewer flows have a relatively high concentration of solids resulting from the wastewater flows; typical untreated municipal wastewater has a TSS concentration range of 100–400 $mg/L$ [9]. As a result, the settling of solids occurs due to increased and long-duration storage of combined sewer flows behind sewer assets. In order to minimize the magnitude of flow and/or TSS load peaks, stored flows must be slowly released, resulting in low velocities from the storage assets and minimal resuspension of settled solids in the sewer network. This allows for settled solids to accumulate in the sewer network. However, most sewers are not designed to manage these solids in the conveyance network and must employ significant maintenance efforts to manually remove these solids or flush them downstream [10]. Hence, control algorithms that operate or inform combined sewer control actions should be designed with solids accumulation as a key consideration. The impact of system importance parameters, $\alpha_1^q$ and $\alpha_1^{tss}$, on solids accumulation is shown in Figure 3.5f.

When TSS load is more strongly weighted than flow (i.e., below the 1:1 line), the sewer network retains less solids mass within the storage assets; this is because flows are released based on the stored TSS concentrations in order to maintain a TSS load threshold downstream. At storage assets experiencing greater settling, the suspended solids concentration will be lower, thus requiring larger volumes to be released, resulting in resuspension. On the other hand, high flow system importance values ($\alpha_1^q \geq 12.5$) consistently resulted in greater than 10% solids retention within the upstream assets, regardless of the TSS load weight. This is likely due to the requirement for flows to be gradually released from the upstream storage assets to achieve flow attenuation and equalization at the downstream network outlet. However, in achieving this, flows are released slowly, resulting in little solids resuspension and thus solids accumulation in the upstream storage assets.

#### 3.3.2.2 Willingness to Hold Water

The formulation of the control algorithm presented here also includes the instantaneous importance weight $\rho$, which determines the willingness of an asset to hold water as levels approach storage capacity. For flow and TSS peak reduction, and dry-weather flow and TSS load variance, a lower $\rho$ value is associated with better performance (Figure 3.6, where $\alpha_1^q = \alpha_1^{tss} = 5.0$). However, for most of these first four metrics, the range of performance does not vary greatly with the values of $\rho$ considered here, compared with the range of performance values in Figure 3.5. The exception to this is dry-weather flow variance. In this case, lower $\rho$ values perform considerably better than higher $\rho$ values (Figures 3.6 and B.3). This is because storage assets fill up with diurnal inflows, and suddenly release flows when at capacity. Lower $\rho$ values buffer this variability by more steadily releasing water and reducing impulses to the WRRF.

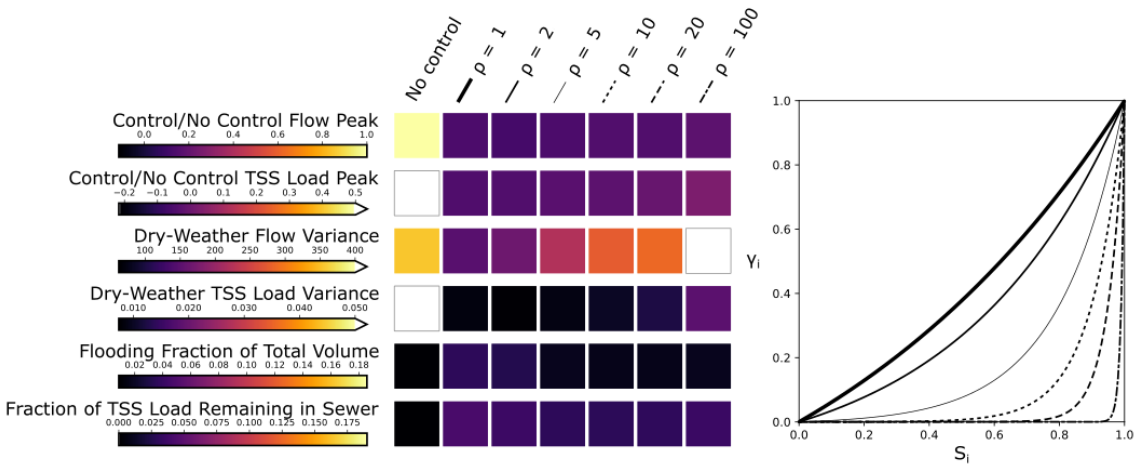


Figure 3.6: Impact of instantaneous importance weight $\rho$ on performance metrics for $\alpha_1^q = \alpha_1^{tss} = 5.0$. The right graph demonstrates the relationship between state $S_i$ and instantaneous importance $\gamma_i$ for each $\rho$ value for reference. In all scales, a darker color indicates better performance in that particular metric.

The impact of the instantaneous importance weight $\rho$ is also assessed for network flooding and solids accumulation (Figure 3.6). While all $\rho$ values considered here

produce little flooding, flooding volume is inversely proportional to $\rho$ value. To account for this behavior with respect to flooding, note that upstream storage assets with higher normalized depths, and thus higher risk for flooding, will release more water than those that are not prone to overflowing at that particular time. Further, $\rho$ has little impact on the solids load remaining in the sewer network, though there is minimal improvement in resuspension with higher $\rho$ values (Figure 3.6).

### 3.3.3 Towards Implementation

A natural extension from these findings would be the separation and customization of control schemes for various system states and inputs. The results suggest a benefit in adjusting control regimes or parameterizations between wet- and dry-weather periods (Figure 3.4 and Table 3.1). Flow attenuation (Scenario 1) resulted in higher flow peak reduction during wet-weather when compared to TSS load attenuation (Scenario 2) (94.17% vs. 78.24%, respectively); however, dry-weather flow and TSS load oscillations were not dampened as successfully via flow attenuation (Scenario 1) as with TSS load attenuation (Scenario 2) (flow oscillation damped: 78.7% vs. 86.8% and TSS load oscillation damped: 78.8% vs. 93.2%). Thus, in this case, flow-driven control during wet-weather events and TSS load-driven control during dry-weather periods would be a viable strategy towards improving sewer operation. Indeed, having weather-dependent regimes is a common strategy in more manual sewer operations [40, 104, 118]. As such, implementations should also look beyond one-size-fits-all parameterizations in the case of real-time control.

Further, while the system importance parameter assignment has been demonstrated to achieve improved downstream performance (e.g., peak reduction and oscillation dampening), beyond a certain level of weighting, downstream performance plateaus ($\alpha_1^q, \alpha_1^{tss} \geq 10$, Figures 3.5a, 3.5b, 3.5d, and 3.5e). What should determine system importance parameter values is a balance with upstream or system-wide performance indicators (e.g., flooding, solids accumulation). In this study, there is an upper limit on downstream system importance values to minimize network flooding ($\alpha_1^q, \alpha_1^{tss} \leq 10$; Figure 3.5c). One approach to mitigate network flooding would be to

build in a heuristic rule for releasing stored water when an asset becomes too full. However, maintaining a connection with actual implementation, this strategy would need to ensure that the emergency release of stored water from upstream assets does not result in too great a surge of flows at downstream storage assets or the WRRF inlet.

More interestingly, perhaps, is the presence of a band of higher performance for solids accumulation across system importance values (for system importance values such that $\alpha_1^q + \alpha_1^{tss} \approx 10$; Figure 3.5f). To explain this, note that settling and resuspension are dictated by water depth and velocity of releases. For lower system importance values, there is shallow upstream storage and thus less distance for solids to settle, and hence more settling. However, the shallow storage also results in lower velocity when water is released, and thus less resuspension. On the other hand, high system importance values result in large quantities of water stored behind upstream assets, requiring small releases due to the strict control against downstream peaks — and thus minimal resuspension of settled solids. However, between these ranges is an area of minimal solids accumulation. This indicates not only a trade-off between high and low system importance values with down- and upstream performance, but a desirable range of values for the control algorithm parameters. In this case study, the most desirable performance across all considered system-wide metrics would be achieved with system importance values that satisfy $\alpha_1^q + \alpha_1^{tss} \approx 10$ and $\rho = 1$ (Figures 3.5 and 3.6). These parameters may be case study-specific, and parameter values for other systems may likely vary based on context and system priorities; this will be explored in future work so that transferability of results can be considered. More generally, this illustrates the need for optimization and parameter analysis in formulating the control problem and determining priority weights in the objective function. Similar conclusions can also be found in other studies that highlight the impact of parameterization on control performance and stability [119, 120]. Overall, this lends support to trying out a simpler control technique first — such as the one presented in this paper — before embarking on the application of more complex algorithms. A first order, simpler analysis may shed insights on performance bands unique to a given system, which may provide insight to tuning more complex algorithms.

Complex and interesting dynamics may be missed if control algorithm formulations fail to account for a breadth of upstream and downstream performance measures. Namely, optimization of one parameter may often come at the cost of another. Indeed, the concern of sewer solids accumulation has been explored in other works [87]. While control algorithms for water systems are typically formulated, tested, and refined in simulation, connection and communication with real-world system operators is crucial to the feasibility of real-time control implementation. For instance, attempting to maintain downstream flow and/or TSS load strictly below a threshold may be too restrictive given available storage in sewer assets during high-stress times (e.g., large and/or flashy storms) and would thus require over-utilization of storage assets insomuch as they exceed their storage capacity and increase the risk of flooding in the network and may increase in-line maintenance needs. This study explored this balance between upstream and downstream objectives using parameters within the control algorithm, namely system importance values $\alpha_1^q$ and $\alpha_1^{tss}$ and instantaneous importance weight $\rho$. The realizable values of these parameters will ultimately not be governed solely by physical constraints, but also human preferences.

The results illustrated here demonstrate a need for further flexibility to avoid or manage the accumulation of settled solids behind control assets in the sewer network. Extending beyond the approach discussed here, this flexibility can be incorporated by introducing dewatering strategies or intentional scour release events that occur after wet-weather events by releasing water from upstream to downstream assets, thereby flushing the system to encourage resuspension and conveyance of solids to the downstream WRRF for treatment and management [10, 121].

## 3.4 Conclusions

In this study, we demonstrate the use of a control algorithm, flexible to multiple water quantity and quality objectives, as well as downstream and upstream objectives. Our parameterization analysis is used to explore trade-offs among these goals. Our findings highlight the importance of identifying a range of near-optimal parameter values for control algorithms. Future work should investigate how these

regions translate to other algorithm formulations. It is critical to note that what defines "optimal" will be dependent on the system context, human preferences, and trade-offs between multiple objectives. Overall, bands of near-optimality may arise and string a balance between most objectives. This however, should be evaluated on a case-by-case basis. In lieu of one optimal point, this may present a range of aspirational values to appeal to system operators. Sensitivity analyses and decision maker preferences should be considered in the control process as early as the formulation of the actual control problem and objective function.

# CHAPTER 4

# Impact of Collection System Control on WRRF Treatment

## 4.1 Introduction

The operation and performance of water resource recovery facilities (WRRFs) is heavily influenced by influent conditions. This is particularly true in combined sewer systems, in which wastewater (dry-weather) and stormwater (wet-weather) flows are integrated into the same pipe network. Both contributions result in flow and pollutant dynamics, such as diurnal wastewater patterns and stormwater hydrograph peaks. Inflow dynamics impact WRRF treatment processes, which in turn affect operator or control decisions. For instance, dynamic chemical addition and aeration need to account for changes in pollutant loads and flows. More examples can be given, but a general notion remains: operations at the WRRF should always adapt since WRRF operators have limited control over what is received from the sewer. As described in prior chapters, however, there is an opportunity to exercise significant control over inflow dynamics by controlling the collection system. This brings to bear the notion that the collection system is simply an extension of the WRRF, and should be operated in a holistic, systems context.

The paradigm of coupled sewer-WRRF control has generally be explored through the concept of *integrated* modeling and control across the sewer system, WRRF, and receiving water body (e.g., river). Most of these efforts rely on the development

and calibration of highly complex, mechanistic or physically-based models, or informing simplified surrogate models using these complex models for the purpose of control optimization [16, 56, 122, 123]. Because these integrated systems are so complex, rule-based control is a frequent basis for exploring the benefits of integrated management [124]. However, these rules require expert knowledge to develop, are system-specific, and are difficult to scale. While recent literature has implemented model predictive control to consider WRRF capacity in sewer-based control actions [125], still little work has been done to evaluate the impacts that expansive sewer-scale control has on WRRF treatment performance and operation. Evaluating the impacts of control on both the sewer and WRRF is critical for highlighting benefits and trade-offs that exist across the urban wastewater system, such as mitigating flooding and overflows, improving treatment, and maintaining overall system function. Even further, developing this understanding is crucial for permitting holistic control of the urban water cycle.

As was demonstrated in previous work (Chapter 3), real-time and coordinated control of distributed sewer storage assets can successfully attenuate stormwater flow and pollutant load peaks, as well as dampen wastewater diurnal patterns. While a key motivation for prior chapters was to improve WRRF efficiency, an explicit analysis of WRRF conditions under controlled inflows was not evaluated. Since many impacts to WRRF conditions could be evaluated, to narrow the scope of this study, this chapter will focus on chemical phosphorus removal in the WRRF primary system, specifically via ferric chloride dosing. This is motivated by ongoing work in the greater Detroit area by the Great Lakes Water Authority (GWLA). The contribution of this chapter is to *quantify the impacts of WRRF influent dynamics and ferric chloride dose on chemical phosphorus treatment efficacy (i.e., phosphorus removal) and efficiency (i.e., ferric chloride consumption).*

### 4.1.1 Background

Variability of influent flow and composition can be detrimental to the operation and performance of WRRF treatment processes, including washing out of microor-

ganisms in bioreactors and disturbing settled solids in clarifiers [9, 10]. The GLWA WRRF exemplifies this, given that it is a combined sewer system with both pronounced wastewater and stormwater influences. As it is one of the largest WRRFs in the world, treatment performance at the GLWA WRRF has the capacity to significantly impact the quality of the downstream receiving water bodies. To demonstrate this, consider the case of phosphorus. The GLWA WRRF is a major source of phosphorus loading to the Detroit River and Lake Erie further downstream. One study found that, among watershed contributions, the GLWA WRRF contributes 10% of the total phosphorus load to the Detroit River system. Moreover, it the largest urban and point source in the region and so it is one of the biggest single-site opportunities to reduce phosphorus loads to Lake Erie [126]. Phosphorus pollution in natural water systems results in eutrophication and algal blooms, both of which have been increasing occurrences in Lake Erie in recent years. Ultimately this has resulted in periods of suspended use for recreation, degradation of drinking water supply, and overall disruption and deterioration of the natural water environment [126, 127]. Hence, phosphorus treatment at the GLWA WRRF is a particularly interesting and impactful case study and is considered here.

#### 4.1.1.1 Case Study Motivation: Chemical Phosphorus Removal in the GLWA WRRF

Chemical phosphorus removal is a common treatment route in many WRRFs. Specifically, at the GLWA WRRF, ferric chloride ($FeCl_3$) is added to precipitate soluble phosphorus and then settle out the particulate form in primary clarifiers. The dosing of ferric chloride is determined by dry- and wet-weather operation, as well as manual measurements of soluble phosphorus in the primary effluent (Appendix C) [128]. The primary treatment system in the GLWA WRRF has a capacity of 4.5 $Mm^3/d$ (1200 $Mgal/d$), while the secondary treatment system has a capacity of 3.5 $Mm^3/d$ (930 $Mgal/d$) [129]. As a result, primary effluent flow over this 3.5 $Mm^3/d$ threshold is discharged as overflow to the environment directly after the primary treatment system (Figure 4.1). Thus, any pollutants in these discharged volumes

receive primary-only treatment before going to the receiving water body, bypassing the remainder of the WRRF [128–130]. Further, while phosphorus removal through chemical addition enables WRRFs to reduce phosphorus discharges through WRRF effluent and overflows, this chemical use comes at cost to the WRRF. For a WRRF as large as the GLWA facility, this cost can be significant. The GLWA WRRF used around 1080 dry metric tons (2.38 million dry pounds) of ferric chloride during the 2018–2019 fiscal year, at a cost of $1.17 million for this chemical resource alone [131]. Thus, improvements in the efficiency of ferric chloride use can result in financial savings.

To generalize the findings of this study, a simulated WRRF is used, which was inspired by the GLWA facility [132]. The goal of this chapter is not to have an exact representation of the GLWA primary system, but rather a realistic enough representation to derive general conclusions. Indeed, though many WRRFs employ chemical phosphorus removal, specifics regarding location of metal addition, mixing, dosing strategies, etc. vary significantly based on WRRF and context. Thus, the ability to discover broad trends is the aim herein. More detail on this simulated representation is found in Section 4.2.1. The subsequent section provides additional background into the mechanisms and factors impacting chemical phosphorus removal.

#### 4.1.1.2 Mechanisms and Factors of Chemical Phosphorus Removal

Chemical phosphorus removal broadly describes the addition of metal salts to react with phosphorus species; these reactions convert soluble phosphorus into insoluble phosphorus, which is removed as a precipitate via settling. In the case of ferric chloride addition, these metal-phosphorus reactions can include several mechanisms: phosphate adsorption on hydrous ferric oxide (HFO), binding and co-precipitation of phosphate in the HFO structure, formation and precipitation of ferric phosphate ($FePO_4$), and precipitation of mixed cation phosphates [133]. Both experimental and model studies have shown that minimal phosphorus removal occurs through the $FePO_4$ pathway, particularly at pH values that are common in a wastewater-context [133, 134] and thus HFO reactions are a primary mechanism for chemical phosphorus

removal [45]. HFO is a solid that forms as a result of acidic ferric cations reacting with the alkalinity in the water into which it is dosed. The oxygen sites on and in the HFO structure enable binding and co-precipitation of phosphate species, thereby enabling settling of phosphorus species in a particulate form [135].

Before the 2000s there was incomplete, if not incorrect, understandings of the mechanisms of chemical phosphorus removal [136]. Consequently, many WRRFs were, and still are, designed to provide unnecessarily high doses of chemical addition, going beyond what is needed for sufficient phosphorus removal. As a result, WRRFs experience high chemical costs and production of large amounts of chemical sludge [45]. However, in the past 10–15 years, extensive experimental and modeling efforts have contributed to a more nuanced and accurate understanding of the mechanisms behind chemical phosphorus removal, as well as factors that influence its efficacy.

**Type of Metal Salt.** The type of metal salt used will impact the efficacy and efficiency of removal of soluble constituents. In fact, a number of studies directly compare a variety of chemicals, including ferric- and aluminum-based compounds [45, 137–140]. Given the use of ferric chloride by the GLWA WRRF chemical phosphorus removal system, this work focuses on its application.

**Dose of Metal Salt.** Metal salt dose plays a significant role in the efficacy of chemical phosphorus removal [45, 133, 138] and removal of soluble phosphorus species increases with relative chemical dose. However, studies have shown that "specific phosphorus removal decreases with increasing coagulant dose" [45]. This has also been observed in the chemical phosphorus removal system at the GLWA WRRF, wherein removal plateaus beyond a ferric chloride dose of 2.5 mg/L [130]. This could be the result of an upper bound on the amount of phosphorus that can be incorporated into ferric-based precipitates, as observed in experimental study [45], though further investigation into the underlying mechanisms of these observations is needed.

**Influent Pollutant Concentrations.** Influent characteristics have been studied to determine influence on chemical phosphorus removal, concluding that influent variability can be of particular consequence for devising and adjusting chemical dosing strategies [138]. The most relevant findings to this chapter include concentrations of species that are being removed via chemical addition. Our focus is on the chemical removal of phosphate [45, 133]; however, competition with other species, such as organics and total suspended solids (TSS), can impact and inhibit chemical phosphorus removal by reacting with the metal added [45, 135, 141]. Additionally, although increases in initial soluble phosphorus concentrations result in increases in phosphorus removal, very high metal doses ($\gg$1 mol $FeCl_3$/mol P, the stoichiometric ratio) may be required to achieve low concentrations of phosphorus ($<$0.1 $g/m^3$ as P) [45]. Further analysis into these interactions is outside of the scope of this study and is left for future work.

**Time and Kinetics.** The role of time, particularly contact time for chemical reactions, in the efficacy of chemical phosphorus removal has been reported in recent studies. Initial, fast removal of phosphorus through the addition of metal salts was observed previously; this removal occurred so quickly it was thought to be nearly instantaneous (and is called *instantaneous phosphorus removal* in the literature). However, experimental studies have shown that further and non-negligible phosphorus removal continues to occur over timescales of hours to days, called *slow phosphorus removal* [45]. This latter removal mechanism will be important when considering the design of reactors for mixing, chemical reactions, and precipitation and binding for both real-world applications and simulations. In particular, the hydraulic residence time (HRT) of reactors will play a role in chemical phosphorus removal as longer HRTs will enable more removal via the slow phosphorus removal mechanisms.

Other operational variables also impact chemical phosphorus removal, including floc age and the mixing regime of the metal salt into the influent wastewater, which both influence the number of sites on HFO for phosphate adsorption and coprecipitation [45, 133]. These factors will vary based on WRRF context and design of the broader primary treatment system; further they are outside of the scope of this study

and will not be considered here.

#### 4.1.1.3 Impact of Influent Dynamics on Chemical Phosphorus Removal

Few studies have explicitly studied the impact of dynamic influent on chemical phosphorus removal. This will be important for assessing the impact of changes in influent conditions (e.g., flow) and operational variables (e.g., metal salt dose) on the effectiveness and efficiency of chemical phosphorus removal. Conidi et al. [135] studied the impact of solids residence time on phosphorus removal using sequencing batch reactors; however, the batch environment eliminates short-term temporal dynamics in influent conditions. Thus the role of influent dynamics within chemical phosphorus removal remains largely unexplored.

Several studies have been conducted with a combination of modeling and full-scale or pilot-scale experiments to explore the potential of control in chemical phosphorus removal applications for the dosing of metal salts [46–48]. A constant dose strategy was often used as a baseline for comparison to other strategies, such as dosing proportional to influent flow or pollutant load. These studies also compared the performance of feedback control, commonly using a proportional-integral (PI) controller. Tik and Vanrolleghem [46] and Ingildsen [47] have reported success of feedback control with real-time dose changes and closely achieved effluent quality setpoints. However, the need to consider operational setup of these systems, as well as lag times between placement of the downstream sensor and location of the metal salt addition must be highlighted, particularly for transitioning from a modeling study to real-world application. Otherwise, instability of the feedback controller can result in oscillatory behavior [48]. Further, there have been no studies found that simultaneously consider ferric chloride (or, in general, metal salt) dosing strategies *and* attenuation or modulation of influent conditions to improve the efficacy and efficiency of chemical phosphorus removal.

### 4.1.2 Opportunity and Motivation

Given the impact WRRFs have on the water quality of their receiving water bodies, maintaining high treatment performance is the key priority. By providing more desirable influent conditions (i.e., equalized), there is an opportunity to enable better WRRF treatment. Specifically, we contend that it is possible to improve chemical phosphorus removal during times of high phosphorus loading (i.e., storm events) and minimize phosphorus received by surrounding water bodies, through both effluent and overflow discharges. Our study quantifies these benefits and informs how WRRF operation can be simultaneously leveraged to improve the efficiency of chemical resource use for this aim.

## 4.2 Methods

### 4.2.1 WRRF Primary System Modeling

For this chapter, we develop a reduced order model of the GLWA WRRF with the desire to produce results that can be broadly generalized to other systems. As such, only phosphorus treatment is presented; other treatment processes are left out to enhance the focus of our study. To promote generalizability of results, this study was intentionally designed so that WRRF influent is received in a single pipe, to which ferric chloride is added before mixing and reaction. More specifically, the WRRF primary system modeled here consists of ferric chloride ($FeCl_3$) addition to the WRRF influent, a small CSTR for chemical mixing and reactions (14,583 $m^3$ volume, 10 $min$ dry-weather average HRT), and a volumeless point separator primary clarifier with a constant solids percent removal of 70% based on previous study [130] (Figure 4.1). Sumo (Dynamita), a wastewater process simulator, was the modeling software employed. It was interfaced with Python for executing simulations and conducting analyses. All code and models for simulation and analysis are provided in a public web repository (github.com/stroutm/sewerWRRF).

Influent to this WRRF primary system includes flow from the upstream combined sewer network. As shown in Chapter 3, real-time and coordinated control of

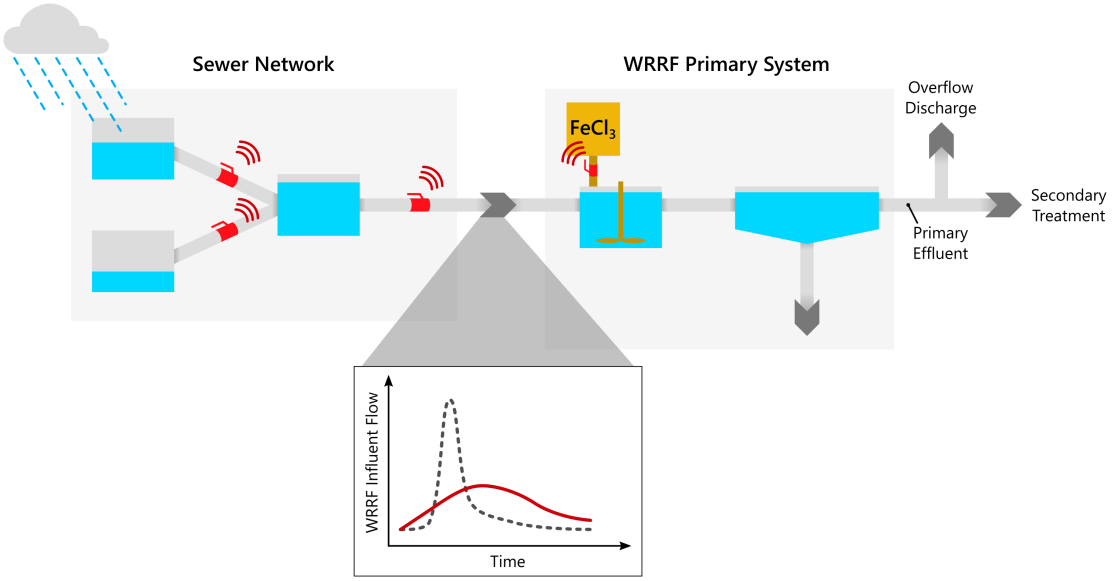


Figure 4.1: Schematic description of the connection between the sewer network and the WRRF primary system. Real-time control of distributed sewer storage assets (depicted as red valve icons) can achieve peak attenuation in WRRF influent flow. Interaction of this control with ferric chloride ($FeCl_3$) dosing strategies is investigated.

distributed sewer assets can attenuate precipitation-driven peaks and dampen diurnal wastewater patterns at the outlet of a combined sewer network [142]. Specifically, this *should* enable improved influent conditions for WRRF operations and performance, as proposed in Figure 4.1. Influent data for the WRRF primary system are generated from Chapter 3 results to simulate dynamic WRRF influent conditions, for cases of varying sewer control; the process of generating these influent inputs is described in Section 4.2.4.

Modeling of the chemical phosphorus removal mechanisms in Sumo build from previous studies, which have shown that HFO reactions with phosphorus are the primary mechanism for chemical phosphorus removal in wastewater treatment contexts [45]. The oxygen sites on and in the HFO structure enable binding and co-precipitation of phosphate species, thereby enabling settling of the phosphorus species in a particulate form [135]. Aging of HFO has been observed to reduce

phosphorus adsorption capacity; specifically, HFO structures become more dense as they age, limiting diffusion and adsorption of soluble phosphorus into the structure [143]. Thus, adsorption properties are determined by HFO age. The underlying model of these processes in Sumo divides HFO species into three classes based on age and adsorption properties, namely $HFO_H$, $HFO_L$, and $HFO_{old}$ for HFO used in instantaneous binding (high adsorption capacity, $H$), slow binding (low adsorption capacity, $L$), and old HFO structures, respectively [133]. Specifically these instantaneous phosphorus removal reactions occur on the order of seconds or shorter, while slow reactions have been observed over minutely, hourly, or daily scales [45, 143]. On the other hand, old HFO structures are modeled as having no phosphorus adsorption capacity. These HFO reactions are modeled in Sumo and thus is the mechanism for chemical phosphorus removal used in this study. More detail of this representation is provided in Appendix C and Figure C.1.

### 4.2.2 Generating Static Influent Conditions

To investigate the direct impacts of WRRF influent flow and ferric chloride dose, specifically via dose concentration ($FeCl_3$ mass rate per influent flow rate) on chemical phosphorus removal, a series of simulations were first conducted, each simulation with a static influent flow and ferric chloride dose. For example, one simulation may have an influent flow of 2.1 $Mm^3/d$ and ferric chloride dose of 2.0 $g/m^3$, while another simulation would have an influent flow of 2.6 $Mm^3/d$ and ferric chloride dose of 2.5 $g/m^3$. In each simulation, the soluble orthophosphate ($SPO_4$) and total phosphorus (TP) concentrations in the primary effluent were measured. Note that in these simulations, the concentrations of the included water quality parameters were not changed regardless of changes in flow conditions. This was done intentionally to keep the ratio of ferric chloride dose *concentration* to influent phosphorus *concentration* constant. Further, by changing only the influent flow, the impact of contact time (via CSTR HRT) was evaluated. Note that HRT is expressed as

$$HRT = \frac{V}{Q} \tag{4.1}$$

where $V$ is the volume of the CSTR (14,583 $m^3$) and $Q$ is the flow through the reactor ($m^3/d$). Thus, increases in flow result in reduced contact and reaction time in the CSTR.

### 4.2.3 Generating Dynamic Influent Conditions

While simulation experiments with static conditions can elucidate how certain variables directly impact chemical phosphorus treatment performance, the reality is that WRRFs receive dynamic influent. More specifically, we are interested in combined sewer dynamics that exhibit both dry- and wet-weather influences. For this study, influent inputs into the WRRF primary system exhibit dynamics and are generated using sewer outflow conditions (at a 30-min temporal resolution) from the load-balancing control algorithm demonstrated in Chapter 3. These sewer outflow conditions include wastewater and stormwater dynamics of flow and TSS concentration for a *sub*section of the Detroit combined sewer system. It should be noted that that the sewer subsection used in Chapter 3 has a dry-weather average flow of 0.49 $Mm^3/d$ compared to 2.1 $Mm^3/d$ for the WRRF considered here. Thus, these subsection results were linearly scaled to match the magnitude of the WRRF influent. This procedure consisted of the following steps:

1. Influent flow and constituent concentrations (total chemical oxygen demand, TCOD; total Kjeldahl nitrogen, TKN; TP), as observed in a previous study [130], are used as the *average dry*-weather influent flow conditions.

2. Series of 75-day sewer outflow conditions (flow and TSS) with various sewer control scenarios from Chapter 3 were selected. Recalling that these time series are for a *sub*section of the Detroit combined sewer network, these dry- and wet-weather events were linearly scaled so that the average dry-weather flow matches the average dry-weather WRRF influent conditions from the above step (Figure 4.2).

3. For simplicity, it is assumed that other constituents in the WRRF influent follow similar dynamics of TSS and so they are scaled in the same fashion.

This has been done for TCOD, TKN, and TP (Figure 4.2) as these are influent inputs in the Sumo model used here. The percentage of orthophosphate ($SPO_4$) within the total phosphorus concentration is assumed constant throughout at 53.3% (as observed in Yan et al. [130]).

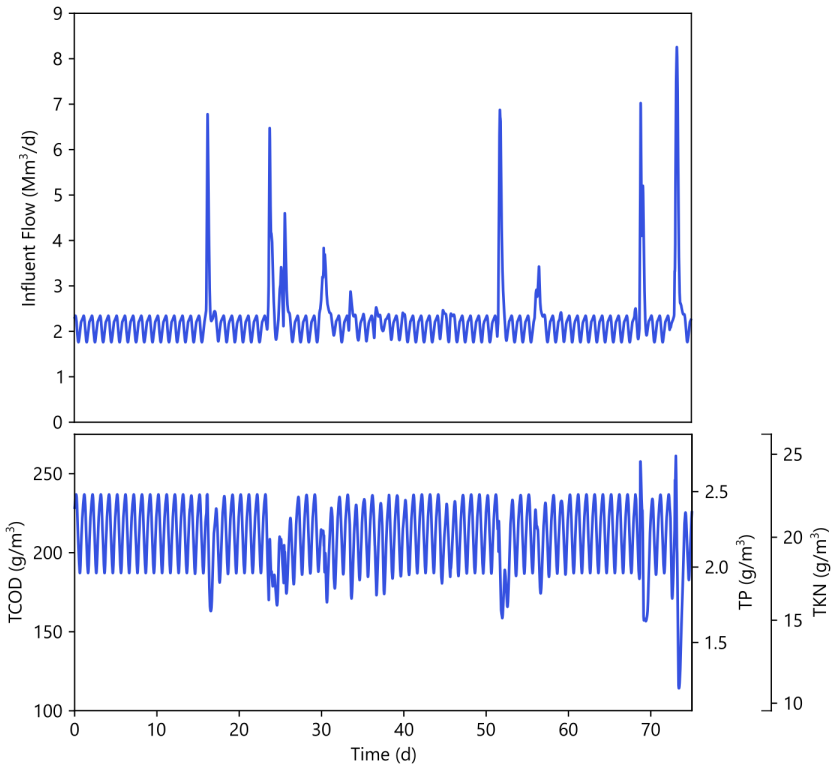


Figure 4.2: WRRF influent flow and water quality composition.

### 4.2.4 Design of Dynamic Influent Simulation Experiments

Within the 75-day simulation period, five storm events were isolated for analysis. These are shown in Figure C.2 and summarized in Table C.2. Pairings between three sewer control scenarios and two ferric chloride dosing strategies were assessed for simulation experiments with dynamic influent conditions. Three assessment metrics were used. These are summarized in Figure 4.3; detail for each follows.

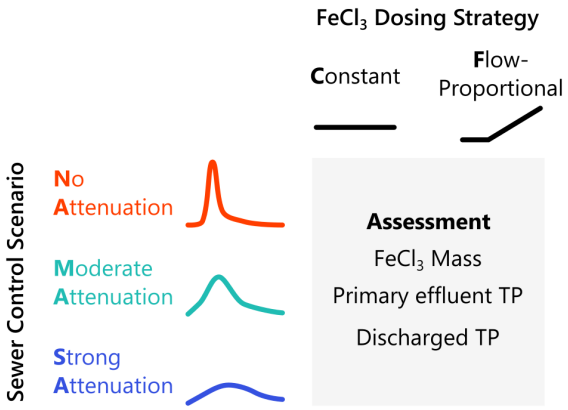


Figure 4.3: Pairings between sewer control scenarios and ferric chloride dosing strategies. The sewer control scenarios compare no attenuation, moderate attenuation, and strong attenuation. The ferric chloride dosing strategies compare constant and flow-proportional dosing approaches.

Sewer control scenarios were chosen from Chapter 3 and were selected to consider a range of stormwater flow peak attenuation scenarios. Namely, these scenarios are **NA**: no flow peak attenuation (i.e., no sewer control); **MA**: moderate flow peak attenuation ($\alpha_1^{tss} = 1.0$ from Chapter 3); **SA**; strong flow peak attenuation ($\alpha_1^{tss} = 10.0$ from Chapter 3). Note that the SA scenario is in the band of high performance identified in Chapter 3.

Two ferric chloride dosing strategies were selected for comparison in the dynamic influent simulations. The first strategy is one of constant ferric chloride dose at 2 $g/m^3$ (**C**). As this is a constant concentration of ferric chloride, as the influent flow increases, the *mass* of ferric chloride added will also increase *linearly*. The second dosing strategy is one of flow-proportional ferric chloride dose (**F**) [128]. In this case, a constant ferric chloride dose of 1.5 $g/m^3$ is used when influent flow is below 2.1 $Mm^3/d$, which corresponds to the average dry-weather flow at the WRRF influent. Above influent flow of 2.1 $Mm^3/d$, the ferric chloride dose increases with flow, following

$$FD = (4.45 \cdot 10^{-7})Q + 0.566 \tag{4.2}$$

where $Q$ is influent flow ($m^3/d$) and $FD$ is ferric chloride dose ($g/m^3$). This cor-

responds to maintaining 1.64 $g/m^3$ TP in the primary effluent based on the results generated in Section 4.3.1 and shown in Figure 4.4b. This concentration of 1.64 $g/m^3$ TP is an estimate of what would be achieved with 1.5 $g/m^3$ ferric chloride at 2.1 $Mm^3/d$ based on Figure 4.4b. By reducing the ferric chloride dose from 2.0 to 1.5 $g/m^3$ below the average dry-weather flow and increasing the dose as flow (and correspondingly phosphorus load) increases, the aim was to prioritize ferric chloride addition during times when phosphorus removal was most crucial. This is based on elevated phosphorus load to the WRRF during storm events; increases in phosphorus mass and flow are a result of stormwater influx. These times of prioritized ferric chloride addition also importantly occur when there is increased likelihood of experiencing primary treatment-only discharges to the environment, which occur when flow is over 3.5 $Mm^3/d$.

Each sewer control scenario and ferric chloride dosing strategy pair is assessed based on:

- Cumulative ferric chloride mass added
- Cumulative total phosphorus mass in the primary effluent
- Cumulative total phosphorus mass discharged via overflow after the WRRF primary treatment system

These are specifically assessed here through *cumulative* totals over the duration of each storm event. To compare the performance of chemical phosphorus removal for each sewer control scenario and ferric chloride dosing strategy pair across the different storm events, which have different volumes and flow peaks (Table C.2), each of the above assessment metrics are also computed relative to that of the C,NA "base case," which exemplifies a simple mode of operation (no sewer control attenuation and constant ferric chloride dosing regardless of weather conditions). These relative assessment metrics are then averaged across the five storm events, with standard deviations also calculated to evaluate consistency.

## 4.3 Results and Discussion

### 4.3.1 Static Influent Simulations

Simulations were first performed using static influent conditions. To investigate the impact of flow magnitude and ferric chloride dose on chemical phosphorus removal, static influent flow rates were considered, ranging from 1.1–3.1 $Mm^3/d$; recall that the average dry-weather WRRF influent flow for the context considered here is 2.1 $Mm^3/d$. For each flow rate, ferric chloride doses were considered, ranging from 1.5–2.5 $g/m^3$. The resulting $SPO_4$ and TP concentrations in the primary effluent vary nearly linearly with influent flow and ferric chloride dose (Figures 4.4a and 4.4b, respectively). Specifically, increases in influent flow rate result in increases for both $SPO_4$ and TP primary effluent concentrations (i.e., reductions in chemical phosphorus removal performance). This is explained through Equation 4.1 in that increases in flow result in decreased HRT in the CSTR and thus reduced contact and reaction time between phosphate and ferric species (e.g., HFO), particularly through the slow phosphorus removal reactions.

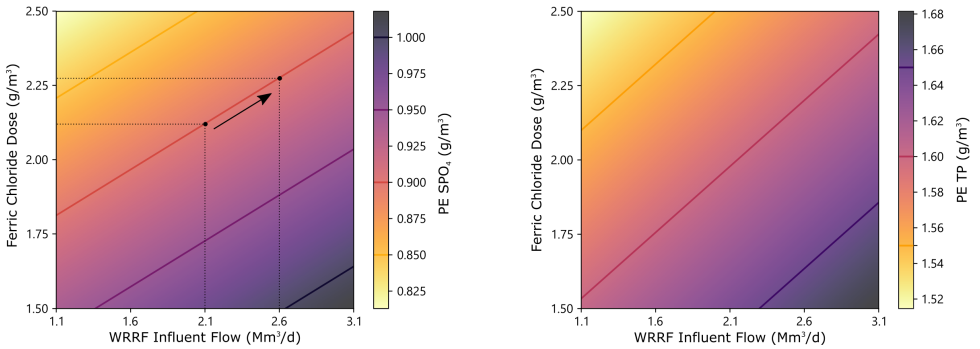


(a) (b)

Figure 4.4: Impact of influent flow and ferric dose on (a) $SPO_4$ and (b) TP primary effluent concentrations as conducted by simulations with static influent conditions. The dashed lines and arrow in Subfigure (a) indicate the increase in ferric chloride dose required for an increase in influent flow from 2.1 to 2.6 $Mm^3/d$ to maintain a $SPO_4$ primary effluent concentration of 0.9 $g/m^3$.

Increases in ferric chloride dose result in decreases in $SPO_4$ and TP concentrations in the primary effluent (Figure 4.4). This is because higher concentrations of ferric chloride support more reactions between phosphate and ferric species, which transform soluble phosphorus components to particulate and then settle in the primary clarifier; this is in line with findings in literature [45, 133, 138].

These trends (Figure 4.4) suggests that increases in ferric chloride dose can compensate for reductions in chemical phosphorus removal that would otherwise occur as a result of increased influent flow. For instance, to achieve a $SPO_4$ primary effluent concentration of 0.9 $g/m^3$ at an influent flow of 2.1 $Mm^3/d$, a ferric chloride dose of 2.1 $g/m^3$ is required. However, if influent flow increased to 2.6 $Mm^3/d$, ferric chloride dose should be increased to 2.3 $g/m^3$, a 9.5% increase, to maintain the 0.9 $g/m^3$ primary effluent $SPO_4$ concentration (Figure 4.4a). Moreover, changing the ferric chloride dose in response to dynamics in influent flow could enable more consistent phosphorus removal. While this is the case in these simulation experiments, it must be noted that previous studies of full- and bench-scale systems have observed that phosphorus removal plateaus beyond certain levels of ferric chloride dose [45, 130]. However, these non-linearities may not be captured in simuation. Moreover, ferric chloride dosing is the consumption of a resource and so imposes costs (e.g., financial expense and production of solids). Therefore, its application should not be without constraint.

Even more promising is the potential to leverage both ferric chloride dosing *and* modulation of the influent flow to achieve better chemical phosphorus removal. Through these static influent condition experiments we can see that by reducing influent flow magnitude to the WRRF, the dose of ferric chloride can be reduced while maintaining consistent phosphorus removal. This suggests that efficiency in dosing can be achieved by regulated inflows, which is explored in the subsequent section.

### 4.3.2 Dynamic Influent Simulations: Single Storm Event

Simulations were carried out with 75-day, dynamic WRRF influent conditions, including both dry- and wet-weather behavior. As described, three sewer control

scenarios are included and correspond to scenarios from Chapter 3: NA, MA, and SA. The two ferric chloride dosing strategies are C: constant dose at 2 $g/m^3$; and F: flow-proportional dose (see Section 4.2.4 for more details). Figure 4.5 shows a comparison of these sewer control scenarios and dosing strategies for a particular 5-day storm event (Storm E: Days 67–72).

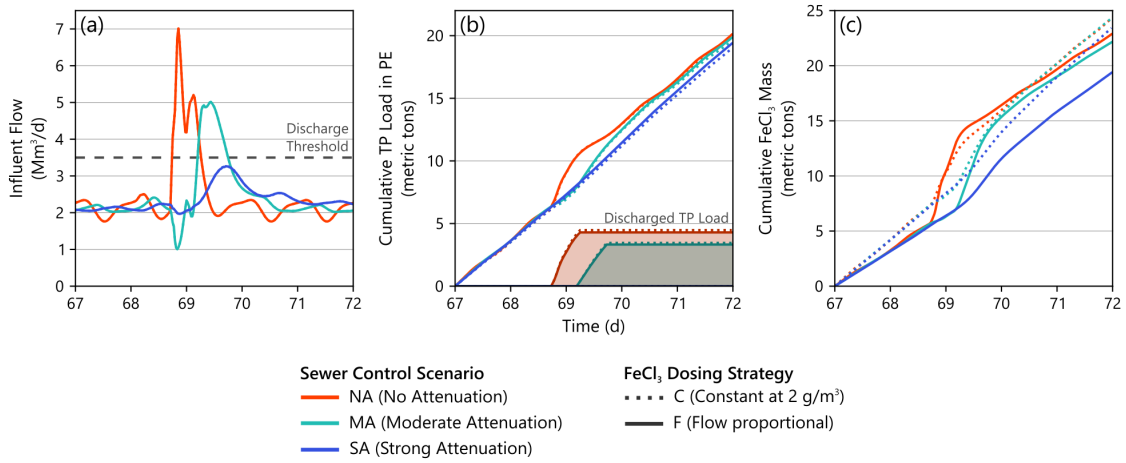


Figure 4.5: Impact of sewer control and ferric chloride dosing strategy on dynamic WRRF response. The time series show (a) WRRF influent flow, (b) cumulative primary effluent TP load, and (c) cumulative $FeCl_3$ mass added. Subfigure (b) also depicts the cumulative TP load in flow that exceeds the 3.5 $Mm^3/d$ threshold and is discharged from the WRRF to the environment after primary treatment. Sewer control scenarios (different colors: NA, MA, SA) and ferric chloride dosing strategies (line styles: C, F) are compared. One storm event (Storm E) is shown as an example and cumulative totals begin at time 67 $d$ for visual clarity.

For both ferric chloride dosing strategies (C and F), the attenuation of influent peaks (both storm-driven and diurnal) results in more consistent phosphorus load in the primary effluent (closer to a straight line in Figure 4.5(b)). Further, the cumulative total phosphorus in the primary effluent at the end of this 5-day period is lower in the scenarios of greater flow peak attenuation, though this difference is very small (Figure 4.5(b) and Table C.3).

Of greater importance is the phosphorus that is discharged after the WRRF

primary system. Primary effluent flows above 3.5 $Mm^3/d$ are discharged to the environment from the WRRF. These discharges result in volumes of combined sewer flow that receive only primary treatment, bypassing secondary treatment benefits and going directly to the receiving water body. The darker shaded regions in Figure 4.5(b) show the cumulative total phosphorus load that would be discharged in these overflows. Influent flow peak attenuation has a substantial impact on reducing the phosphorus load that is discharged after primary-only treatment. This is the result of the reductions of flow above the 3.5 $Mm^3/d$ threshold and thus reductions in the overflow volume. Indeed, in the MA scenario, less primary effluent volume is discharged, resulting in less total phosphorus discharged as well (Figure 4.5(b) and Table C.3). In the SA scenario, there is sufficient attenuation of flow peaks so that no primary effluent is discharged and all flow proceeds to later stages of treatment in the WRRF. Not only could this mitigate instances of regulatory non-compliance, but also enable other means of phosphorus and other pollutant (e.g., carbon and nitrogen species, depending on the WRRF) treatment that occur later in the WRRF.

For the constant ferric chloride dosing strategy (C), there was little impact of flow peak attenuation on ferric chloride consumption (Figure 4.5(c) and Table C.3). This is because the total volume of the storm is the same for each sewer control scenario (NA, MA, SA). Since the ferric chloride dose remains constant at 2 $g/m^3$ regardless of flow, the total ferric chloride mass consumed is simply

$$C \cdot V \tag{4.3}$$

where $C$ is the ferric chloride dose concentration (2 $g/m^3$) and $V$ is the volume of the event ($m^3$). However, the cumulative consumption of ferric chloride changes substantially in the flow-proportional dosing strategy (F) (Figure 4.5(c)). More specifically, with this ferric chloride dosing strategy, increased flow peak attenuation results in reduced consumption of ferric chloride. For this particular 5-day storm event (Storm E), the cumulative ferric chloride consumption in each scenario is (in metric tons) NA: 22, MA: 22, SA: 19 — a 14% reduction for SA compared to NA. Relative to the C,NA case (24 metric tons of ferric chloride consumed), the F,SA case

shows a 21% reduction in ferric chloride consumption (Table C.3). For the GLWA WRRF, a reduction of this magnitude corresponds with a potential cost savings of $250,000 per year from ferric chloride usage alone based on historical ferric chloride expenditures at the WRRF [131].

### 4.3.3 Dynamic Influent Simulations: Overall Behavior

While Figure 4.5 compares sewer control scenarios and ferric chloride dosing strategies for a single storm event (Storm E), these results are compiled for the five storm events in the 75-day simulation (Tables 4.1 and C.3, and Figure C.2). In Table 4.1, each table entry shows the result (e.g., cumulative ferric chloride mass added) *relative* to the C,NA base case. Table 4.1 averages these *relative* results across the five storm events.

Each pairing of ferric chloride dose strategy and sewer control scenario results in nearly equal total phosphorus loads in the primary effluent compared to the base case of C,NA. While this was exemplified with Storm E (Figure 4.5), even when averaging across the five storm events in the 75-day simulation period, this remains so (Table 4.1). Again, of more significant result is the reductions in TP that are discharged after the WRRF primary system. The moderate attenuation scenario (MA) for both constant (C) and flow-proportional (F) dosing strategies discharge cumulative TP mass that is 79% ($\pm$ 14%) and 77% ($\pm$ 14%) of the C,NA case, respectively, when averaged across the five storm events (TP discharge reductions of 21% and 23%, respectively). Further, in all five storm events, the strong attenuation scenario (SA) for both dosing strategies (C and F) completely eliminates primary effluent discharges, resulting in no TP mass discharged after the WRRF primary system (Table 4.1).

Table 4.1: Relative values for each row are summarized by averaging (± standard deviations) across the five storm events in the 75-day simulation period. This is done for each of the three sewer control scenarios (NA, MA, SA) and the two ferric chloride dosing strategies (C, F). *Percentages are used to compare cases relative to the C,NA case.* Note that cases in which the percentage is over 100% indicate that values were greater than the C,NA case (e.g., the F,NA case has 2% greater cumulative TP mass in the primary effluent compared to the C,NA case).

| **$FeCl_3$ Dosing Strategy** | **Sewer Control Scenario** | **Cumulative $FeCl_3$ Mass Added** | **Cumulative TP Mass in Primary Effluent** | **Cumulative TP Mass Discharged** |
|---|---|---|---|---|
| **C** | **NA** | 100% (± 0%) | 100% (± 0%) | 100% (± 0%) |
| | **MA** | 100% (± 0%) | 99% (± 1%) | 79% (± 14%) |
| | **SA** | 98% (± 2%) | 97% (± 2%) | 0% (± 0%) |
| **F** | **NA** | 89% (± 3%) | 102% (± 0%) | 97% (± 1%) |
| | **MA** | 86% (± 2%) | 100% (± 1%) | 77% (± 14%) |
| | **SA** | 80% (± 2%) | 99% (± 2%) | 0% (± 0%) |

When considering reductions in ferric chloride consumption, the dosing strategy has an important role. For the constant dose (C), there is little to no change in the mass of ferric chloride added across the sewer control scenarios (NA, MA, SA) when compared to the C,NA case (Table 4.1 and Figure C.2). This is because the total volume of each storm event remains the same and thus the ferric chloride mass does as well. However, in the flow-proportional strategy, reductions in ferric chloride consumption are observed across the three sewer control scenarios. Even in the case of no attenuation (F,NA), only 89% (± 3%) of the ferric chloride mass

added in C,NA is used (11% reduction). Moreover, flow peak attenuation further reduces ferric chloride consumption by reducing times of elevated ferric chloride dose. Respectively, the moderate and strong attenuation scenarios (F,MA and F,SA) utilize 86% (± 2%) and 80% (± 2%) of the ferric chloride mass in C,NA (Table 4.1) (14% and 20% reductions, respectively). The small standard deviations in these cases suggest that these results are also consistent across the five storm events in the 75-day simulation period considered here, even though these storm events vary in total volume and flow peak (Figure C.2).

While not the primary focus of this study, other factors were briefly investigated for their impact on the efficacy of chemical phosphorus removal and are included as supplemental to these results. First, in the previously discussed simulation experiments, a constant temperature of 20°C was used; however, some of the reactions in chemical phosphorus treatment have temperature-dependent rates [133]. To illustrate this dependence, simulation experiments were conducted for the C,NA case over the 75-day period, considering wastewater temperatures of 10, 20, and 30°C. Based on the results of these experiments, temperature plays a negligible role in the efficacy of chemical phosphorus removal; specifically, temperature changes of ±10°C to 20°C result in at most 0.4% change in cumulative total phosphorus mass in the primary effluent over 75 days, with higher temperatures being associated with slightly greater phosphorus removal (Appendix C and Table C.4). The second factor considered is the primary clarifier model used within the WRRF primary system model. Specifically, previous experiments discussed here use a volumeless point separator model; however, we also compare this to a three compartment model. This model choice is considered for comparison as the three compartment model has volume for additional reactions between HFO and phosphorus to potentially occur beyond the mixing CSTR. Again, simulation experiments over the 75-day period were conducted for the C,NA case, comparing the volumeless point separator (used previously) and the three compartment clarifier model (with an additional 2-hr HRT). The additional reaction time provided by the primary clarifier with the three compartment model resulted in 1.08% less total phosphorus mass in the primary effluent (Appendix C and Table C.5). Additional details for both of these experiments are in Appendix C.

### 4.3.4 Broader Implications

The key findings of this work are summarized as:

- **Influent flow attenuation reduces variability of phosphorous loads to downstream treatment processes and plant outflows.** The benefits of more equalized conditions are passed to downstream treatment, such as more stable conditions for biological treatment systems. It also results in fewer pollutant shocks in the receiving water body, particularly during and after storm events.

- **Influent flow attenuation mitigates overflows from the WRRF and therefore the mass of phosphorus to receiving water bodies.** In certain cases (SA scenarios), these overflows were completely eliminated, meaning that all primary effluent is able to be treated in downstream treatment processes before leaving the WRRF.

- **The combination of influent flow attenuation *and* flow-proportional ferric chloride dosing reduces the amount of ferric chloride required.** Reduction of this chemical consumption can realize financial savings, possibly substantial, and potential decreases in chemical sludge production.

While not evaluated here, it is likely these results would extend to the coagulation of other species, such as TSS, in the WRRF primary treatment system. The GLWA WRRF is working towards having an on-line analyzer for chemical phosphorus removal and ferric dosing [128]. This feedback control mechanism may allow for more precise control of phosphorus in the primary effluent and the WRRF at large. Ingildsen [47] saw that feedback control with a simple PI controller yielded good results in the removal of phosphorus via ferric-based dosing. However, tuning will be important to ensure precision and robustness, and reduce lag and instability [48]. Based on results presented here, it is likely that attenuation of influent flow peaks (via sewer control) will only further improve treatment performance by reducing variability, enabling more stable treatment performance, and reducing ferric chloride

consumption. The financial savings from reductions in ferric chloride usage can be considerable and depend on the size of the WRRF. For the GLWA WRRF, the F,SA case has potential savings of around $250,000 per year when compared to the C,NA case.

In Chapter 3, we concluded that trade-offs across the sewer and urban wastewater system do exist when conducting system-wide sewer control, specifically noting a need to balance WRRF influent peak attenuation, local sewer network flooding, and accumulation of solids in the sewer. Similar trade-offs should also be considered when planning coordination between sewer and WRRF operational control decisions. The sewer control scenarios used here (NA, MA, SA) were specifically chosen to show a range of peak attenuation while experiencing minimal flooding (Figure 3.5 in Chapter 3). However, a full characterization of costs (financial *and* operational) to the sewer network and WRRF should be conducted before making control decisions in the real system.

## 4.4 Conclusions

There is a large challenge and opportunity for coordinated management across the urban wastewater system. There is significant potential to leverage sewer storage and control resources to benefit the downstream WRRF. This work has demonstrated that, when deployed in concert, sewer control to augment WRRF influent flow dynamics *and* ferric chloride dosing at the WRRF impact both the efficacy and efficiency of chemical phosphorus removal. This can result in improved conditions for treatment further downstream in the WRRF, reduced discharges of partially-treated wastewater from the WRRF, and savings from reduced chemical consumption. As control actions and decisions take place in both the sewer and WRRF, coordination and trade-offs across the urban wastewater system should be evaluated to strike a balance between the multiple, often competing objectives in this system. Computational algorithms and quantitative assessment of impacts across the sewer and WRRF, as presented in this and previous work [142], will inform coordinated decisions and enable coupled urban wastewater system management.

# CHAPTER 5

# Conclusions, Contributions, and Future Research Directions

## 5.1 Conclusions and Contributions

With a data-driven emphasis, this dissertation contributes to the broader knowledge of real-time modeling and control of urban wastewater systems. By working in the context of a real-world system, this work has focused on technical solutions that consider and address challenges of implementation. Summaries of these contributions are detailed below.

Chapter 2 highlights the influence of data quality, age, and volume for training data-driven models of dynamic and uncertain systems, specifically urban wastewater systems. This is particularly important in considering the modeling toolchain and re-calibration scheme for accurately representing such systems. As was illustrated here, wastewater and stormwater flow components in combined sewers exhibit distinct spatial *and* temporal variation across the scale of cities. This work illustrates that signal processing and machine learning techniques are effective tools to decouple and separately model these components, learning from the unique characteristics in the underlying hydraulic and hydrologic processes that are reflected in sensor measurements. At the crux of the effectiveness of such an approach is the flexibility to separately and continuously re-calibrate each model component of the broader system based on individual data requirements.

Chapter 3 extends the ability to monitor the sewer network towards actual control of distributed assets. Specifically, through the development and application of a control algorithm, this work illustrates coordinated control of distributed sewer storage assets in order to balance multiple water quantity and quality objectives. Parameterization analysis within this approach elucidates trade-offs that exist between a number of objectives. For instance, sole priority given to flow attenuation can result in sewer network flooding and operational challenges. Rather control strategies should seek to balance objectives of the system and strongly consider those that would impede its adoption. To do so, consultation with decision makers and operators must take place at the beginning of the problem formulation process. Informing control decisions based on these trade-offs is key to the operation and performance of the urban wastewater system itself.

Building from the ability to coordinate the control of sewer assets and attenuate WRRF influent flows, Chapter 4 establishes the connection between sewer and WRRF control and decision making. While focusing on chemical phosphorus removal, this work demonstrates the potential to jointly leverage sewer control and chemical dosing strategies to maintain or improve phosphorus treatment while simultaneously reducing chemical resource requirements. By evaluating the impacts of sewer control on the WRRF, priorities and trade-offs of each must be more explicitly considered.

## 5.2 Future Research Directions

Further investigation is needed into the role of uncertainty in decision making and control strategies at the scale of urban wastewater systems [144]. Uncertainties within these systems arise from a number of sources, including sensor measurements and weather predictions. As a key illustration, consider rainfall measurements and forecasts which are critical for estimating conditions and making decisions in urban water systems. Traditional means of generating these data (e.g., rain gauges, weather radar) are subject to both temporal *and* spatial uncertainties [145]. At the scale of cities, the propagation of both measurement and modeling uncertainties will most

certainly influence control actions. Understanding the robustness of control strategies to these uncertainties is critical for ensuring proper function and mitigating risks of system failure [22, 107]. Even further, evaluation and quantification of uncertainty will be critical for developing effective means to communicate, plan for, and build trust of operators in monitoring and control decision support systems in light of uncertainty [144]. For illustration, consider noise and anomalies present in sensor measurements that will directly or indirectly (through model training and prediction) impact control actions that are dictated, especially in data-driven contexts. In real-time applications, data quality must be assessed and erroneous data corrected to ensure that high fidelity data can be used for a variety of purposes (e.g., model calibration, decision making) [146]. Even in the sensor deployment stage, sensor placement and redundancy to protect against sensor failure are non-trivial problems that must be addressed. This will be particularly important for expanding the deployment of water quality sensors, which require significant maintenance efforts to ensure consistent reliability [147]. Further, literature related to optimal sensor placement is present in the field of water distribution systems [148], yet remains largely unexplored in wastewater and stormwater contexts [117]. Recent work into digital twin applications and real-time calibration is laying the groundwork towards this end [149], but this remains an emerging area of research for urban wastewater systems.

While the goal of this work has been to reside in the context and considerations of real-world systems, significant research efforts must be devoted towards enabling true adoption and implementation of real-time modeling and control in urban wastewater systems. Namely, sociotechnical approaches seek to understand the deep coupling of technical and social aspects of such problems [150]. While some of the technical challenges have been discussed and addressed here, urban wastewater systems are inherently complex and umbrella over numerous stakeholders, each with distinct and often competing priorities and incentives, as well as decision-making processes and abilities [121, 151]. Technological means alone will not be able to overcome these social barriers and fully realize the implementation of real-time modeling and control in urban wastewater systems [150]. Instead, sociotechnical approaches are essential for understanding the underlying organizational structures [43, 152] and developing

context-driven decision support processes [44].

# APPENDICES

# APPENDIX A

# Supplementary Information for Chapter 2.

### Linear Dynamical System Representation

Equation 2.12 can also be represented as a linear dynamical system [65]

$$\dot{h} = Ah + Bp, \tag{A.1}$$

where

$$A = \begin{bmatrix} 0 & \cdots & 0 & 0 & -a_n \\ 1 & \cdots & 0 & 0 & -a_{n-1} \\ \vdots & \ddots & \vdots & \vdots & \vdots \\ 0 & \cdots & 1 & 0 & -a_2 \\ 0 & \cdots & 0 & 1 & -a_1 \end{bmatrix} ; \; B = \begin{bmatrix} b_n - a_n b_0 \\ b_{n-1} - a_{n-1} b_0 \\ \vdots \\ b_2 - a_2 b_0 \\ b_1 - a_1 b_0 \end{bmatrix}. \tag{A.2}$$

Table A.1: Evaluation of GP dry-weather flow prediction via mean NRMSE using various look-back windows for model training. Red text indicates model with best relative performance.

| **Lookback Window** | **Site** | | | | | | | | | |
|---|---|---|---|---|---|---|---|---|---|---|
| | **Q01** | **Q02** | **Q03** | **Q04** | **Q05** | **Q06** | **Q07** | **Q08** | **Q09** | **Q10** |
| 1 Mo | 0.2251 | 0.4123 | 0.2575 | 0.4934 | 0.6043 | 0.4785 | 0.2962 | 0.5922 | 0.3706 | 0.3952 |
| 2 Mo | 0.2560 | 0.4170 | 0.2654 | 0.5174 | 0.6384 | 0.4912 | 0.3211 | 0.6118 | 0.4304 | 0.4171 |
| 3 Mo | 0.2967 | 0.4378 | 0.2839 | 0.5298 | 0.6309 | 0.4906 | 0.3764 | 0.5986 | 0.5165 | 0.4132 |
| 4 Mo | 0.3083 | 0.4217 | 0.2787 | 0.5310 | 0.6253 | 0.4926 | 0.3764 | 0.5895 | 0.4607 | 0.4044 |
| 5 Mo | 0.3293 | 0.4243 | 0.3058 | 0.5302 | 0.6224 | 0.4934 | 0.4098 | 0.5943 | 0.5209 | 0.4081 |
| 6 Mo | 0.3454 | 0.4281 | 0.3093 | 0.5354 | 0.6194 | 0.4983 | 0.4476 | 0.6083 | 0.5170 | 0.4072 |
| 7 Mo | 0.3755 | 0.4312 | 0.3145 | 0.5354 | 0.6273 | 0.5136 | 0.4435 | 0.6064 | 0.5145 | 0.3986 |
| 8 Mo | 0.3985 | 0.4321 | 0.3357 | 0.5357 | 0.6274 | 0.5233 | 0.4523 | 0.6143 | 0.5162 | 0.3914 |
| 9 Mo | 0.4107 | 0.4227 | 0.3345 | 0.5384 | 0.6252 | 0.5204 | 0.4505 | 0.6140 | 0.5220 | 0.3886 |
| 10 Mo | 0.4331 | 0.4107 | 0.3345 | 0.5410 | 0.6245 | 0.5179 | 0.4367 | 0.6183 | 0.5259 | 0.3602 |
| 11 Mo | 0.4479 | 0.4095 | 0.3389 | 0.5526 | 0.6293 | 0.5232 | 0.4245 | 0.6233 | 0.5299 | 0.3367 |
| 12 Mo | 0.4798 | 0.4053 | 0.3314 | 0.5569 | 0.6365 | 0.5310 | 0.4042 | 0.6276 | 0.5315 | 0.3208 |
| 15 Mo | 0.4613 | 0.3692 | 0.3216 | 0.5525 | 0.6267 | 0.5324 | 0.4234 | 0.6176 | 0.5606 | 0.2815 |
| 18 Mo | 0.4455 | 0.3671 | 0.3985 | 0.5724 | 0.6201 | 0.5264 | 0.5270 | 0.6117 | 0.5551 | 0.1537 |
| 24 Mo | - | 0.3415 | - | 0.5470 | 0.6029 | 0.5587 | - | 0.5931 | 0.5640 | -0.0710 |

Table A.2: Evaluation of System Identification for wet-weather flow prediction via mean NRMSE using various lookback windows for model learning. Red text indicates model with best relative performance.

| **Lookback Window** | **Site** | | | | | | | | | |
|---|---|---|---|---|---|---|---|---|---|---|
| | **Q01** | **Q02** | **Q03** | **Q04** | **Q05** | **Q06** | **Q07** | **Q08** | **Q09** | **Q10** |
| 1 Mo | 0.2096 | 0.3475 | 0.3914 | 0.1921 | 0.3510 | 0.0992 | 0.2176 | 0.0646 | 0.1003 | 0.2643 |
| 2 Mo | 0.2803 | 0.3369 | 0.2691 | 0.2250 | 0.3043 | 0.1237 | 0.3525 | -0.0323 | -0.0875 | 0.2590 |
| 3 Mo | 0.2672 | 0.3478 | 0.2894 | 0.2183 | 0.2634 | 0.1214 | 0.3266 | 0.0727 | -0.0870 | 0.3834 |
| 4 Mo | 0.2672 | 0.3125 | 0.4034 | 0.2336 | 0.2713 | 0.0674 | 0.3280 | 0.0656 | -0.2686 | 0.3529 |
| 5 Mo | 0.2672 | 0.3213 | 0.4411 | 0.1796 | 0.2119 | 0.1190 | 0.3758 | 0.1126 | -0.3553 | 0.3588 |
| 6 Mo | 0.2672 | 0.3453 | 0.4586 | 0.1979 | 0.2748 | 0.1259 | 0.4875 | 0.1126 | -0.4484 | 0.3530 |
| 7 Mo | 0.2672 | 0.3665 | 0.4602 | 0.1697 | 0.2488 | 0.1826 | 0.5004 | 0.1148 | -0.3058 | 0.3615 |
| 8 Mo | 0.2672 | 0.4057 | 0.4898 | 0.1591 | 0.2766 | 0.1081 | 0.4242 | 0.1299 | -0.2658 | 0.2526 |
| 9 Mo | 0.2672 | 0.3463 | 0.5256 | 0.1539 | 0.4684 | 0.1339 | 0.4322 | 0.1124 | -0.2654 | 0.2735 |
| 10 Mo | 0.2249 | 0.3633 | 0.5185 | 0.1694 | 0.4615 | 0.1936 | 0.5170 | 0.1688 | -0.2859 | 0.1775 |
| 11 Mo | 0.3304 | 0.3628 | 0.4910 | 0.1626 | 0.4863 | 0.1832 | 0.4558 | 0.1221 | -0.2804 | 0.2285 |
| 12 Mo | 0.3573 | 0.4160 | 0.5266 | 0.1514 | 0.4679 | 0.3009 | 0.4658 | -0.0038 | -0.0004 | 0.1191 |
| 15 Mo | 0.1931 | 0.4014 | 0.4821 | 0.2099 | 0.5637 | 0.2744 | - | - | 0.1692 | 0.0948 |
| 18 Mo | 0.1931 | 0.4443 | 0.5422 | 0.3263 | 0.5618 | 0.2234 | - | - | 0.1607 | -0.4938 |
| 24 Mo | 0.1931 | 0.5411 | 0.3364 | 0.4032 | 0.5660 | 0.1302 | - | - | 0.0848 | -0.1329 |

# APPENDIX B

# Supplementary Information for Chapter 3.

Table B.1: System subcatchment and storage asset physical characteristics.

| **Controllable Storage Asset** | **Directly Contributing Subcatchment Area** $(km^2)$ | **Diameter of In-line Conduit** $(m)$ |
|---|---|---|
| 2 | 1.66 | 4.48 |
| 3 | 5.78 | 2.74 |
| 4 | 21.67 | 4.27 |
| 5 | 2.64 | 4.72 |
| 6 | 0.00 | 4.72 |
| 7 | 0.00 | 4.72 |
| 8 | 6.64 | 4.72 |
| 9 | 5.08 | 3.73 |
| 10 | 13.60 | 4.72 |
| 11 | 3.54 | 3.20 |
| 12 | 6.68 | 3.51 |

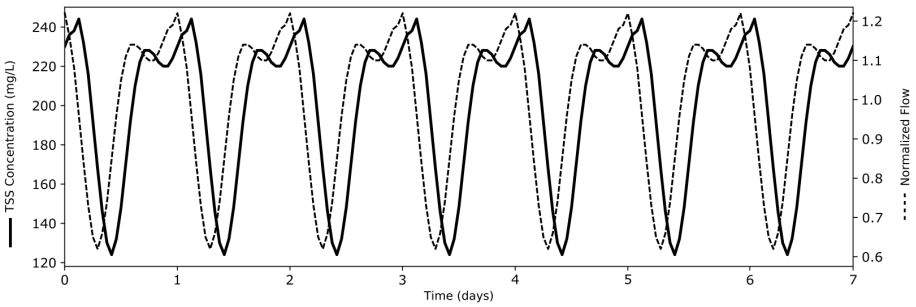


Figure B.1: Dry-weather inputs to the sewer network. The flow and TSS concentration dynamics at each network inlet follow diurnal wastewater patterns, where the magnitude of flow (scaled from the normalized flow shown here) is dictated by the corresponding subcatchment area and TSS has an average concentration of 200 $mg/L$.

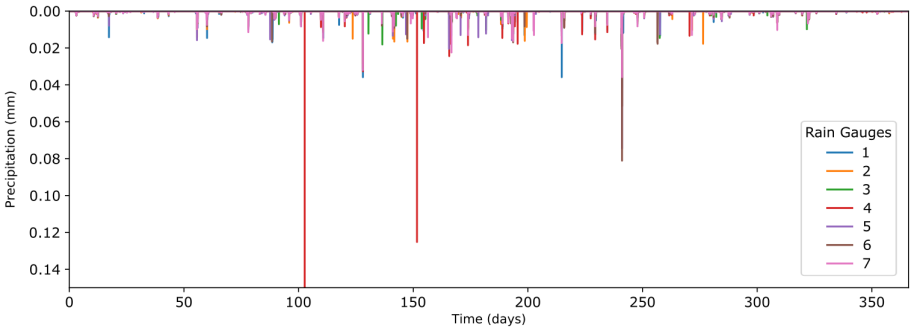


Figure B.2: Precipitation data used for wet-weather inputs into sewer network. Each subcatchment receives precipitation from one of the seven rain gauges.

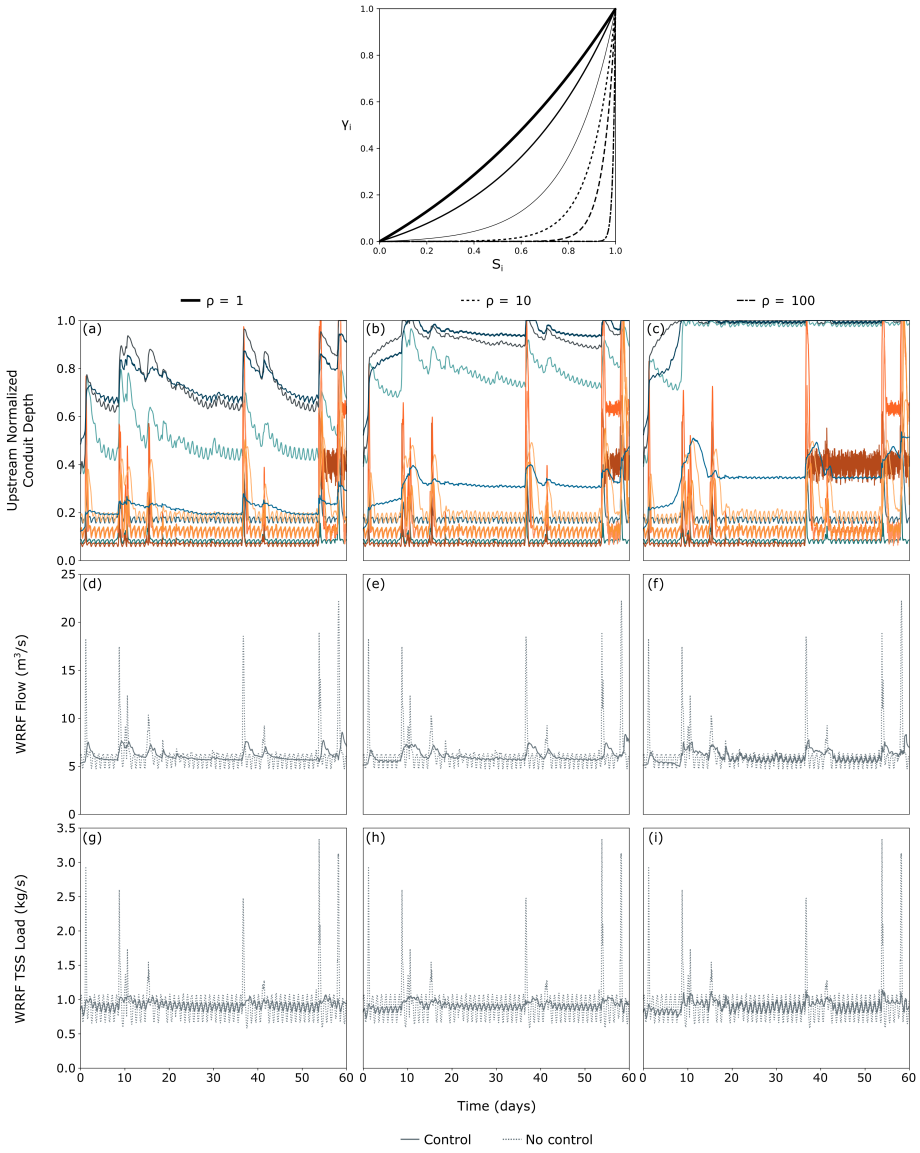


Figure B.3: Comparison of control performance with system importance values $\alpha_1^q = 5.0$ and $\alpha_1^{tss} = 5.0$ during the first two months of the simulation period. Three $\rho$ values used in the state-dependent instantaneous importance $\gamma_i$ are shown in the columns; the upstream normalized depth behind the storage assets, flow at the network outlet, and TSS load at the network outlet are shown in the rows. Dashed and solid lines in (d)–(i) denote uncontrolled and controlled cases, respectively.

# APPENDIX C

# Supplementary Information for Chapter 4

### Dosing Scheme of Ferric Chloride in the GLWA WRRF

In the GLWA WRRF primary treatment system, ferric chloride ($FeCl_3$) is dosed for chemical phosphorus removal. There are two lines that receive WRRF influent from different sections of the sewer network. In the first line, which receives combined sewer flow, ferric chloride is added in a surge basin, which is then followed by a wet well, pump, and preliminary treatment (bar screen and grit removal), before heading to the primary system. In this case, mixing of ferric chloride is considered to be very good. In the second line, which receives sanitary sewer flow, ferric chloride is added after preliminary treatment and before the primary system; mixing is not assumed to be good in this case [128].

The ferric chloride dose for these two lines is determined by dry- and wet-weather operation. During dry-weather, ferric chloride is added at a constant dose of 1.5 $g/m^3$ to the first line (combined sewer), while the second line (sanitary sewer) receives variable ferric chloride dose based on the measured concentration of soluble phosphorus (SP) in the primary effluent; these measurements are taken 2–3 times a day. Specifically, if primary effluent SP is 0.5–0.75 $g/m^3$, a ferric chloride dose of 1.5 $g/m^3$ is used; if SP is 0.75–1.0 $g/m^3$, the dose is 2.0 $g/m^3$; if the dose is >1.0 $g/m^3$, the dose

is 2.5 $g/m^3$. In both lines, if SP is <0.5 $g/m^3$, no ferric chloride is added. When there is a storm event, the ferric chloride dose in both lines is 2.0 $g/m^3$. However, if there has been more than 7 days of antecedent dry-weather, the ferric chloride dose to the first line (combined sewer) is 2.5 $g/m^3$. These elevated doses remain until the measured primary effluent SP concentrations go below 0.5 $g/m^3$ [128].

### Chemical Phosphorus Removal via the HFO Pathway

The chemical phosphorus removal mechanisms as modeled in Sumo include the following reactions:

- Oxidation of ferric cations to form HFO

$$Fe \rightarrow HFO_H$$

- This newly formed HFO can experience:
  - Instantaneous binding of phosphorus species on HFO (denoted by subscript $H$)

$$HFO_H + P \rightarrow (HFO_H + P)$$

    or

  - Aging

$$HFO_H \rightarrow HFO_L$$

    followed by slow binding of phosphorus species (denoted by subscript $L$) due to reduced phosphorus adsorption capacity

$$HFO_L + P \rightarrow (HFO_L + P)$$

- Desorption of phosphorus from HFO can occur in either of the above cases

$$(HFO + P) \rightarrow HFO + P$$

- In all of these cases, aging of HFO will reduce phosphorus adsorption capacity

$$HFO_H \rightarrow HFO_L$$
$$HFO_L \rightarrow HFO_{old}$$
$$(HFO + P) \rightarrow (HFO + P)_{old}$$

- Throughout this, HFO can also be reduced with organic matter back to ferric ions

$$HFO \rightarrow Fe$$

This is summarized in Figure C.1 and the reaction rates used in Sumo are given in Table C.1.

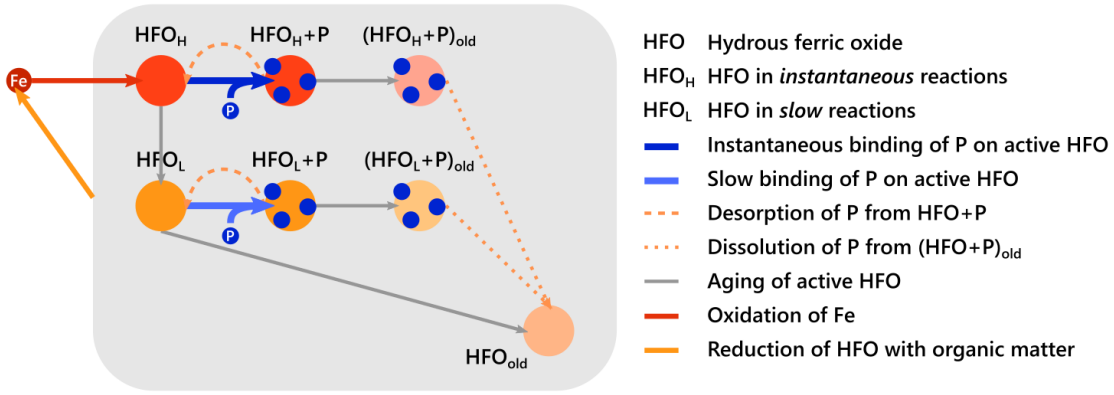


Figure C.1: Reactions between hydrous ferric oxide (HFO) and phosphorus (P) in chemical phosphorus removal, including both instantaneous and slow reactions.

Table C.1: Default hydrous ferric oxide (HFO) kinetics parameters in Sumo, specifically rates of reactions for both (nearly) *instantaneous* (instan.) and *slow* chemical phosphorus (P) removal.

| **Reaction Rates** $(1/d)$ | **Instan.** | **Slow** |
|---|---|---|
| Binding of P on Active HFO | 150 | 1 |
| Desorption of P from HFO | 100 | 10 |
| Dissolution of P from Old HFO | 100 | 100 |
| Aging of Active HFO | 250 | 1 |
| Oxidation of Fe | 1 | |
| Reduction of HFO with Organic Matter | 2 | |

Table C.2: Storm event characteristics in the 75-day simulation period.

| | | Storm | | | | |
|---|---|---|---|---|---|---|
| | | **A** | **B** | **C** | **D** | **E** |
| | **Days** | 15–19 | 22–29 | 29–34 | 50–59 | 67–72 |
| **Volume** ($Mm^3$) | **NA** | 9.7 | 17.3 | 11.9 | 21.3 | 12.2 |
| | **MA** | 9.7 | 17.3 | 11.9 | 21.3 | 12.2 |
| | **SA** | 9.4 | 17.2 | 11.8 | 21.3 | 11.8 |
| **Flow Peak** ($Mm^3/d$) | **NA** | 6.8 | 6.5 | 3.8 | 6.8 | 7.0 |
| | **MA** | 4.4 | 4.1 | 3.6 | 4.9 | 5.0 |
| | **SA** | 3.1 | 3.0 | 2.9 | 3.1 | 3.3 |

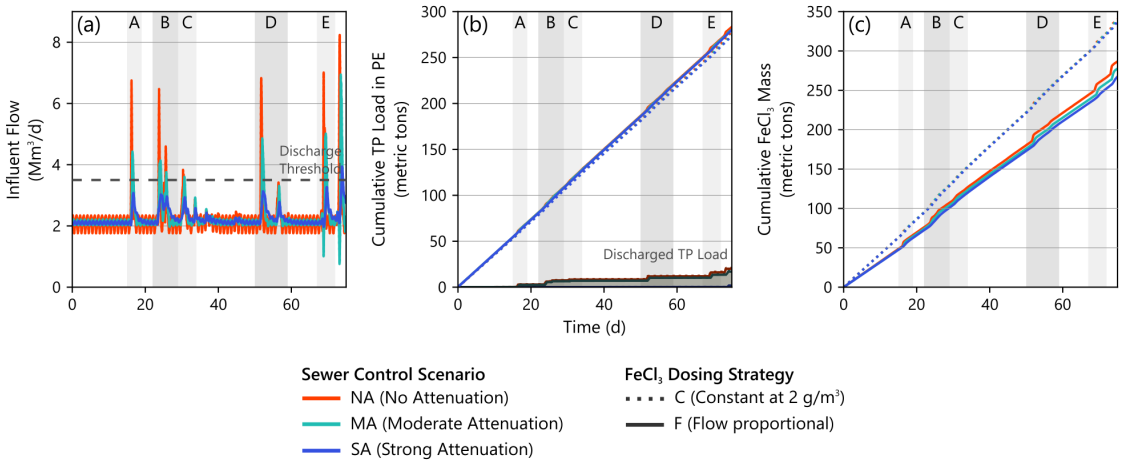


Figure C.2: Impact of sewer control on WRRF response. Time series show (a) WRRF influent flow, (b) cumulative primary effluent TP mass and that discharged after the primary WRRF system, (c) cumulative $FeCl_3$ mass added. These compare sewer control scenarios (different colors: no attenuation, moderate attenuation, strong attenuation) and ferric chloride dosing strategies (line styles: constant at 2 $g/m^3$ and flow proportional with 1.5 $g/m^3$ dose when influent flow is less than 2.1 $Mm^3/d$ and a linear increase in dose proportional to flow). These show all of the 75-day simulation. The grey vertical blocks indicate the five storm events that were isolated within this period and letters at the top of each block indicate the storm event corresponding to Tables C.2 and C.3.

Table C.3: Cumulative performance for each storm event comparing the three sewer control scenarios (no attenuation (NA), moderate attenuation (MA), strong attenuation (SA)) and the two ferric chloride dosing strategies (constant at 2 $g/m^3$ (C), flow proportional (F)).

| $FeCl_3$ Dosing Strategy | Sewer Control Scenario | Cumulative $FeCl_3$ Mass Added (metric tons) | Cumulative TP Mass in Primary Effluent (metric tons) | Cumulative TP Mass Discharged (metric tons) | Cumulative $FeCl_3$ Mass Added (metric tons) | Cumulative TP Mass in Primary Effluent (metric tons) | Cumulative TP Mass Discharged (metric tons) |
|---|---|---|---|---|---|---|---|
| | | **Storm A: Days 15–19** | | | **Storm D: Days 50–59** | | |
| C | NA | 19 | 16 | 3.0 | 43 | 34 | 3.6 |
| | MA | 19 | 15 | 2.5 | 43 | 34 | 3.3 |
| | SA | 19 | 15 | 0.0 | 43 | 34 | 0.0 |
| F | NA | 18 | 16 | 2.9 | 38 | 35 | 3.4 |
| | MA | 17 | 16 | 2.4 | 36 | 35 | 3.2 |
| | SA | 15 | 15 | 0.0 | 35 | 34 | 0.0 |
| | | **Storm B: Days 22–29** | | | **Storm E: Days 67–72** | | |
| C | NA | 35 | 27 | 4.6 | 24 | 20 | 4.5 |
| | MA | 35 | 27 | 4.1 | 24 | 20 | 3.4 |
| | SA | 34 | 27 | 0.0 | 24 | 19 | 0.0 |
| F | NA | 31 | 28 | 4.5 | 22 | 20 | 4.3 |
| | MA | 30 | 28 | 4.0 | 22 | 20 | 3.3 |
| | SA | 29 | 28 | 0.0 | 19 | 19 | 0.0 |
| | | **Storm C: Days 29–34** | | | | | |
| C | NA | 24 | 19 | 0.94 | | | |
| | MA | 24 | 19 | 0.52 | | | |
| | SA | 24 | 19 | 0.00 | | | |
| F | NA | 20 | 19 | 0.93 | | | |
| | MA | 20 | 19 | 0.52 | | | |
| | SA | 19 | 19 | 0.00 | | | |

### Impact of Temperature on Chemical Phosphorus Removal

To examine the impact of temperature on chemical phosphorus removal, the 75-day simulation for the C (constant ferric dose), NA (no attenuation) case was conducted at temperatures of 10, 20, and 30°C (original simulations were at 20°C). The cumulative total phosphorus (TP) mass in the primary effluent (metric tons) at these temperatures are shown in Table C.4. From these results, varying the temperature ±10°C (from 20°C) changes the total phosphorus mass by only 0.4%.

Table C.4: Impact of temperature on chemical phosphorus removal for the C,NA case and the 75-day simulation.

| **Temperature (°C)** | **Cumulative TP Mass in Primary Effluent (metric tons)** |
|---|---|
| 10 | 278 |
| 20 | 278 |
| 30 | 277 |

To ground these results in the underlying modeled mechanisms, note that temperature plays a limited role in chemical phosphorus removal reactions as developed in Hauduc et al. [133]. Specifically, only rates of Fe oxidation and HFO reduction with organic matter are temperature corrected using the Arrhenius equation. This temperature correction modeled as:

$$q_T = q \cdot \theta^{T-T_{base}}$$

where $q$ is the base reaction rate, $\theta$ is the Arrhenius coefficient for the reaction, $T$ is the temperature of interest, and $T_{base}$ is the base temperature (20°C). For both Fe oxidation and HFO reduction, the Arrhenius coefficient is $\theta = 1.040$. The base reaction rate for Fe oxidation is $q_{Fe,OX} = 1.0d^{-1}$ and the base reaction rate for HFO reduction is $q_{HFO,RED} = 2.0d^{-1}$. Thus, for $T = 30°C$, the temperature-corrected

reaction rates for Fe oxidation and HFO reduction are respectively:

$$q_{30^\circ C,Fe,OX} = q_{Fe,OX} \cdot \theta^{T-T_{base}} = 1.0d^{-1} \cdot 1.040^{30^\circ C-20^\circ} = 1.48d^{-1}$$
$$q_{30^\circ C,HFO,RED} = q_{HFO,RED} \cdot \theta^{T-T_{base}} = 2.0d^{-1} \cdot 1.040^{30^\circ C-20^\circ C} = 2.96d^{-1}$$

and for $T = 10^\circ C$,

$$q_{10^\circ C,Fe,OX} = q_{Fe,OX} \cdot \theta^{T-T_{base}} = 1.0d^{-1} \cdot 1.040^{10^\circ C-20^\circ C} = 0.68d^{-1}$$
$$q_{10^\circ C,HFO,RED} = q_{HFO,RED} \cdot \theta^{T-T_{base}} = 2.0d^{-1} \cdot 1.040^{10^\circ C-20^\circ C} = 1.35d^{-1}$$

While these temperature-corrected reaction rates are up to 50% different than the base rates, other reaction rates, which are not temperature dependent, are still orders of magnitude greater. These include that of instantaneous phosphorus binding on HFO at 150 $d^{-1}$, $HFO_H$ aging at 250 $d^{-1}$, and desorption of phosphorus from HFO at 100 $d^{-1}$. This thus results in minimal impacts of temperature on chemical phosphorus removal, as evidenced here.

### Impact of Primary Clarifier Model on Chemical Phosphorus Removal

To consider the impact of the primary clarifier model on chemical phosphorus removal, the original choice of a volumeless point separator was changed to a three compartment model in Sumo. This change specifically allows for volume, and thus time for reaction, in the primary clarifier, and thus possibly increased phosphorus and HFO reactions. This three compartment model was designed to have a dry-weather average hydraulic residence time (HRT) of 2 hr (the dry-weather average flow is 2.1 $Mm^3/d$ and the clarifier volume is 175,000 $m^3$). Based on conversation with personnel at the Great Lakes Water Authority (GLWA), the time between WRRF influent and primary effluent is approximately 1.5–2 hrs [128]. Thus the HRT in this three-compartment model will be slightly more than the estimate of the real WRRF primary system. The solids percent removal was kept consistent with that of the volumeless point separator primary clarifier (70%), as observed in previous study for the GLWA WRRF [130].

For this comparison, the 75-day simulation was conducted for the C (constant ferric dose), NA (no attenuation) case. Table C.5 compares the cumulative orthophosphate ($SPO_4$) and total phosphorus (TP) mass in the primary effluent for the volumeless point separator and three compartment primary clarifier models. The additional 2 hrs of reaction time in the three compartment model yielded a reduction of approximately 3 metric tons in primary effluent phosphorus mass over the 75-day simulation; this is a 1.96% reduction in orthophosphate mass and 1.08% reduction in total phosphorus mass. Because this 3 metric ton reduction is observed in the *orthophosphate* mass, it is concluded that this is the result of additional binding and co-precipitation between soluble phosphorus species and HFO occurring in the primary clarifier. This is a relatively small difference despite the substantially large addition of HRT and is likely due to balance struck between HFO-P binding and HFO aging. As discussed previously, aging of HFO decreases its phosphorus adsorption capacity. Note that aging of fresh HFO ($HFO_H$) has a reaction rate of 250 $d^{-1}$, while the reaction rate of instantaneous phosphorus binding with fresh HFO is 150 $d^{-1}$ and slow binding with aging HFO is 1 $d^{-1}$. Thus, as HRT increases, there is substantial aging of HFO and HFO-P binding ability plateaus.

Table C.5: Impact of primary clarifier model on chemical phosphorus removal for the C,NA case and the 75-day simulation, comparing both orthophosphate and total phosphorus for the volumeless point separator and three compartment clarifier model.

| | **Cumulative P Mass in Primary Effluent (metric tons)** | |
|---|---|---|
| **Clarifier Model** | **$SPO_4$** | **TP** |
| Volumeless Point Separator | 153 | 278 |
| Three Compartment | 150 | 275 |

# APPENDIX D

# `pystorms`: A Simulation Sandbox for the Development and Evaluation of Stormwater Control.

Full paper in preparation for submission. In collaboration and co-authored with S. P. Rimer (Argonne National Laboratory), A. Mullapudi (University of Michigan), B. Kerkez (University of Michigan).

## D.1 Introduction

The advent of smart cities is poised to transform the management of our built environment [153, 154]. Specific to stormwater, a new generation of smart and connected stormwater systems promises to reduce flooding and improve water quality management by autonomously sensing watershed parameters and subsequently controlling corresponding hydraulic components across complete watersheds, both *adaptively* and *in real-time*. These smart systems will provide an alternative to costly concrete-and-steel construction by squeezing even more performance out of existing stormwater and sewer infrastructure, and reimagining the design and operation of new infrastructure. While the idea of controlling distributed stormwater systems in real-time dates back to the 1970s [155], the concept has only recently gained

widespread traction in large part due to the affordability of internet-connected sensors, the increased capacity of data services, and the broader acceptance and popularity of other autonomous systems (e.g. self-driving cars and robots). Relative to other fields of autonomy, however, smart water systems are still early in their stage of adoption. Thus, developing and implementing smart water systems presents an exciting opportunity for researchers and practitioners alike to propose new visions, standards, and technologies.

The intelligence of smart stormwater systems broadly refers to the acquisition (i.e. "sensing") and processing of data into decisions and actions (i.e. "control strategies") that are then used to guide the operation of gates, valves, pumps, and other actuators within a water system. Ultimately, the logic embedded via these control rules determines how water is moved around the collection system to meet specific performance objectives or reduce adverse outcomes (e.g. flooding, overflows, and/or water quality impairments). As such, the emerging field of smart stormwater systems stands to benefit greatly from researchers and stakeholders who can bring to bear new control strategies and techniques.

However, due to the complex, bureaucratic nature of watershed management, it can be impenetrable for new groups working in this field to obtain the necessary details of how real-world stormwater systems operate, as those details are unlikely to be opened up to just anyone who wants to try out new ideas of controlling them. To that end, computational toolchains exist for simulating stormwater systems and then evaluating various control rules implemented by them. Yet, developing these simulations and adapting them to specific control strategies often requires a significant amount of effort and expertise. Furthermore, while a number of promising control algorithms have been proposed, they have all been evaluated on highly specific examples and simulators, making it difficult to establish cross-comparisons of their performance. In an effort to address these limitations, the contribution of this paper is `pystorms`, an open-source Python package comprised of:

(i) A collection of real world-inspired smart stormwater control scenarios that facilitate the quantitative evaluation of control strategies, coupled with

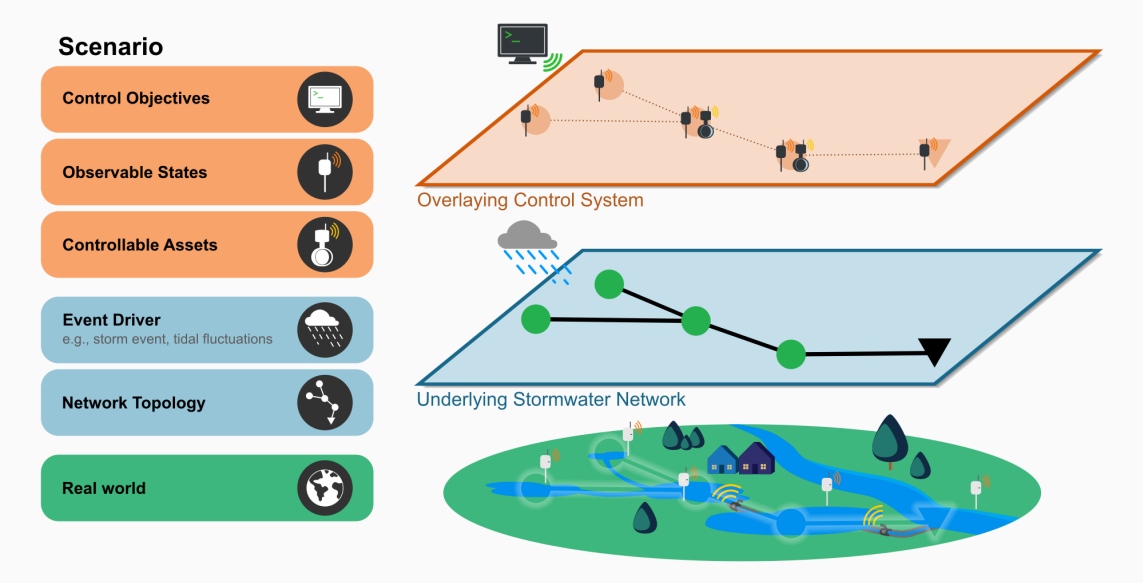


Figure D.1: `pystorms` abstracts the control of stormwater systems as scenarios, which are characterized by a computational representation of a stormwater network, a corresponding event driver, set of observable states, and controllable assets that can be leveraged to manipulate the behavior of a stormwater network in real-time to achieve control objectives. This is coupled with a streamlined programming interface and a stormwater simulator to provide the users with a standalone package for the development and evaluation of control algorithms.

(ii) A programming interface and a stormwater simulator to provide a stand alone package for developing stormwater control strategies.

Our aspiration is for `pystorms` to emerge as a community-driven resource that fosters accessibility and collaboration amongst smart stormwater control's field of researchers and practitioners, both novices and experts alike.

## D.2 Background

### D.2.1 Control of Stormwater Systems

A stormwater control problem can be defined as the development of an infrastructural strategy to manipulate the behavior of stormwater in order to achieve a

desired response. Traditionally, stormwater control has relied on *passive* solutions, in which control strategies are large-scale, construction-heavy, and often financially-burdensome. However, the emergence of microcontrollers, wireless communication technologies, and low-cost sensors has allowed for small-scale, modular, and automated control components (e.g. hydraulic valve operated by cellularly-connected actuator) to be installed at strategic locations throughout a stormwater network for *active* control, with decisions that can be automated, adjusted remotely, and made in real-time. Consequently, stormwater infrastructure can now be instantly redesigned to respond to its dynamic environment.

Although implemented smart stormwater control engineering solutions were documented at least a decade earlier, research-oriented discussion of these implementations did not occur until 1989 [156]. Furthermore, while implementation of smart stormwater control began at the end of the 20th-century, the 21st-century has seen far more extensive systematic successes, as seen beginning with the foundational reviews of Schütze et al. [54] and Vanrolleghem et al. [16]. Some notable adaptive real-time stormwater control implementations that have been installed hand-in-hand with extensive research dissemination include Mullapudi et al. [23], García et al. [90], Ocampo-Martinez [93], Montestruque [96], Gaborit et al. [98], Vezzaro and Grum [107], Gaborit et al. [116], Sadler et al. [157]. These references we specifically emphasize as to us they represent diverse and well-documented implementations of smart stormwater control from single control assets to watershed-scale implementations. For more comprehensive reviews of stormwater control implementations, we direct the reader to some recently published survey articles on the topic [14, 85, 90, 121, 158].

#### D.2.1.1 Simulating Stormwater Systems

Due to the variability of storm events and the safety concerns of experimental uncertainty, it is infeasible to test various control strategies on *actual* stormwater networks. Thus, a more practical method to test the outcomes of different control decisions is to use a computational simulation of a stormwater network that is able

to give us a "good enough" estimate of what the actual in-situ physical results might be. Often, these simulations can be carried out using computational stormwater models that have already been developed to inform the design and operation of the stormwater system being studied.

As a stormwater system is designed to route rainfall and other runoff to a wastewater treatment plant and/or discharge to a receiving body of water, the computational components of stormwater models primarily include a (i) runoff module and (ii) a routing module, and are driven by (iii) precipitation events (e.g. rain, snow). The runoff module converts precipitation into overland runoff; the overland runoff then undergoes hydrological processes (e.g. infiltration, evaporation) and is hydraulically transported to the stormwater collection system, which is carried out computationally via the routing module.

Over the years, several different software applications have been developed for modeling and simulating stormwater networks. The different software applications all function in a similar manner in which they computationally estimate the dynamics of stormwater as it moves through predefined temporal and spatial bounds to varying degrees of mathematical accuracy and fidelity to the underlying hydraulic and hydrological governing processes. The US-EPA's Stormwater Management Model (SWMM) [114], MIKE URBAN+ from the MIKE Powered by DHI software suite[1], and the Model for Urban Stormwater Improvement Conceptualisation (MUSIC) by eWater[2] are a few examples of widely-used stormwater software applications. Furthermore, in addition to modeling runoff and its routing, some of these software applications have also been developed with the capabilities of modeling urban flooding (e.g. MIKE FLOOD) as well as the generation and transport of pollutants (e.g. SWMM). The computational details underlying the models produced by these software applications are not the purpose of this paper, and instead for clarity and further detail, the reader is directed to Rossman and Huber [159], Rossman [160], and Rossman and Huber [115]. Additionally, we provide further detail about the hydraulic simulator we utilize in Section D.3.3.

[1] mikepoweredbydhi.com
[2] ewater.org.au

#### D.2.1.2 Implementing Control

For those unfamiliar with control theory and control systems engineering, the field can be evasive. Here, we aim to maintain the idea of control in its broadest but most straightforward meaning: after receiving some sort of *cue* (for our systems, this cue may be readings from sensors), an *action* is taken on the system to alter it for a desired outcome (an action for stormwater systems may be as simple as the opening and closing of a valve). When we implement *control*, we are making decisions and taking actions that try to optimize our system in order to meet some specified objective. Thus, a stormwater control strategy can be simplified as the method of developing rules that determine actions to be implemented by the stormwater system. The computational process of implementing this method to find these actions is what we define as the *stormwater control algorithm*.

It is easy to imagine how finding the "best" actions to implement is a complex undertaking. Suppose a stormwater system with only one valve was installed, and that valve could be either completely opened or closed every hour. Deciding on a pattern for the complete opening and closing of the valve — even over the period of a few days — in order to meet some sort of objective is actually quite difficult, with no guarantee of a singularly "correct" solution. Now, imagine if the action could be to open the valve as a percentage between 0–100% — the combination of actions that can be implemented becomes even more endless. From an initial perspective, this process of finding the "best" and "correct" solution from what is an inexhaustible set of possibilities might seem futile. However, for stormwater applications, finding such an absolute "best" solution is usually not necessary, and most likely does not even exist. Instead, a solution that provides a "better" outcome than the current one is often sufficient and can still drastically benefit the system. Additionally, such better solutions are actually dependent on how a system's underlying needs are even defined. That is, *how we define the objective determines what is considered optimal*. Thus, research on stormwater control focuses on both (i) the formulation of control objectives and (ii) analyzing and differentiating the myriad potential solutions based on said formulations. While the former research is essential in this field, it is not

the focus of this paper. Rather, our initiative here concentrates on the latter: via the presented simulation sandbox `pystorms`, we aim to develop a systematic means for analyzing and differentiating control solutions for stormwater systems with predefined objectives.

Thus far, we have discussed "smart stormwater control" in its broadest sense, which encompasses all layers that a smart stormwater control system would entail — from the sensors chosen, the communication protocol implemented for those sensors, the data management of what is sensed, the wireless actuators controlling a control asset, even to the human operators who may interact or intervene physically with the system. However, from here on out, we focus our discussion of smart stormwater control strategies strictly on *the computational algorithm that is used to determine the discrete actions to be taken by the system's control assets based on information known regarding the system's past, current, and/or future state.* This algorithm can allow for the control strategy to be implemented and adjusted over any number of given time periods, and can be coordinated amongst any number of control assets within the system. By focusing strictly on the computational algorithm, we are able to isolate one component of smart stormwater systems that can allow for *quantitative* cross-comparisons of strategies used across a multitude of stormwater systems. Additionally, the focus on the computational algorithm also centers the component of a smart stormwater system that can specifically benefit from experts outside the discipline of water resources engineering.

### D.2.2 The Need for a Simulation Sandbox

Even though smart stormwater control has been successfully implemented for decades, there still does not exist a standard to systematically evaluate the performance of different control strategies across diverse stormwater networks and contexts. Consequently, this inability to systematically evaluate smart stormwater control directly impedes our field's ability to bring new and necessary expertise to solve some of our most essential and complex problems.

As demonstrated by the smart stormwater control survey papers referenced in

Section D.2.1, this desire for direct and systematized comparisons of control strategies is not an isolated realization. While there have been previous efforts to introduce benchmarking stormwater networks for evaluating control strategies [41, 161], we identify the need to make available a more extensive assortment of example stormwater networks to the broader research community. This assortment of networks must be both nonexclusive and nonrestrictive, and capture the complexity and diversity of features unique to stormwater. Furthermore, we recognize that there is a need for an unambiguous programming interface that explicates the computational backend and aids researchers to easily utilize the example networks for prototyping stormwater control solutions.

We developed `pystorms` as a Python-based *simulation sandbox* to accelerate a researcher's ability to computationally simulate and evaluate stormwater control strategies. `pystorms` provides a collection of diverse stormwater control scenarios, which are drawn from real-world urban watersheds to encompass diverse features appertaining to stormwater systems. These scenarios are coupled with a stormwater simulator and streamlined programming interface, which together provide researchers with a standalone package that focuses its usage on stormwater control algorithm development and testing. Our intention is that `pystorms` reduces the programming learning curve that can be a barrier to those aspiring to learn stormwater control, and also curates an open repository of smart stormwater control examples which foster the development and evaluation of any number of new control strategies applied to them. In the following section, we present a detailed overview of the design and architecture of `pystorms`, and how it facilitates the systematic evaluation of stormwater control strategies.

## D.3 `pystorms`

Developed in Python, `pystorms` is supported on all major operating systems (OSX, Windows, and Linux) and can be installed using `pip`[3]. `pystorms` is distributed

[3] pypi.org/project/pystorms

Table D.1: Terminology defined for the `pystorms` package and to delineate stormwater scenarios.

| | |
|---|---|
| **Network Topology** | We distinguish a *network* to be the physical system of conduits (e.g. pipes, culverts), storage elements (e.g. retention and detention basins), and any other subcatchment infrastructure (e.g. green infrastructure, wetlands) that collect, convey, and/or treat stormwater runoff. |
| **Event Driver** | Any inputs or "disturbances" to the network that govern the generation and flow of runoff are defined as event drivers. Most often, an event driver is the precipitation generating runoff in the watershed. It can also include wastewater flows, tidal fluctuations of connected water bodies, or any other such phenomenon that influence the flow of runoff in the network. |
| **Controllable Assets** | Any elements (e.g. basins, wetlands, CSO pump stations) that are equipped with valves, pumps, or any other flow control infrastructure that can be actuated to manipulate stormwater flow. |
| **Observable States** | The collection of states in the network (e.g. water levels, flows, pollutants) that can be accessed by the users during a simulation. |
| **Control Objectives** | The overall goal or set of goals (e.g. preventing flooding, improving water quality, reducing erosion) of manipulating the behavior of a stormwater network using controllable assets during a simulation. The ability of a controller to achieve a particular objective is quantified using a performance metric. |

under the GNU General Public GPLv3 license[4], which ensures that this package and its derivatives remain open-source and can be used free of cost. Additionally, source code for the package is available on Github[5], alongside comprehensive documentation and tutorials to utilize and contribute to its broader development[6].

Table D.2: `pystorms` includes a curated collection of real world-inspired stormwater scenarios for developing and quantitatively evaluating the performance of stormwater control algorithms.

| Scenario | Network | Control Objectives |
|---|---|---|
| `theta` | 2 $km^2$ idealized separated stormwater network | Maintain the flows at the outlet below a threshold and avoid flooding (2 storage basin outlets) |
| `alpha` | 0.12 $km^2$ residential combined sewer network | Minimize total combined sewer overflow volume (5 weirs at interceptor connections) |
| `beta` | 1.3 $km^2$ separated stormwater network with a tidally-influenced receiving river | Minimize flooding (1 detention pond outlet, 1 storage basin outlet, 1 pump) |
| `gamma` | 4 $km^2$ highly urban separated stormwater network | Maintain channel flows below threshold and avoid flooding (11 detention pond outlets) |
| `delta` | 1.7 $km^2$ combined sewer network in which the stormwater ponds also serve as waterfront | Maintain water levels within upper and lower thresholds for water quality and aesthetic objectives (5 storage basin outlets) |
| `epsilon` | 67 $km^2$ highly urban combined sewer network | Maintain sewer network outlet TSS load below threshold and avoid flooding (11 in-line storage dams) |
| `zeta` | 1.8 $km^2$ combined and separated sewer network (based on the Astlingen benchmarking network [161, 162]) | Maximize flow to downstream wastewater treatment plant and minimize total combined sewer overflow volume (4 storage basin outlets) |

### D.3.1 Scenarios

`pystorms` abstracts smart stormwater systems as *scenarios*. Each scenario is described by (i) *an underlying stormwater network*–which includes the network's topology (e.g. a sewer system draining into a water body) and its event driver (e.g.

[4] gnu.org/licenses/gpl-3.0.html
[5] github.com/kLabUM/pystorms
[6] open-storm.org/pystorms

storm event)–and its *overlaying control system*, which includes a set of observable states (e.g. water levels), controllable assets (e.g. basins with controllable valves at outlet), and a specific control objective (e.g. preventing flooding). The specific terminology for a scenario in `pystorms` is described in further detail in Table D.1, and the corresponding delineation between (i) and (ii) is illustrated in Figure D.1.

By abstracting our stormwater systems as scenarios, we are able to create new scenarios with relative ease by interchanging different scenario components. For example, let us assume we have evaluated a control algorithm when applied to an individual scenario. We can now broaden our inquiry and test the algorithm's *scalability* by interchanging components of our scenario's overlaying control system (e.g. sequentially increase its number of controllable assets), and evaluating the algorithm on this newly derived set of scenarios. Similarly, we can quantify the *generalizability* of a control algorithm as it is applied to a specific control objective (e.g. maintaining water level set points) by systematically altering the underlying stormwater network (e.g. cycle through a set of design storms as the event driver) while retaining the overall control system. We can then calculate a performance metric of the algorithm when applied across this new subsequent set of scenarios. Thus, not only can can now evaluate a control algorithm applied to an individual stormwater scenario, but we can also evaluate it more universally when applied across a spectrum of these interchanged scenarios.

`pystorms` provides an collection of seven scenarios, drawn from real-world smart stormwater systems across North America and Europe and named as a letter from the Greek alphabet. The collection of scenarios span a multitude of stormwater systems that address a diverse set of urban watershed needs with various smart control objectives. The subcatchment areas range from 0.12–67 $km^2$ in size, and include both combined and separated stormwater arrangements. A brief summary of the collection's scenarios are presented in Table D.2, with their more detailed descriptions provided throughout this paper's appendices.

While our aim is for this collection of scenarios to be representative of a myriad of smart stormwater control, we recognize that it is certainly not exhaustive. As such, we aspire to grow the `pystorms` repository of stormwater scenarios through

community-driven contributions of new scenarios. Accordingly, we provide extensive documentation [7] for users to contribute their own scenarios, or modify the existing ones.

To demonstrate what is a scenario in the context of `pystorms`, we present here Scenario `theta`, an idealized stormwater network that can be used for rapid prototyping of control strategies. Scenario `theta`'s *network topology* can be described as two 1000 $m^3$ storage basins connected in parallel and draining through a shared outlet into a downstream water body. The *event driver* is a synthetic rain event lasting 9 *hr* with a peak intensity of 3.2 *in*. We stipulate the *observable states* to be the water levels at the two basins at each 15 *min* time-step of the simulation, and the *controllable assets* are outlet valves of both storage basins adjustable at each time-step between 0–100% open. The *control objective* is to maintain the outflow into the downstream water body below a specified threshold of 0.5 $m^3 s^{-1}$, while simultaneously preventing flooding at the basins. The ability of a control strategy to meet `theta`'s control objective is quantified using a pre-defined performance metric that computes a penalty for violating the control objective at each time-step, and sums these penalties across the whole simulation. We provide the specific details on this performance metric (Equation D.1a) in Section D.4 where we evaluate the performance of two different example control strategies applied to `theta`.

### D.3.2 Programming Interface

The `pystorms` programming interface is inspired by the principles of control theory, where the control of a system is abstracted as an iterative process (also known as a control loop) in which a controller monitors the underlying state(s) of the system of interest, and makes calculated adjustments — via control actions — to the system for it to achieve a desired behavior. In the context of smart stormwater control, our system of interest is our stormwater network, and the states and control actions are represented by the set of observable states and the specific control asset configurations (e.g. valve positions and pump settings). Thus, we have discretized

[7] open-storm.org/pystorms/docs/build-scenarios

```python
import pystorms


def controller(state):
    # your control algorithm goes here
    return actions


# initialize scenario
env = pystorms.scenarios.theta()
done = False

while not done:
    # query current state
    state = env.state()
    # compute the control action
    actions = controller(state)
    # implement the action
    done = env.step(actions)

# check your controller's performance
env.performance()
```

Figure D.2: `pystorms` provides a high-level abstraction for simulating control in stormwater networks for users to quantitatively evaluate the performance of control strategies with minimal overhead.

the simulation of stormwater control in `pystorms` as the following series of steps:

1. **Query the set of observable states** for specified locations in the stormwater network at the current time-step; then potentially use these queried states to
2. **Compute control actions** to manipulate the system to achieve a desired behavior; and finally,
3. **Implement the control actions** by adjusting the settings of the controllable assets that serve as inputs into the underlying system.

We initialize a `pystorms` scenario by creating an instance of it using the statement: `pystorms.scenarios.<scenario name>()`. As seen in Figure D.2, `theta` is initialized with `pystorms.scenarios.theta()`. The initialization then configures

the stormwater simulator with the computational representations necessary to simulate the respective scenario, and returns it as a Python object. This Python object (`env` in Figure D.2) can be used to progress and/or pause the stormwater simulator, read and/or write parameters to the network, and utilize any additional `pystorms` functionality. The current state of the underlying stormwater network in the scenario can be queried using the `<scenario object>.state()` call (`env.state()` in Figure D.2). `<scenario object>.step(<actions>)` implements the control actions in the stormwater network, progresses the simulation forward a time-step, and returns the current status of simulation (`True` when the simulation has terminated and `False` otherwise). In Figure D.2, `done = env.step(actions)` implements `actions` in the stormwater network and progresses the simulation being handled by the `env` Python object, which in this case is the Scenario `theta`. `done` is assigned `True` when the simulation has terminated, and `False` otherwise.

During the each time-step of the simulation, the ability for the implemented control actions to achieve the scenario's control objective are evaluated by computing the time-step's corresponding performance metric. This computed value is then stored for each time-step, and can be accessed at any time during the simulation using `<scenario object>.performance()` (`env.performance()` in Figure D.2). Additional parameters are logged throughout the simulation. While an initial set of these logged parameters is predefined, the user is able to customize this set for any additional parameters of interest.

The series of steps for implementing a control loop into our stormwater simulation is seamlessly integrated throughout the `pystorms` programming interface. Users carry out Step 1 using `<scenario object>.state()`, and Step 3 using `<scenario object>.step(<actions>)`. Separated out to be defined by the user is the controller (Step 2), which maps the observed states to control actions. While implementing the controller into `pystorms` is ultimately left to the user, for our example presented here, we implement it as a Python function block (see Figure D.2).

### D.3.3 Architecture

The `pystorms` architecture follows the object oriented programming paradigm which relies on classes as its core building blocks. This style of software architecture was chosen to allow `pystorms` to be modular such that users can customize it to meet their own specific requirements and/or workflows. While the `pystorms` programming interface is designed with the intent to be intuitive for all potential users, it particularly caters to those who may only have a rudimentary understanding of stormwater dynamics and/or basic familiarity with programming in Python. However, it can also be easily customized to meet the requirements of researchers who want to incorporate advanced functionality, such as custom water quality or rainfall-runoff modules (for details on how to utilize `pystorms` modularity and customization, we again direct the reader to its online documentation).

The `pystorms` architecture is organized to accomplish two tasks: (1) the configuration of the scenario metadata, and (2) the simulation of the stormwater network. These two tasks are carried out using three core interacting modules: `environment`, `scenario`, and `config`. These three modules interface with each other to build and execute the various scenarios. Figure D.3 provides a schematic of this architecture. The first two modules handle the stormwater simulation, while the latter handles the computational representation of the stormwater networks and the metadata pertaining to the control problem (i.e. states, actions, and objectives).

#### D.3.3.1 Configuration

The `config` module is used to manage the configuration in the `pystorms` architecture. `config` contains a configuration file for each scenario, which delineates the stormwater network, its set of observable states and controllable assets, and the set of parameters that are used to compute its control objective's corresponding performance metric. The configuration files are written using YAML, a mark-up language commonly used for developing configuration files in software applications. With YAML, the parameters of interest defined in the configuration file are formatted as vertical lists rather than data structures. As a result, the configuration file be-

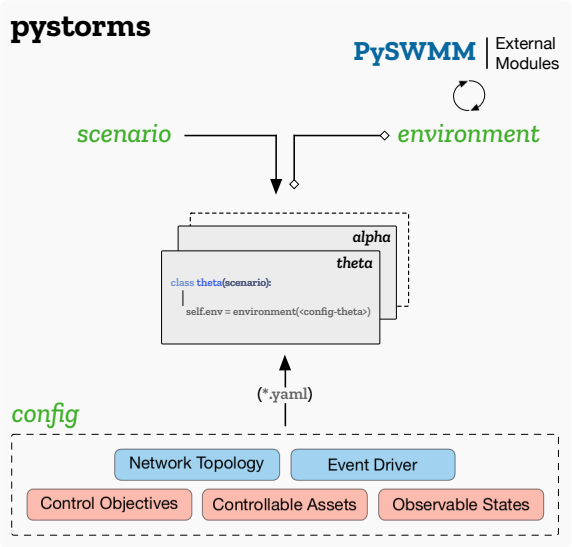


Figure D.3: `pystorms` is built with three interacting core modules: (i) `config` represents the metadata and computational representations of the stormwater network and event driver; (ii) `environment` acts as an interface for scenarios to interact with the stormwater simulators; and (iii) `scenario` provides a consistent structure for the scenarios in the package. A scenario object in `pystorms` inherits (represented by arrows) from the base `scenario` class, and interfaces (represented by line) with the stormwater simulator though the `environment`.

comes more human-readable, and creates a scalable and easy workflow for developing scenarios.

#### D.3.3.2 Simulation

Scenarios in `pystorms` are implemented as Python classes. To ensure consistent functionality across scenarios, each scenario is instantiated as its own independent class with an inherited structure from a base `scenario` module. The scenario classes interface their corresponding configuration files with the stormwater simulator and implement any of the functions specific to that scenario (e.g. functions used for computing performance metrics of corresponding control objectives).

The `environment` module is the interface between the stormwater simulator (e.g. EPA-SWMM) and the scenarios. This module is specifically included to ensure

`pystorms` is able to remain agnostic to whatever stormwater simulator is used. For instance, if a user wants to utilize a customized hydrologic solver for simulating stormwater, they can do so by modifying the `environment` module to call their solver when the scenarios query it, thus ensuring compatibility to a wide array of simulators with minimal overhead.

`pystorms` uses SWMM as its default stormwater simulator. SWMM, developed by the US-EPA, is an open-source stormwater simulation model that is extensively used for the design and analysis of stormwater systems across the world. SWMM is built with the C programming language, a low-level language that results in significant computational efficiency. However, the trade-off for using C is SWMM's difficulty to be interfaced with the latest scientific libraries. As a result, there have been several efforts over the years to build wrappers for SWMM such that its functionality can be exploited via high-level programming languages, such as Python.

PySWMM is a Python implemented package that not only provides a wrapper to communicate with SWMM, but also yields a high-level user interface for querying the various stormwater parameters. `pystorms` — by means of the `environment` module — interfaces with SWMM using PySWMM, and as a result, all functionality included in PySWMM can also be accessed using `pystorms`. Readers are directed to the documentation for additional details and examples to customize `pystorms` to meet their requirements.

## D.4 Demo: Evaluating Control Strategies

Throughout this section, we demonstrate how `pystorms` facilitates developing smart stormwater control strategies by evaluating the performance of two control algorithms applied to Scenario `theta`.

While there exist many control strategies that can be adopted to achieve `theta`'s control objective, to simplify our illustration of `pystorms`, we implement two basic control strategies here. The algorithms used to implement the control strategies are described below and in Figure D.4. Both control strategies are simple reactive control strategies, in which the valve settings of `theta`'s two basin outlets are adjusted to

**Algorithm 2:** Equal-Filling Control Algorithm: Let $i$ be a tank in the network of $\mathcal{N}$ tanks. In scenario theta, $\mathcal{N} = 2$ and Max depth in each tank is 2.0m

Let $\lambda$ be the target flow to be achieved
**for** *all* $\mathcal{N}$ *tanks* **do**
    Compute the *filling degree*; $f_i = {}^{\text{depth}_i}/_{\text{Max depth}_i}$
Estimate the *average filling degree*; $\bar{f} = \Sigma_i^N \, {}^{f_i}/_N$
**for** *all* $\mathcal{N}$ *tanks* **do**
    Let $\psi_i = f_i - \bar{f}$
    **if** $\psi_i < 0.0$ **then**
        $\psi_i = 0.0$
    **else if** $\psi_i = 0.0$ **then**
        $\psi_i = \bar{f}$
**for** *all* $\mathcal{N}$ *tanks* **do**
    Assign valve positions; $v_i \propto \lambda \times \{{}^{\psi_i}/_{\sum_i^N \psi_i}\}$

```python
def controller(depths,
               N=2,
               LAMBDA=0.3,
               MAX_DEPTH=2.0):
    # Compute the filling degree
    f = depths/MAX_DEPTH

    # Estimate the average filling degree
    f_mean = np.mean(f)

    # Compute psi
    psi = np.zeros(N)
    for i in range(0, N):
        psi[i] = f[i] - f_mean
        if psi[i] < 0.0:
            psi[i] = 0.0
        elif psi[i] == 0.0:
            psi[i] = f_mean

    # Assign valve positions
    actions = np.zeros(N)
    for i in range(0, N):
        if depths[i] > 0.0:
            k = 1.0 / np.sqrt(2 * 9.81 * depths[i])
            action = k * LAMBDA * psi[i]/np.sum(psi)
            actions[i] = min(1.0, action)

    return actions
```

Figure D.4: Equal-filling controller maintains the flows at the outlet below a desired threshold by coordinating its actions such that it equally utilizes the storage in the controllable assets of the network. Algorithm 2 and the corresponding code snippet illustrate the algorithm and its Python implementation. An interactive example of algorithm implementation and its evaluation on Scenario `theta` can be accessed at open-storm.org/pystorms/demo.

either retain or release storage depending on the observed states compared some corresponding water level limits.

**Rule-Based Control** Our basic rule-based control strategy adjusts our basin outlets based on their respective water levels. Specifically, each basin's outlet setting is equal to its relative water level (i.e., the current water level of the basin divided by its maximum depth). Therefore, our control algorithm will set a full basin's outlet to 100% open, and a basin that is half full will have its outlet set to 50% open, etc. While this strategy provides a means to mitigate local flooding at each basin, it notably does not consider the other control objective for the network's outflow into the downstream water body to stay below a given threshold.

**Equal-Filling Degree Control** The equal-filling degree is a control strategy often applied to stormwater networks with distributed stormwater storage assets, and has commonly been used as a starting point when comparing more than one control

strategies [41, 105–108]. For this strategy, we begin by defining a storage asset's "filling degree" — which is typically the ratio a storage asset is full based on its volume or depth — and compute it for each asset in the collection system. The algorithm seeks to "balance" these filling degrees across the system based on its average. The exact manner in which this balancing is carried out is not necessarily consistent in literature. Our method for this balancing is delineated in the algorithm in Figure D.4. If all assets have a filling degree equal to the average (i.e., all assets are equally filled), then each should release an equal fraction of the target outflow. Otherwise, the released flows across the assets should be differentiated such that, when an asset has a filling degree less than the average, it does not release any flow; but if an asset is greater than the average, it releases flows based on its deviation from the average.

The implementation of the equal-filling degree algorithm using `pystorms` can be seen in Figure D.4. We carry out the simulation for each of the two algorithms, as well as for the *uncontrolled case*, in which control actions are never implemented and the basin outlets are always open. The resulting hydraulic behavior at the two basins and the network's outflow for each of these simulation runs can be seen in Figure D.5.

Our aim to find a control strategy that can meet `theta`'s *control objective* to maintain the outflow into the downstream water body below a specified threshold of $0.5\ m^3 s^{-1}$ and also minimize flooding at the basins. As discussed in Section D.3.1, we pre-define a performance metric to quantify our control algorithm's ability to meet the corresponding control objective. For Scenario `theta`, this performance metric, $P$, is defined as:

$$P = \sum_{t=0}^{T} \left( \mathcal{H}_t + \sum_{i=1}^{2} \mathcal{G}_{i,t} \right) \tag{D.1a}$$

$$\mathcal{H}_t = \begin{cases} Q_t - 0.5\,, & \text{if } Q_t > 0.5 \\ 0.0\,, & \text{otherwise} \end{cases} \tag{D.1b}$$

$$\mathcal{G}_{i,t} = \begin{cases} 10^3\,, & \text{if any flooding at basin } i \\ 0.0\,, & \text{otherwise} \end{cases} \tag{D.1c}$$

where $\mathcal{H}_t$ is a flow exceedance penalty of the stormwater network's outflow, $Q_t$, over the 0.5 $m^3 s^{-1}$ threshold; and $\mathcal{G}_{i,t}$ is an arbitrary flooding penalty of $10^3$ added whenever there exists flooding at either of our two basins, both calculated and summed across every time-step $t$ in the simulation.

The performance metric calculated across the simulations for both implemented control algorithms and the uncontrolled case can be seen in Table D.3). Additionally, the hydraulic behavior of our two basins and the network outlet when these algorithms are applied versus the uncontrolled case can be seen in Figure D.5.

As can be seen, the equal-filling degree strategy is able to achieve the control objective of the outflow threshold, as well as avoidance of flooding. Alternatively, the rule-based control strategy only is able to avoid flooding at the basins. The stormwater network behavior for both strategies follow their corresponding implemented algorithm. For example, as the rule-based control strategy does not directly consider the outflow threshold when determining the implemented control actions, it follows that the outflow in the network's outlet exceeds this threshold (see the outlet plot in Figure D.5).

The results for each implemented control strategy versus the uncontrolled case are also captured using `theta`'s performance metric seen in Equation D.1. As the performance metric is ultimately a sum of penalties for violating the control objective, a smaller calculated performance metric value indicates a better performing control algorithm. The respective performance metric values for each control strategy presented here can be seen in Table D.3. With a calculated performance metric of 0, the equal-filling degree strategy perfectly meets `theta`'s control objective; comparatively, the rule-based and uncontrolled cases have higher performance metric values, and thus, we can conclude perform worse than the equal-filling degree.

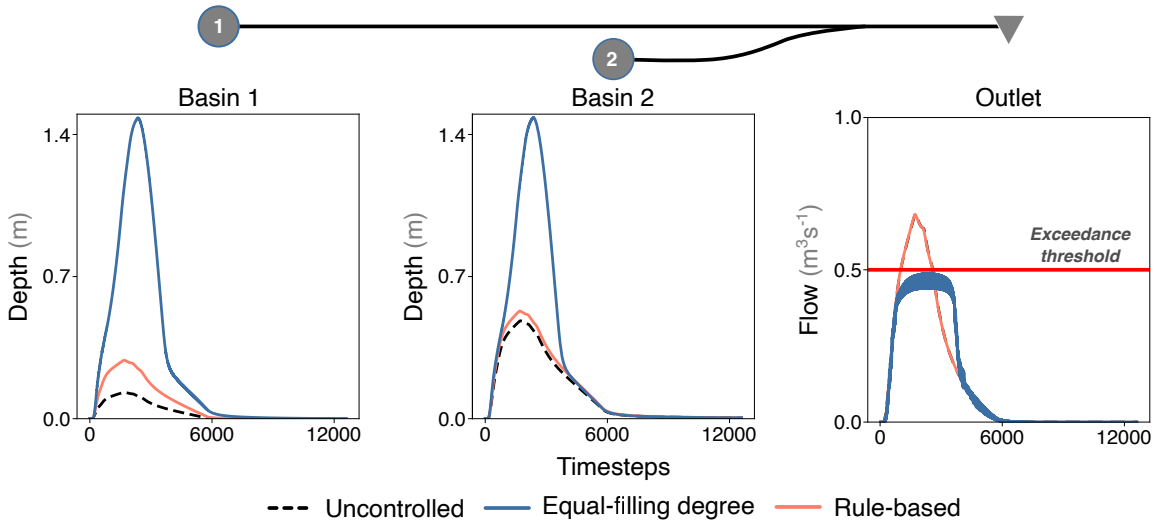


Figure D.5: In Scenario `theta`, the equal-filling degree control strategy is successfully able to maintain the flows at the outlet of the watershed below the desired threshold of 0.5 $m^3s^{-1}$ by uniformly using the storage in the networks. Static rule-based control and uncontrolled responses of the networks are also presented for comparison. The maximum depth in each of the two basins is 2 $m$.

Table D.3: Calculated performance metric values from Equation D.1 for simulations corresponding to the two implemented control algorithms and the uncontrolled simulation. As can be seen, the equal-filling degree control strategy performs better than the rule-based control strategy, which then outperforms the uncontrolled case.

| **Control Strategy** | **Performance Metric** |
|---|---|
| Uncontrolled | 1630 |
| Rule-based | 1624 |
| Equal-filling Degree | 0 |

## D.5 Discussion

This ability for stormwater systems to be instantly modified is critical as communities prepare for more frequent, uncertain, and destructive weather events due to climate change. More so, *often the most basic control strategies* can have large-scale impacts on the complex, dynamic systems they operate, potentially leading to millions of dollars in savings for the communities they serve. Even though sensor-actuator components may be successfully deployed at individual sites throughout a stormwater network, determining strategies for their coordination across the entire watershed may only add further complexity. As a result, there is a great need — along with endless opportunities — to develop and implement novel control strategies for transforming stormwater systems. While the sandboxing efforts of `pystorms` serves as an initial effort to foster the development of these strategies, we see specific opportunities to, first, methodically facilitate the development of new simulation frameworks and control algorithms, and subsequently, to then validate and extend their efficacy. We expound on these points here, and discuss next steps to put them into practice.

As discussed in Section D.2.2, a critical limitation to progressing smart stormwater control research forward is the inability to systematically develop and analyze smart stormwater simulation workflows and control algorithms. `pystorms` can be customized and adapted for a multitude of other uses beyond its initially provided collection of scenarios and stormwater simulator provided. For example, alternative stormwater simulation software be easily integrated into `pystorms`. Furthermore, new scenarios can be assembled from the assortment of components in the scenario collection such that additional research questions can be studied. For instance, for each of the scenarios we provide at the outset, `pystorms` specifies only a subset of a scenario's total observable states that are able to be queried throughout the simulation. However, this initial subset of observable states is never claimed as the optimal; in fact, to the best of our knowledge, there does not yet exist a methodology for identifying an optimal set of observable states. Thus, new scenarios can be made with different subsets of observable states (e.g. flows, pollutant concentrations), and

new research questions can now be asked about which states may be most critical for informing control actions to be taken.

Beyond the coordination and integration of smart stormwater control methods, we view a more expansive opportunity for `pystorms` to impel the research community to extend its analysis of "control." Specifically, we see a need for improved validation of control methods, and an opportunity for new approaches in defining a control method's success. In the current iteration of `pystorms` discussed here, we present a means to assess the performance of a control algorithm via its ability to achieve the pre-defined control objective (e.g. maintain flow below a threshold, avoid flooding). However, there are many other assessment metrics that can define a control algorithm's "success," including computational efficiency, applicability across real-world contexts, and the incorporation of social considerations for actual implementation. `pystorms` can serve as a mechanism for assessing the performance of control algorithms across these definitions. For example, by increasing the number of controllable assets available out of the eleven pond outlets presented in Scenario `gamma`, one can assess the *scalability* of a control algorithm as the state-action space increases. Additionally, control algorithm *generalizability* across storm characteristics can be assessed with the multiple rain events provided in Scenario `epsilon`. These are just a few illustrations of how `pystorms` provides a way to broaden and assess the definition of control efficacy to include factors that are critical for the implementation of smart stormwater approaches in real-world systems.

## D.6 Conclusions and Next Steps

`pystorms` provides a curated collection of scenarios, coupled with an accessible programming interface, to enable the development and quantitative evaluation of stormwater control algorithms. We have developed `pystorms` with the intent to make research into smart stormwater control more accessible to the broader research community. It is our hope that this package will emerge as a community-driven resource that is able to address key knowledge gaps and enable the advancement of smart stormwater systems. To this extent, we see proximate opportunities for the

broader research community to collaborate on `pystorms` by contributing their own stormwater scenarios and/or control algorithms to the package initiated here. Likewise, we encourage the broader research community to further build upon `pystorms` by imparting their own smart stormwater control instances using the `pystorms` architecture and integrating their own stormwater control simulation workflows into it.

# BIBLIOGRAPHY

# BIBLIOGRAPHY


[1] R. Field and E. J. Jr. Struzeski. Management and Control of Combined Sewer Overflows. *Journal (Water Pollution Control Federation)*, 44(7):1393–1415, 1972.

[2] J. G. Langeveld, R. P. S. Schilperoort, and S. R. Weijers. Climate change and urban wastewater infrastructure: There is more to explore. *Journal of Hydrology*, 476:112–119, 2013. doi: 10.1016/j.jhydrol.2012.10.021.

[3] P. Willems, K. Arnbjerg-Nielsen, J. Olsson, and V. T. V. Nguyen. Climate change impact assessment on urban rainfall extremes and urban drainage: Methods and shortcomings. *Atmospheric Research*, 103:106–118, 2012. doi: 10.1016/j.atmosres.2011.04.003.

[4] R. Robison. The tunnel that cleaned up Chicago. *Civil Engineering - ASCE*, 56(7):34–37, 1986.

[5] C. Scalise and K. Fitzpatrick. Chicago deep tunnel design and construction. In *Structures Congress*, pages 1485–1495, 2012.

[6] C. H. Emerson, C. Welty, and R. G. Traver. Watershed-scale evaluation of a system of storm water detention basins. *Journal of Hydrologic Engineering*, 10 (3):237–242, 2005. doi: 10.1061/(ASCE)1084-0699(2005)10:3(237).

[7] A. Mullapudi, M. D. Bartos, B. P. Wong, and B. Kerkez. Shaping streamflow using a real-time stormwater control network. *Sensors*, 18, 2018. doi: 10.3390/s18072259.

[8] S. A. Neshaei, A. Ahmadnejad, F. Yousefi, and F. Ghanbarpour. Estimating groundwater and rainfall infiltration into sewerage. *International Journal of Sustainable Development and Planning*, 12(1):185–193, 2017.

[9] Metcalf & Eddy, Inc., G. Tchobanoglous, F. L. Burton, and H. D. Stensel. *Wastewater Engineering: Treatment and Resource Recovery*. McGraw-Hill, 5 edition, 2013.

[10] U.S. Environmental Protection Agency. Flow Equalization, 1974. EPA Technology Transfer Seminar Publication, EPA 625/4-74-006.

[11] S. Arthur, H. Crow, and L. Pedezert. Understanding blockage formation in combined sewer networks. *Proceedings of the Institution of Civil Engineers: Water Management*, 161(4):215–221, 2008. doi: 10.1680/wama.2008.161.4.215.

[12] D. R. Marlow, F. Boulaire, D. J. Beale, C. Grundy, and M. Moglia. Sewer performance reporting: Factors that influence blockages. *Journal of Infrastructure Systems*, 17(1):42–51, 2011. doi: 10.1061/(ASCE)IS.1943-555X.0000041.

[13] C. Rosén. *A Chemometric Approach to Process Monitoring and Control - With Applications to Wastewater Treatment Operation*. PhD thesis, Lund University, 2001.

[14] P. van Daal, G. Gruber, J. G. Langeveld, D. Muschalla, and F. Clemens. Performance evaluation of real time control in urban wastewater systems in practice: Review and perspective. *Environmental Modelling and Software*, 95: 90–101, 2017. doi: 10.1016/j.envsoft.2017.06.015.

[15] J. Vaze, D. A. Post, F. H. S. Chiew, J.-M. Perraud, N. R. Viney, and J. Teng. Climate non-stationarity – Validity of calibrated rainfall–runoff models for use in climate change studies. *Journal of Hydrology*, 394(3–4):447–457, 2010. doi: https://doi.org/10.1016/j.jhydrol.2010.09.018.

[16] P. A. Vanrolleghem, L. Benedetti, and J. Meirlaen. Modelling and real-time control of the integrated urban wastewater system. *Environmental Modelling and Software*, 20(4):427–442, 2005. doi: 10.1016/j.envsoft.2004.02.004.

[17] J. Meirlaen, J. Van Assel, and P. A. Vanrolleghem. Real time control of the integrated urban wastewater system using simultaneously simulating surrogate models. *Water Science and Technology*, 45(3):109–116, 2002.

[18] A. Doglioni, F. Primativo, D. Laucelli, V. Monno, S.-T. Khu, and O. Giustolisi. An integrated modelling approach for the assessment of land use change effects on wastewater infrastructures. *Environmental Modelling & Software*, 24(12): 1522–1528, 2009.

[19] T. D. Fletcher, H. Andrieu, and P. Hamel. Understanding, management and modelling of urban hydrology and its consequences for receiving waters: A state of the art. *Advances in Water Resources*, 51:261–279, 2013.

[20] Y. Liu, V. F. Bralts, and B. A. Engel. Evaluating the effectiveness of management practices on hydrology and water quality at watershed scale with a rainfall-runoff model. *Science of The Total Environment*, 511:298–308, 2015.

[21] D. Hill, B. Kerkez, A. Rasekh, A. Ostfeld, B. Minsker, and M. K. Banks. Sensing and cyberinfrastructure for smarter water management: The promise and challenge of ubiquity. *Journal of Water Resources Planning and Management*, 140(7):1–3, 2014.

[22] B. Kerkez, C. Gruden, M. Lewis, L. Montestruque, M. Quigley, B. P. Wong, A. Bedig, R. Kertesz, T. Braun, O. Cadwalader, A. Poresky, and C. Pak. Smarter stormwater systems. *Environmental Science and Technology*, 50(14): 7267–7273, 2016. doi: 10.1021/acs.est.5b05870.

[23] A. Mullapudi, B. P. Wong, and B. Kerkez. Emerging investigators series: Building a theory for smart stormwater systems. *Environmental Science: Water Research and Technology*, 3(1):66–77, 2017. doi: 10.1039/C6EW00211K.

[24] T. Hastie, R. Tibshirani, and J. Friedman. *The Elements of Statistical Learning*. Springer, 2009.

[25] C. W. Dawson and R. L. Wilby. Hydrological modelling using artificial neural networks. *Progress in Physical Geography*, 25(1):80–108, 2001.

[26] A. G. El-Din and D. W. Smith. A neural network model to predict the wastewater inflow incorporating rainfall events. *Water Research*, 36(5):1115–1126, 2002.

[27] O. Kisi, J. Shiri, and M. Tombul. Modeling rainfall-runoff process using soft computing techniques. *Computers and Geosciences*, 51:108–117, 2013. doi: http://dx.doi.org/10.1016/j.cageo.2012.07.001.

[28] A. Kurth, A. Saul, S. Mounce, W. Shepherd, and D. Hanson. Application of Artificial Neural Networks (ANNs) for the prediction of CSO discharges. In *11th International Conference on Urban Drainage*, 2008.

[29] X. Li, F. Zhou, and S. Lodewyk. Applications of artificial neural networks in urban water system. In *Proceedings of Watershed Management 2010: Innovations in Watershed Management Under Land Use and Climate Change*, 2010.

[30] S. R. Mounce, W. Shepherd, G. Sailor, J. Shucksmith, and A. J. Saul. Predicting combined sewer overflows chamber depth using artificial neural networks with rainfall radar data. *Water Science and Technology*, 69(6):1326–1333, 2014.

[31] J. Smith and R. N. Eli. Neural-network models of rainfall-runoff process. *Journal of Water Resources Planning and Management*, 121(6):499–508, 1995.

[32] H. R. Maier and G. C. Dandy. Neural networks for the prediction and forecasting of water resources variables: A review of modelling issues and applications. *Environmental Modelling & Software*, 15(1):101–124, 2000.

[33] D. P. Solomatine and K. N. Dulal. Model trees as an alternative to neural networks in rainfall-runoff modelling. *Hydrological Sciences Journal*, 48(3): 399–411, 2003. doi: 10.1623/hysj.48.3.399.45291.

[34] M. Bruen and J. Yang. Combined hydraulic and black-box models for flood forecasting in urban drainage systems. *Journal of Hydrologic Engineering*, 11 (6):589–596, 2006.

[35] Z. Vojinovic, V. Kecman, and V. Babovic. Hybrid approach for modeling wet weather response in wastewater systems. *Journal of Water Resources Planning and Management*, 129(6):511–521, 2003.

[36] A. Campisano, J. Cabot Ple, D. Muschalla, M. Pleau, and P. A. Vanrolleghem. Potential and limitations of modern equipment for real time control of urban wastewater systems. *Urban Water Journal*, 10(5):300–311, 2013. doi: 10.1080/1573062X.2013.763996.

[37] M. Mahmoodian, O. Delmont, and G. Schutz. Pollution-based model predictive control of combined sewer networks, considering uncertainty propagation. *International Journal of Sustainable Development and Planning*, 12(1):98–111, 2017. doi: 10.2495/SDP-V12-N1-98-111.

[38] E. Meneses, M. Gaussens, C. Jakobsen, P. S. Mikkelsen, M. Grum, and L. Vezzaro. Coordinating rule-based and system-wide model predictive control strategies to reduce storage expansion of combined urban drainage systems: The case study of Lundtofte, Denmark. *Water*, 10(1):76, 2018. doi: 10.3390/w10010076.

[39] M. Pleau, H. Colas, P. Lavallée, G. Pelletier, and R. Bonin. Global optimal real-time control of the Quebec urban drainage system. *Environmental Modelling and Software*, 20(4):401–413, 2005. doi: 10.1016/j.envsoft.2004.02.009.

[40] D. Fiorelli, G. Schutz, K. Klepiszewski, M. Regneri, and S. Seiffert. Optimised real time operation of a sewer network using a multi-goal objective function. *Urban Water Journal*, 10(5):342–353, 2013. doi: 10.1080/1573062x.2013.806560.

[41] P. Borsányi, L. Benedetti, G. Dirckx, W. De Keyser, D. Muschalla, A. Solvi, V. Vandenberghe, M. Weyand, and P. A. Vanrolleghem. Modelling real-time control options on virtual sewer systems. *Journal of Environmental Engineering and Science*, 7(4):395–410, 2008. doi: 10.1139/S08-004.

[42] A. Mullapudi, M. J. Lewis, C. L. Gruden, and B. Kerkez. Deep reinforcement learning for the real time control of stormwater systems. *Advances in Water Resources*, 140(March), 2020. doi: 10.1016/j.advwatres.2020.103600.

[43] S. Elsawah, T. Filatova, A. J. Jakeman, A. J. Kettner, M. L. Zellner, I. N. Athanasiadis, S. H. Hamilton, R. L. Axtell, D. G. Brown, J. M. Gilligan, M. A. Janssen, D. T. Robinson, J. Rozenberg, I. I. T. Ullah, and S. J. Lade. Eight grand challenges in socio-environmental systems modeling. *Socio-Environmental Systems Modelling*, 2:16226, 2020. doi: 10.18174/sesmo.2020a16226.

[44] E. A. Moallemi, F. Zare, P. M. Reed, and S. Elsawah. Structuring and evaluating decision support processes to enhance the robustness of complex human-natural systems. *Environmental Modelling and Software*, 123:104551, 2020. doi: 10.1016/j.envsoft.2019.104551.

[45] A. Szabó, I. Takács, S. N. Murthy, G. T. Daigger, I. Licskó, and S. Smith. Significance of design and operational variables in chemical phosphorus removal. *Water Environment Research*, 80(5):407–416, 2008. doi: 10.2175/106143008x268498.

[46] S. Tik and P. A. Vanrolleghem. Chemically enhancing primary clarifiers: Model-based development of a dosing controller and full-scale implementation. *Water Science and Technology*, 75(5):1185–1193, 2017. doi: 10.2166/wst.2016.600.

[47] P. Ingildsen. *Realising full-scale control in wastewater treatment systems using in situ nutrient sensors*. PhD thesis, Lund University, 2002.

[48] J. Väänänen, S. Memet, T. Günther, M. Lilja, M. Cimbritz, and J. La Cour Jansen. Automatic control of the effluent turbidity from a chemically enhanced primary treatment with microsieving. *Water Science and Technology*, 76(7): 1770–1780, 2017. doi: 10.2166/wst.2017.358.

[49] J. B. Ellis. Sewer infiltration/exfiltration and interactions with sewer flows and groundwater quality. In *2nd International Conference Interactions between sewers, treatment plants and receiving waters in urban areas–Interurba II*, pages 19–22, 2001.

[50] C. Karpf and P. Krebs. Quantification of groundwater infiltration and surface water inflows in urban sewer networks based on a multiple model approach. *Water Research*, 45(10):3129–3136, 2011. doi: http://dx.doi.org/10.1016/j.watres.2011.03.022.

[51] C. W. Pawlowski, L. Rhea, W. D. Shuster, and G. Barden. Some factors affecting inflow and infiltration from residential sources in a core urban area: Case study in a Columbus, Ohio, Neighborhood. *Journal of Hydraulic Engineering*, 140(1):105–114, 2013.

[52] R. Löwe, L. Vezzaro, P. S. Mikkelsen, M. Grum, and H. Madsen. Probabilistic runoff volume forecasting in risk-based optimization for RTC of urban drainage systems. *Environmental Modelling & Software*, 80:143–158, 2016.

[53] L. P. Risholt, W. Schilling, V. Erbe, and J. Alex. Pollution based real time control of wastewater systems. *Water Science and Technology*, 45(3):219–228, 2002.

[54] M. Schütze, A. Campisano, H. Colas, W. Schilling, and P. A. Vanrolleghem. Real time control of urban wastewater systems - Where do we stand today? *Journal of Hydrology*, 299(3-4):335–348, 2004. doi: 10.1016/j.jhydrol.2004.08.010.

[55] K. Seggelke and K.-H. Rosenwinkel. Online-simulation of the WWTP to minimise the total emission of WWTP and sewer system. *Water Science and Technology*, 45(3):101–108, 2002.

[56] P. M. Bach, W. Rauch, P. S. Mikkelsen, D. T. Mccarthy, and A. Deletic. A critical review of integrated urban water modelling - Urban drainage and beyond. *Environmental Modelling & Software*, 54:88–107, 2014.

[57] T. Beeneken, V. Erbe, A. Messmer, C. Reder, R. Rohlfing, M. Scheer, M. Schuetze, B. Schumacher, M. Weilandt, and M. Weyand. Real time control (RTC) of urban drainage systems – A discussion of the additional efforts compared to conventionally operated systems. *Urban Water Journal*, 10(5): 293–299, 2013. doi: 10.1080/1573062X.2013.790980.

[58] K. Seggelke, R. Löwe, T. Beeneken, and L. Fuchs. Implementation of an integrated real-time control system of sewer system and waste water treatment plant in the city of Wilhelmshaven. *Urban Water Journal*, 10(5):330–341, 2013.

[59] M. Häck and J. Wiese. Trends in instrumentation, control and automation and the consequences on urban water systems. *Water Science and Technology*, 54 (11-12):265–272, 2006.

[60] M. Schütze, D. Butler, and M. B. Beck. *Modelling, simulation and control of urban wastewater systems*. Springer Science & Business Media, 2011.

[61] S. S. Haykin. *Neural Networks: A Comprehensive Foundation*. Prentice Hall, 2nd edition, 1999.

[62] E. Todini. Hydrological catchment modelling: Past, present and future. *Hydrology and Earth System Sciences*, 11(1):468–482, 2007.

[63] A. E. Ruano. *Intelligent Control Systems using Computational Intelligence Techniques*, volume 70. IET, 2005.

[64] B. K. Banik, L. Alfonso, C. Di Cristo, A. Leopardi, and A. Mynett. Evaluation of different formulations to optimally locate sensors in sewer systems. *Journal of Water Resources Planning and Management*, 143(7), 2017.

[65] F. Golnaraghi and B. C. Kuo. *Automatic Control Systems*, volume 2. Wiley, 9 edition, 2009.

[66] L. Ljung. *System Identification: Theory for the User*. Prentice Hall, 2nd edition, 1999.

[67] A. Andreas. *Digital Filters, Analysis, Design, and Applications*. McGraw-Hill, Inc, 2 edition, 1993.

[68] R. Saagi, X. Flores-Alsina, G. Fu, D. Butler, K. V. Gernaey, and U. Jeppsson. Catchment & sewer network simulation model to benchmark control strategies within urban wastewater systems. *Environmental Modelling & Software*, 78: 16–30, 2016.

[69] D. Butler and M. Schütze. Integrating simulation models with a view to optimal control of urban wastewater systems. *Environmental Modelling & Software*, 20 (4):415–426, 2005.

[70] K. V. Gernaey, X. Flores-Alsina, C. Rosen, L. Benedetti, and U. Jeppsson. Dynamic influent pollutant disturbance scenario generation using a phenomenological modelling approach. *Environmental Modelling & Software*, 26(11):1255–1267, 2011.

[71] C. K. I. Williams and C. E. Rasmussen. *Gaussian Processes for Machine Learning*. The MIT Press, 2006.

[72] Z. Yang and D. Han. Derivation of unit hydrograph using a transfer function approach. *Water Resources Research*, 42(1), 2006. doi: 10.1029/2005WR004227.

[73] InfluxDB, 2017. URL `https://www.influxdata.com/time-series-platform/influxdb/`.

[74] Grafana, 2017. URL `http://grafana.org/`.

[75] Google Maps, 2017. URL `http://maps.google.com`.

[76] Å. Björck. *Numerical Methods for Least Squares Problems*. SIAM, 1996.

[77] M. Métadier and J.-L. Bertrand-Krajewski. From mess to mass: A methodology for calculating storm event pollutant loads with their uncertainties, from continuous raw data time series. *Water Science and Technology*, 63(3):369–376, 2011.

[78] M. van Bijnen and H. Korving. Application and results of automatic validation of sewer monitoring data. In *Proceedings on 11th International Conference on Urban Drainage, Edinburgh, Scotland, UK*, 2008.

[79] S.-Y. Leu, D. Rosso, L. E. Larson, and M. K. Stenstrom. Real-time aeration efficiency monitoring in the activated sludge process and methods to reduce energy consumption and operating costs. *Water Environment Research*, 81 (12):2471–2481, 2009. doi: 10.2175/106143009x425906.

[80] R. C. Leitão, A. C. Van Haandel, G. Zeeman, and G. Lettinga. The effects of operational and environmental variations on anaerobic wastewater treatment systems: A review. *Bioresource Technology*, 97(9):1105–1118, 2006. doi: 10.1016/j.biortech.2004.12.007.

[81] C. P. L. Grady, Jr., G. T. Daigger, N. G. Love, and C. D. M. Filipe. *Biological Wastewater Treatment*. CRC Press, 2011.

[82] J. Bolmstedt. *Controlling the Influent Load to Wastewater Treatment Plants*. PhD thesis, Lund University, 2004.

[83] I. Aymerich, L. Rieger, R. Sobhani, D. Rosso, and L. Corominas. The difference between energy consumption and energy cost: Modelling energy tariff structures for water resource recovery facilities. *Water Research*, 81:113–123, 2015. doi: 10.1016/j.watres.2015.04.033.

[84] M. Gatterdam and R. Johnson. Operating a collection system like a treatment plant: A cost effective way to reduce overflows. In *Proceedings of the Water Environment Federation*, volume 8, pages 1853–1868, 2016. doi: https://doi.org/10.2175/193864716819714078.

[85] N. S. V. Lund, A. K. V. Falk, M. Borup, H. Madsen, and P. S. Mikkelsen. Model predictive control of urban drainage systems: A review and perspective towards smart real-time water management. *Critical Reviews in Environmental Science and Technology*, 48(3):279–339, 2018. doi: 10.1080/10643389.2018.1455484.

[86] H. Colas, M. Pleau, J. Lamarre, G. Pelletier, and P. Lavallee. Practical perspective on real-time control. *Water Quality Research Journal of Canada*, 39 (4):466–478, 2004. doi: 10.2166/wqrj.2004.058.

[87] R. M. Ashley, J. Dudley, J. Vollertsen, A. J. Saul, A. Jack, and J. R. Blanksby. The effect of extended in-sewer storage on wastewater treatment plant performance. *Water Science and Technology*, 45(3):239–246, 2002.

[88] G. Weinrich, W. Schilling, A. Birkely, and T. Moland. Pollution based real time control strategies for combined sewer systems. *Water Science and Technology*, 36(8-9):331–336, 1997.

[89] W. Schilling, B. Andersson, U. Nyberg, H. Aspegren, W. Rauch, and P. Harremoës. Real time control of wastewater systems. *Journal of hydraulic research*, 34(6):785–797, 1996.

[90] L. García, J. Barreiro-Gomez, E. Escobar, D. Téllez, N. Quijano, and C. Ocampo-Martinez. Modeling and real-time control of urban drainage systems: A review. *Advances in Water Resources*, 85:120–132, 2015. doi: 10.1016/j.advwatres.2015.08.007.

[91] M. Jørgensen, W. Schilling, and P. Harremoës. General assessment of potential CSO reduction by means of real time control. *Water Science and Technology*, 32(1):249–257, 1995. ISSN 02731223. doi: 10.1016/0273-1223(95)00562-2.

[92] G. Cembrano, J. Quevedo, M. Salamero, V. Puig, J. Figueras, and J. Mart. Optimal control of urban drainage systems - A case study. *Control Engineering Practice*, 12:1–9, 2004.

[93] C. Ocampo-Martinez. *Model predictive control of wastewater systems*. Springer, 2010. doi: 10.1007/978-1-84996-353-4.

[94] C. Sun, B. Josep-Duran, G. Cembrano, V. Puig, and J. Meseguer. Advanced integrated real-time control of combined urban drainage systems using MPC: Barcelona case study. In *EPiC Series in Engineering: International Conference on Hydroinformatics*, volume 3, pages 2033–2041. EasyChair, 2018.

[95] K.-J. van Heeringen, J. Gooijer, and D. Schwanenberg. Practical application of drainage system control by using MPC in Noorderzijlvest. In *EGU General Assembly Conference Abstracts*, volume 15, 2013.

[96] L. A. Montestruque. An agent-based storm water management system. In Panagiotis Tsakalides, Athanasia Panousopoulou, Grigorios Tsagkatakis, and Luis Montestruque, editors, *Smart Water Grids: A Cyber-Physical Systems Approach*, chapter 6, pages 151–168. CRC Press, 2018.

[97] M. D. Bartos, B. P. Wong, and B. Kerkez. Open storm: A complete framework for sensing and control of urban watersheds. *Environmental Science: Water Research and Technology*, 4:346–358, 2018. doi: 10.1039/c7ew00374a.

[98] E. Gaborit, F. Anctil, G. Pelletier, and P. A. Vanrolleghem. Exploring forecast-based management strategies for stormwater detention ponds. *Urban Water Journal*, 13(8):841–851, 2016. doi: 10.1080/1573062X.2015.1057172.

[99] D. Muschalla, B. Vallet, F. Anctil, P. Lessard, G. Pelletier, and P. A. Vanrolleghem. Ecohydraulic-driven real-time control of stormwater basins. *Journal of Hydrology*, 511:82–91, 2014. doi: 10.1016/j.jhydrol.2014.01.002.

[100] S. Sharior, W. McDonald, and A. J. Parolari. Improved reliability of stormwater detention basin performance through water quality data-informed real-time control. *Journal of Hydrology*, 573(March):422–431, 2019. doi: 10.1016/j.jhydrol.2019.03.012.

[101] J. F. Carpenter, B. Vallet, G. Pelletier, P. Lessard, and P. A. Vanrolleghem. Pollutant removal efficiency of a retrofitted stormwater detention pond. *Water Quality Research Journal of Canada*, 49(2):124–135, 2014. doi: 10.2166/wqrjc.2013.020.

[102] A. Gilpin and M. Barrett. Interim report on the retrofit of an existing flood control facility to improve pollutant removal in an urban watershed. In *World Environmental and Water Resources Congress*, pages 65–74, 2014.

[103] S. Eggimann, L. Mutzner, O. Wani, M. Y. Schneider, D. Spuhler, M. Moy de Vitry, P. Beutler, and M. Maurer. The potential of knowing more: A review of data-driven urban water management. *Environmental Science and Technology*, 51(5):2538–2553, 2017. doi: 10.1021/acs.est.6b04267.

[104] A. L. Mollerup, P. S. Mikkelsen, D. Thornberg, and G. Sin. Controlling sewer systems – A critical review based on systems in three EU cities. *Urban Water Journal*, 14(4):435–442, 2017. doi: 10.1080/1573062X.2016.1148183.

[105] A. Campisano, W. Schilling, and C. Modica. Regulators' setup with application to the Roma–Cecchignola combined sewer system. *Urban Water*, 2(3):235–242, 2000. doi: 10.1016/S1462-0758(00)00061-3.

[106] G. Dirckx, M. Schütze, S. Kroll, C. Thoeye, G. De Gueldre, and B. Van De Steene. Cost-efficiency of RTC for CSO impact mitigation. *Urban Water Journal*, 8(6):367–377, 2011. doi: 10.1080/1573062X.2011.630092.

[107] L. Vezzaro and M. Grum. A generalised Dynamic Overflow Risk Assessment (DORA) for real time control of urban drainage systems. *Journal of Hydrology*, 515:292–303, 2014. doi: 10.1016/j.jhydrol.2014.05.019.

[108] S. Kroll, G. Dirckx, B. M. R. Donckels, M. Van Dorpe, M. Weemaes, and P. Willems. Modelling real-time control of WWTP influent flow under data scarcity. *Water Science and Technology*, 73(7):1637–1643, 2016. doi: 10.2166/wst.2015.641.

[109] M. Marinaki and M. Papageorgiou. Linear-quadratic regulators applied to sewer network flow control. In *European Control Conference*, pages 2407–2412. IEEE, 2003. doi: 10.23919/ECC.2003.7085327.

[110] S. Darsono and J. W. Labadie. Neural-optimal control algorithm for real-time regulation of in-line storage in combined sewer systems. *Environmental Modelling and Software*, 22:1349–1361, 2007. doi: 10.1016/j.envsoft.2006.09.005.

[111] B. P. Wong and B. Kerkez. Real-time control of urban headwater catchments through linear feedback: Performance, analysis, and site selection. *Water Resources Research*, 54:7309–7330, 2018. doi: 10.1029/2018WR022657.

[112] S. P. Rimer, A. Mullapudi, S. C. Troutman, and B. Kerkez. A benchmarking framework for control and optimization of smart stormwater networks. *Proceedings of the 10th ACM/IEEE International Conference on Cyber-Physical Systems - ICCPS '19*, pages 350–351, 2019. doi: 10.1145/3302509.3313336.

[113] Open Water Analytics. PYSWMM. `https://github.com/OpenWaterAnalytics/pyswmm`, 2019.

[114] L. A. Rossman. Storm Water Management Model User's Manual Version 5.1, 2015.

[115] L. A. Rossman and W. C. Huber. Storm Water Management Model Reference Manual Volume III - Water Quality, 2015.

[116] E. Gaborit, D. Muschalla, B. Vallet, P. A. Vanrolleghem, and F. Anctil. Improving the performance of stormwater detention basins by real-time control using rainfall forecasts. *Urban Water Journal*, 10(4):230–246, 2013. doi: 10.1080/1573062X.2012.726229.

[117] M. D. Bartos and B. Kerkez. Hydrograph peak-shaving using a graph-theoretic algorithm for placement of hydraulic control structures. *Advances in Water Resources*, 127:167–179, 2019. doi: 10.1016/j.advwatres.2019.03.016.

[118] A. L. Mollerup, P. S. Mikkelsen, D. Thornberg, and G. Sin. Regulatory control analysis and design for sewer systems. *Environmental Modelling and Software*, 66:153–166, 2015. doi: 10.1016/j.envsoft.2014.12.001.

[119] S. Kroll, M. Weemaes, J. Van Impe, and P. Willems. A methodology for the design of RTC strategies for combined sewer networks. *Water*, 10(11):1675, 2018. doi: 10.3390/w10111675.

[120] A. L. Mollerup, P. S. Mikkelsen, and G. Sin. A methodological approach to the design of optimising control strategies for sewer systems. *Environmental Modelling and Software*, 83:103–115, 2016. doi: 10.1016/j.envsoft.2016.05.004.

[121] Z. Yuan, G. Olsson, R. Cardell-Oliver, K. van Schagen, A. Marchi, A. Deletic, C. Urich, W. Rauch, Y. Liu, and G. Jiang. Sweating the assets – The role of instrumentation, control and automation in urban water systems. *Water Research*, 155:381–402, 2019. doi: 10.1016/j.watres.2019.02.034.

[122] L. Benedetti, J. G. Langeveld, A. Comeau, L. Corominas, G. T. Daigger, C. Martin, P. S. Mikkelsen, L. Vezzaro, S. Weijers, and P. A. Vanrolleghem. Modelling and monitoring of integrated urban wastewater systems: Review on status and perspectives. *Water Science and Technology*, 68(6):1203–1215, 2013. doi: 10.2166/wst.2013.397.

[123] J. G. Langeveld, I. Nopens, R. P. S. Schilperoort, L. Benedetti, J. J. M. De Klein, Y. Amerlinck, and S. Weijers. On data requirements for calibration of integrated models for urban water systems. *Water Science and Technology*, 68 (3):728–736, 2013. doi: 10.2166/wst.2013.301.

[124] J. G. Langeveld, L. Benedetti, J. J. M. De Klein, I. Nopens, Y. Amerlinck, A. van Nieuwenhuijzen, T. Flameling, O. van Zanten, and S. Weijers. Impact-based integrated real-time control for improvement of the Dommel River water quality. *Urban Water Journal*, 10(5), 2013. doi: 10.1080/1573062X.2013.820332.

[125] C. Sun, L. Romero, B. Joseph-Duran, J. Meseguer, E. Muñoz, R. Guasch, M. Martinez, V. Puig, and G. Cembrano. Integrated pollution-based real-time control of sanitation systems. *Journal of Environmental Management*, 269, 2020. doi: 10.1016/j.jenvman.2020.110798.

[126] J. Read, D. Scavia, B. Kerkez, Y. Hu, A. Dagnew, R. Muenich, S. Bocaniov, Y.-C. Wang, C. Long, and L. Vaccaro. Watershed Assessment of Detroit River Phosphorus Loads to Lake Erie. Technical report, University of Michigan Water Center, 2019.

[127] D. Scavia, J. D. Allan, K. K. Arend, S. Bartell, D. Beletsky, N. S. Bosch, S. B. Brandt, R. D. Briland, I. Daloğlu, J. V. DePinto, D. M. Dolan, M. A. Evans, T. M. Farmer, D. Goto, H. Han, T. O. Höök, R. Knight, S. A. Ludsin, D. Mason, A. M. Michalak, P. R. Richards, J. J. Roberts, D. K. Rucinski, E. Rutherford, D. J. Schwab, T. M. Sesterhenn, H. Zhang, and Y. Zhou. Assessing and addressing the re-eutrophication of Lake Erie: Central basin hypoxia. *Journal of Great Lakes Research*, 40(2):226–246, 2014. doi: 10.1016/j.jglr.2014.02.004.

[128] M. Khan (Ph.D.). Director of Operations, Wastewater, Great Lakes Water Authority. Personal communication, 2020.

[129] C. Yang, W. Barrott, A. Busch, A. Mehrotra, J. Madden, and G. T. Daigger. How much data is required for a robust and reliable wastewater characterization? *Water Science and Technology*, 79(12):2298–2309, 2019. doi: 10.2166/wst.2019.233.

[130] J. Yan, C. Yang, Z. Tian, and G. T. Daigger. Characterizing the Performance and Operational Characteristics of the Bioreactors at the Detroit, MI, Water Resource Recovery Facility. Technical report, 2018.

[131] L. Kostrzewski. Chemist 3, Great Lakes Water Authority. Email, 2020.

[132] C. Yang. Ph.D. Student, University of Michigan. Personal communication, 2020.

[133] H. Hauduc, I. Takács, S. Smith, A. Szabó, S. N. Murthy, G. T. Daigger, and M. Spérandio. A dynamic physicochemical model for chemical phosphorus removal. *Water Research*, 73:157–170, 2015. doi: 10.1016/j.watres.2014.12.053.

[134] S. Smith, I. Takács, S. N. Murthy, G. T. Daigger, and A. Szabó. Phosphate complexation model and its implications for chemical phosphorus removal. *Water Environment Research*, 80(5):428–438, 2008. doi: 10.1002/j.1554-7531.2008.tb00349.x.

[135] D. Conidi, W. J. Parker, and S. Smith. Effect of solids residence time on dynamic responses in chemical P removal. *Water Environment Research*, 91:250–258, 2019. doi: 10.1002/wer.1052.

[136] D. S. Parker, J. Barnard, G. T. Daigger, R. J. Tekippe, and E. J. Wahlberg. The future of chemically enhanced primary treatment: Evolution not revolution. *Water Research*, 2001.

[137] S. Haydar and J. A. Aziz. Characterization and treatability studies of tannery wastewater using chemically enhanced primary treatment (CEPT): A case study of Saddiq Leather Works. *Journal of Hazardous Materials*, 163 (2-3):1076–1083, 2009. doi: 10.1016/j.jhazmat.2008.07.074.

[138] D. R. Neupane, R. Riffat, S. N. Murthy, M. R. Peric, and T. E. Wilson. Influence of source characteristics, chemicals, and flocculation on chemically enhanced primary treatment. *Water Environment Research*, 80(4):331–338, 2008. doi: 10.2175/106143007x221355.

[139] M. Umar, F. Roddick, and L. Fan. Comparison of coagulation efficiency of aluminium and ferric-based coagulants as pre-treatment for UVC/H2O2 treatment of wastewater RO concentrate. *Chemical Engineering Journal*, 284(2016): 841–849, 2016. doi: 10.1016/j.cej.2015.08.109.

[140] H. Wang, F. Li, A. A. Keller, and R. Xu. Chemically enhanced primary treatment (CEPT) for removal of carbon and nutrients from municipal wastewater treatment plants: A case study of Shanghai. *Water Science and Technology*, 60(7):1803–1809, 2009. doi: 10.2166/wst.2009.547.

[141] Y. Mao, A. Ninh Pham, Y. Xin, and T. D. Waite. Effects of pH, floc age and organic compounds on the removal of phosphate by pre-polymerized hydrous ferric oxides. *Separation and Purification Technology*, 91:38–45, 2012. doi: 10.1016/j.seppur.2011.09.045.

[142] S. C. Troutman, N. G. Love, and B. Kerkez. Balancing water quality and flows in combined sewer systems using real-time control. *Environmental Science: Water Research & Technology*, 2020. doi: 10.1039/C9EW00882A.

[143] I. Takács. *Experiments in Activated Sludge Modelling*. PhD thesis, Ghent University, 2008.

[144] E. Belia, Y. Amerlinck, L. Benedetti, B. R. Johnson, G. Sin, P. A. Vanrolleghem, K. V. Gernaey, S. Gillot, M. B. Neumann, L. Rieger, A. Shaw, and K. Villez. Wastewater treatment modelling: Dealing with uncertainties. *Water Science and Technology*, 60(8):1929–1941, 2009. doi: 10.2166/wst.2009.225.

[145] M. D. Bartos, H. Park, T. Zhou, B. Kerkez, and R. Vasudevan. Windshield wipers on connected vehicles produce high-accuracy rainfall maps. *Scientific Reports*, 9(1), 2019. doi: 10.1038/s41598-018-36282-7.

[146] D. J. Hill and B. S. Minsker. Anomaly detection in streaming environmental sensor data: A data-driven modeling approach. *Environmental Modelling and Software*, 25(9):1014–1022, 2010. doi: 10.1016/j.envsoft.2009.08.010.

[147] J. M. Ledergerber, É. Leray, T. Maruéjouls, and P. A. Vanrolleghem. Optimization of installation and maintenance of water quality sensors in combined sewers. In *International Conference on Urban Drainage*, Prague, Czech Republic, 2017.

[148] A. Krause, J. Leskovec, C. Guestrin, J. VanBriesen, and C. Faloutsos. Efficient sensor placement optimization for securing large water distribution networks. *Journal of Water Resources Planning and Management*, 134(6):516–526, 2008. doi: 10.1061/(ASCE)0733-9496(2008)134:6(516).

[149] C Makropoulos and D. A. Savić. Urban hydroinformatics: Past, present and future. *Water*, 11(1959), 2019. doi: 10.3390/w11101959.

[150] Z. Vojinovic and M. B. Abbott. *Flood risk and social justice*. IWA Publishing, 2012.

[151] L. Rieger and G. Olsson. Why many control systems fail. *Water and Environment Technology*, pages 42–45, 2012. doi: 10.2175/193864711802764779.

[152] S. Gray, A. Voinov, M. Paolisso, R. Jordan, T. Bendor, P. Bommel, P. Glynn, B. Hedelin, K. Hubacek, J. Introne, N. Kolagani, B. Laursen, C. Prell, L. Schmitt Olabisi, A. Singer, E. Sterling, and M. L. Zellner. Purpose, processes, partnerships, and products: Four Ps to advance participatory socio-environmental modeling. *Ecological Applications*, 28(1):46–61, 2018. doi: 10.1002/eap.1627.

[153] H. Chourabi, T. Nam, S. Walker, J. R. Gil-Garcia, S. Mellouli, K. Nahon, T. A. Pardo, and H. J. Scholl. Understanding smart cities: An integrative framework. In *Proceedings of the Annual Hawaii International Conference on System Sciences*, pages 2289–2297. IEEE, 2012. doi: 10.1109/HICSS.2012.615.

[154] C. Harrison and I. A. Donnelly. A theory of smart cities. In *Proceedings of the 55th Annual Meeting of the International Society for the Systems Sciences*, volume 55, 2011.

[155] P. D. Trotta, J. W. Labadie, and N. S. Grigg. Automatic control strategies for urban stormwater. *Journal of the Hydraulics Division*, pages 1443–1459, 1977.

[156] W. Schilling. Real-time control of urban drainage systems: The state-of-the-art. *IAWPRC Task Group on Real-Time Control of Urban Drainage Systems, London*, 1989.

[157] J. M. Sadler, J. L. Goodall, M. Behl, M. M. Morsy, T. Culver, and B. D. Bowes. Leveraging open source software and parallel computing for model predictive control of urban drainage systems using EPA-SWMM5. *Environmental Modelling and Software*, 2019. doi: 10.1016/j.envsoft.2019.07.009.

[158] S. Shishegar, S. Duchesne, and G. Pelletier. Optimization methods applied to stormwater management problems: A review. *Urban Water Journal*, 15(3): 276–286, 2018.

[159] L. Rossman and W. Huber. *Storm Water Management Model Reference Manual Volume I – Hydrology.* US EPA Office of Research and Development, Washington, DC, epa/600/r-15/162a edition, 2015.

[160] L. Rossman. *Storm Water Management Model Reference Manual Volume II – Hydraulics.* US EPA Office of Research and Development, Washington, DC, epa/600/r-17/111 edition, 2017.

[161] M. Schütze, M. Lange, M. Pabst, and U. Haas. Astlingen - a benchmark for real time control (RTC). *Water Science and Technology*, 2017(2):552–560, 2017.

[162] C. Sun, J. L. Svensen, M. Borup, V. Puig, G. Cembrano, and L. Vezzaro. An MPC-enabled SWMM implementation of the Astlingen RTC benchmarking network. *Water*, 12(1034):1–13, 2020. doi: 10.3390/w12041034.